APPENDIX 3.9.1
DSC SHELL STRUCTURAL ANALYSIS

Table of Contents

List of Tables

List of Figures

3.9.1 DSC SHELL STRUCTURAL ANALYSIS

The purpose of this appendix is to present the structural evaluation of the shell assembly of the EOS-37PTH dry shielded canister (DSC) and the EOS-89BTH DSC under all applicable normal, off-normal and accident loading conditions during storage in the EOS horizontal storage module (HSM) and during transfer in the EOS transfer cask (TC). The EOS system consists of the EOS-HSM, the EOS-TC, the dual-purpose (transportable/storage) EOS-37PTH and EOS-89BTH DSC, and associated ancillary equipment.

The design of the DSC includes five design options: EOS-37PTH (short, medium and long) and EOS-89BTH (short and medium). The longest and heaviest EOS-37PTH DSC, which uses TC135 for transfer operations, is analyzed to bound all DSC design options in the NUHOMS® EOS System.

3.9.1.1 General Description

The DSC consists of a fuel basket and a shell assembly. The DSC pressure boundary consists of DSC shell with two cover plates at each end. Non-pressure boundary shield plugs are included at each end of the assembly. The inner bottom shield (IBS) is confined between the inner bottom cover plate (IBCP) and outer bottom cover plate (OBCP). The top shield plug (TSP) is confined by the inner top cover plate (ITCP) and four lifting lugs, which are welded to the inside of the DSC shell. The grapple ring support is welded to the OBCP using full penetration weld. The ITCP is welded along the top perimeter with partial penetration weld. The IBCP is welded using a full penetration weld. Grapple ring assembly connections are all made using full penetration welds.

The DSC shell thickness is 0.50 inch, and the top and bottom closure assemblies are 10.0 inches and 8.0 inches, respectively. The DSC shell is constructed entirely from stainless steel or duplex steel. There are no penetrations through the pressure boundary. The draining and venting systems are covered by the port plugs. The outer top cover plate (OTCP) and the ITCP are welded to the cylindrical shell with multilayer welds. The DSC cavity is pressurized above atmospheric pressure with helium. The DSC shell assembly geometry and the materials used for its analysis and fabrication are shown on drawings EOS01-1000-SAR, EOS01-1001-SAR, EOS01-1005-SAR and EOS01-1006-SAR included in Chapter 1.

3.9.1.2 DSC Shell Assembly Stress Analysis

An enveloping technique of combining various individual loads in a single analysis is used in this evaluation for several load combinations. This approach reduces the number of computer runs, while remaining conservative. For some load combinations, stress intensities under individual loads are added to obtain resultant stress intensities for the specified combined loads. This addition at the stress intensity level for the combined loads, instead of at component stress level, is also a conservative method for reducing the number of analysis runs.

The stresses of all components are assessed by means of elastic analysis methodology for all load combinations, except the side drop load combination. Elastic-plastic analysis methodology is used to assess the stresses for Service Level D side drop load combination.

The DSC component stress results are post-processed using the ANSYS LPATH and PRSECT commands [3.9.1-9], which linearize the stress distribution through a requested section, resulting in a breakdown of the various stress components. Stress linearization for DSC components (DSC shell, top and bottom cover plates and grapple assembly) are performed on the critical selected paths using ANSYS post-processing macros.

In the case of elastic analysis methodology, average stress intensity across the path (including general primary stress intensities, P_m and local primary stress intensities, P_L) are conservatively classified and reported as P_m stresses, and consequently assessed against P_m stress allowable. The linearized membrane plus bending stresses at classification path surfaces are classified as primary membrane and bending stresses, $P_m + P_b$, and assessed against the $P_m + P_b$ stress allowable.

In case of elastic-plastic analysis methodology, ANSYS procedure is set to extract the membrane stress for the path (classified conservatively as P_m stress), as well as the maximum total stress intensity (classified conservatively as the primary stress) for the classification path derived from the total (not linearized) path stresses.

The thermal stress intensities are classified as secondary stress intensities, Q, for code evaluations.

3.9.1.2.1 Material Properties

For elastic analysis, temperature dependent material properties used for each component of DSC shell assembly are obtained from the American Society of Mechanical Engineers (ASME) code [3.9.1-2], and are summarized in Chapter 8. Material properties used for stress evaluations are conservatively taken at 500 °F.

For plastic analysis, a bilinear stress-strain curve with a 5% tangent modulus is used for steel components. The non-linear material properties at 500 °F for side drop analysis are shown in Table 3.9.1-3. Steel material (except shield plugs) is modeled by bilinear kinematic hardening method (TB, BKIN – [3.9.1-9]).

3.9.1.2.2 DSC Shell Stress Criteria

The calculated stresses in the DSC shell assembly structural components are compared with the allowable stresses set forth by ASME Boiler and Pressure Vessel (B&PV) Code, Section III, Subsection NB [3.9.1-3] under normal (Level A), and off-normal (Level B) loading conditions. Appendix F of the ASME B&PV Code is used to evaluate the calculated stresses in the DSC shell assembly under accident (Level D) loading conditions. Allowable stress limits for Levels A, B and D service loading conditions, as appropriate, are summarized in Table 3-1, and the corresponding allowable stress values at different temperatures are summarized in Table 3.9.1-5.

The OTCP-to-DSC shell weld and the ITCP-to-DSC shell weld, which are both partial penetration welds, are to be evaluated using a joint efficiency factor of 0.8. Per NUREG-1536 [3.9.1-7], the minimum inspection requirement for end closure welds is multi-pass dye penetrant testing (PT) using a stress (allowable) reduction factor of 0.8. The allowable weld stresses are summarized in Table 3.9.1-4.

3.9.1.2.3 Finite Element Models

The EOS-37PTH DSC shell assembly is analyzed for the postulated load conditions using a three-dimensional (3D), 180-degree, half-symmetric finite element model (FEM). The FEM is developed using the nominal dimensions of the long cavity DSC.

Each of the DSC shell assembly components is modeled using (ANSYS SOLID185) 3D solid elements. The top end of the DSC is assembled so that no gaps initially exist between the OTCP, ITCP and TSP. Similarly, the bottom end of the DSC is assembled so that no gaps initially exist between the OBCP, IBS, and IBCP. The interfaces between the mating surfaces are modeled using (ANSYS CONTA178) 3D, node-to-node contact elements that allow the transfer of compressive (bearing) loads. The contact elements are defined to allow the surfaces to slide freely (no shear transfer), assuming that there is no friction.

The partial penetration welds of the outer cover plates (OTCP and OBCP) to the DSC shell are modeled by coupling the nodes of the appropriate components in all directions. The weld of the ITCP to the DSC shell is also modeled in the same manner. The IBCP is connected to the DSC shell with a full penetration weld. Therefore, all nodes through the thickness of the plate along the perimeter are merged with the DSC shell nodes. The lifting lug is connected to the DSC shell using a partial penetration groove weld on the top and bottom side, and a fillet weld on the other two sides. The welds are represented in the model by coupling nodes along the lug plate with the DSC shell nodes. The grapple ring is assembled and connected to the OBCP using full penetration welds. Since the grapple ring and grapple support plate welds are also full penetration welds, nodes at their interfaces are merged.

For DSC geometry, dimensions are taken from the drawings in Chapter 1 and material specifications are taken from Chapter 8. Figure 3.9.1-1 through Figure 3.9.1-4 shows the meshed model of EOS-37PTH DSC. Figure 3.9.1-5 through Figure 3.9.1-13 show the boundary conditions and load application for different load cases. Table 3.9.1-1 lists the major dimensions of the bounding model, and Table 3.9.1-2 lists material designations, used in the analysis, of each modeled component to envelop the material options available.

3.9.1.2.4 Load Cases for DSC Shell Stress Analysis

This section discusses the different load cases considered to evaluate the stresses generated in the EOS-37PTH DSC and EOS-89BTH DSC shell assembly during transfer operations and in storage conditions under normal, off-normal and accident loading. During fuel transfer, the DSC is oriented horizontally inside the EOS-TC, which is mounted to the transfer skid and transferred from the reactor or fuel building to the independent spent fuel storage installation (ISFSI). During storage, the DSC is in the horizontal position within EOS-HSM.

Each load case analysis utilizes the finite element model that is described in Section 3.9.1.2.3, along with pertinent loads and boundary conditions. Bounding storage load cases, transfer load cases and load combinations used to evaluate the DSC shell assembly are tabulated in Table 2-5. In general, major loads (ram push/pull loading with internal/external pressure) are combined within the ANSYS analyses, while stress intensities from minor loads (i.e. dead weight and pressure) are added algebraically.

3.9.1.2.4.1 Dead weight

The dead weight is analyzed for three basic configurations: DSC in vertical and horizontal position in the EOS-TC, and DSC in horizontal position in the EOS-HSM. The analytical model applicable to EOS-TC and EOS-HSM differ in boundary conditions representing support rails.

3.9.1.2.4.1.1 Vertical Position in EOS-TC

The DSC shell supports the entire weight of the top end components in addition to its self-weight. The weight of the fuel is assumed to be uniformly distributed over the area of the IBCP. The fuel load and the weight of the bottom end components are transferred directly to the DSC shell bottom through bearing between the IBCP, IBS, and OBCP.

Symmetric boundary conditions are applied at the plane of symmetry of the model. The bottom end surface of the EOS-TC is constrained in vertical direction. The contact elements are generated between DSC shell and OBCP outermost nodes (excluding the surface of OBCP, which is bounded by the grapple ring support) and the EOS-TC surface. The weight of the basket and fuel assemblies is conservatively taken as a total load of 105 kips, and is applied as uniform pressure acting on the IBCP.

3.9.1.2.4.1.2 Horizontal Position in EOS-TC

When the DSC is in a horizontal position in the EOS-TC, the end components and basket assembly bear against the DSC shell and the DSC Shell is supported by six, 3-inch wide canister rails spaced symmetrically at ±6.5°, ±17.5°, and ±25.5° from the bottom centerline.

For the horizontal dead weight load case when the DSC is inside the EOS-TC, dead weight for DSC internals are accounted for by applying an equivalent pressure on the inside surface of the DSC. The pressure is applied at the projection of the first 6.5° canister rail only. The pressure is determined based on the payload of 105 kips and projected area of DSC shell that is in interface with the EOS-TC canister rail.

The interface between the DSC and the EOS-TC canister rails is modeled through node-to-node contact elements CONTA178. Nodes that are interfacing the rails are copied, creating new pattern of nodes. These new nodes are restrained in all degrees of freedom and connected to the original nodes belonging to the DSC shell through the CONTA178 contact elements.

Gaps at the 6.5° rail are set to zero placing the DSC shell and the EOS-TC canister rail in initial contact. The initial gaps are defined in the case of the second and third rail, at 17.5° and 25.5° from the plane of symmetry.

Symmetric boundary conditions are applied at the cut section (Y-symmetry).

3.9.1.2.4.1.3 Horizontal Position in EOS-HSM

When stored horizontally in the EOS-HSM, the DSC shell is supported by two 3-inch wide nitronic plates on the DSC support structure at ±30° from the bottom centerline.

For the horizontal dead weight load case, dead weight of DSC internals are accounted for by applying equivalent pressure onto the inner surface of DSC shell at the EOS-HSM DSC support rail locations. The pressure is determined based on 105 kips and projected area of selected elements that are in interface with the EOS-HSM DSC support rail. Sum of reactions are checked to verify that the intended load consisting of the dead weight of the payload and the DSC is correctly applied.

The interface between the DSC and the EOS-HSM DSC support rail is modeled through node-to-node contact elements CONTA178. Nodes that are interfacing the EOS-HSM DSC support rail are copied creating a new pattern of nodes. Each row of nodes represents the width of the EOS-HSM DSC support rail (there are three nodes across the width of the rail). Each node of the row is coupled with its neighboring node in all degrees of freedom using CERIG command, creating a rigid interface.

Each middle node of this platform is connected in the axial direction of the DSC through BEAM188 element. Finally, these new nodes representing the EOS-HSM are connected to the original nodes belonging to the DSC shell through the CONTA178 contact elements. Gaps are set to zero, placing the DSC shell and the EOS-HSM DSC support rail in initial contact. Nodes representing the EOS-HSM DSC support rail are constrained in all degrees of freedom near the bottom end and the top end. The BEAM188 elements have the properties of the wide-flange steel beam, which supports the DSC inside the EOS-HSM. Therefore, the flexibility of the support beam is considered in the analysis.

3.9.1.2.4.2 Fabrication Pressure and Leak Testing

Pressurization and leak testing is performed on the DSC shell and IBCP during fabrication. No other DSC components are in place during this test. A seal plate is placed on the open top of the DSC shell, and preloaded by eight bolts that are connected to a flange at the bottom of the DSC shell. A total preload of 155 kips is considered in the evaluation. The DSC is then evacuated to a partial vacuum and then re-pressurized with helium. Therefore, two load conditions are evaluated for the DSC Shell and IBCP:

- Leak Test: 155 kip axial compression + 14.7 psig external pressure (full vacuum) on the DSC shell between the top edge and the IBCP + 14.7 psig external pressure on the IBCP. Note that the vacuum will add axial load to the 155 kips preload.
- Pressure Test: 155 kip axial compression + 23.0 psig internal pressure on the DSC shell between the top edge and the IBCP + 23.0 psig internal pressure on the IBCP. Note that the internal pressure will not affect the reaction on the DSC Shell due to the preload.

Symmetric boundary conditions are applied at the plane of symmetry of the model. The bottom surface of the DSC Shell surface is constrained in vertical direction. The 155 kips load is represented by equivalent pressure that is applied at the top surface of the DSC Shell.

External pressure is applied at all external nodes of the DSC Shell-IBCP assembly with the exception of the top surface of the DSC Shell that is loaded with the 155 kips preload. Internal pressure is applied at all nodes on the inside surface of DSC Shell-IBCP assembly. Two load steps are performed, one for the internal pressure and the second one for the external pressure as stated above.

3.9.1.2.4.3 Internal and External Pressure

The DSC pressure boundary is defined by the DSC Shell, the IBCP, the ITCP and the associated welds. Because there are no gaps between the top end plate components, the ITCP bears against the OTCP. Also, because the ITCP meets the leak tight requirements of ANSI N14.5 [3.9.1-5], no leakage is feasible and therefore, the pressure load is shared by the two plates according to their relative stiffness.

Similarly, the absence of gaps between the bottom end components allows the IBCP to bear against the IBS, which, in turn, bears against the OBCP.

A bounding pressure of 30 psig is used for normal and off-normal conditions and 130 psig for accident condition. Two load cases are analyzed – one with internal pressure of 30 psig and second with internal pressure of 130 psig.

All the nodes of the inner surface of DSC shell confined by ITCP and IBCP are selected for application of internal pressure. The inner surface of IBCP and ITCP are also subjected to internal pressure. Symmetric boundary conditions are applied to cut section (Y-plane symmetry).

In addition to the internal pressure loads listed above, the DSC will be subjected to hydrostatic, blowdown, vacuum, and test pressures during the fuel loading and draining/drying processes. Prior to loading fuel and without the top end components in place, the TC/DSC annulus is filled with water resulting in a hydrostatic external load on the DSC Shell. The hydrostatic load is then balanced by filling the DSC with water.

After the fuel is loaded, the TSP and ITCP are installed and an internal blowdown pressure of 15 psig is applied to evacuate the DSC of water. The DSC internals are then dried under vacuum conditions. The DSC is backfilled with helium at 20 psig. The pressure is then reduced to 3.5 psig and the OTCP is welded in place.

External pressure is applied at all external nodes of the DSC at a level below 12 inches from top of DSC. Internal pressure is applied at all surface nodes inside the DSC from the inside of the IBCP up to the coupled node between the ITCP and the DSC Shell. Nodes in contact between the lifting lugs and the DSC Shell are not subject to pressure load.

Two load steps are performed for the Blowdown/Pressure test and the Vacuum Drying with combinations of internal and external pressures without the OTCP installed. See Table 2-5 for list of pressure loads.

3.9.1.2.4.4 EOS-HSM Loading/Unloading

To load the DSC into the EOS-HSM, the DSC is pushed out of the EOS-TC using a hydraulic ram. The load is applied at the center of the OBCP within the diameter of the Grapple Ring Support. Based on the relative stiffness of the cover plates and IBS, a portion of the insertion load will be transferred through the IBS to the IBCP (and associated welds).

- Loading is defined as:
  - Service Level A/B: 135 kips (Ram Push)
- Unloading (grapple) loads are defined as:
  - Service Level A/B: 80 kips (Grapple Pull)
  - Service Level D: 135 kips (Grapple Pull)

To unload the EOS-HSM, the DSC is pulled using grapple hooks which engage the Grapple Ring.

For Grapple push simulation, the cask is modelled by copying outer surface nodes of DSC creating a new pattern of nodes representing cask inner surface. These new nodes are restrained in all degrees of freedom and connected to the original nodes belonging to the DSC Shell through the CONTA178 contact elements. Furthermore, gaps are set to zero at the first rail placing the DSC and the first rail in initial contact. Real constants of contact elements at the second rail are set to gap calculated based on nodal coordinates of the contact element node at the DSC side and the rail side.

Symmetric boundary conditions are applied at the plane of symmetry of the model. Outer top nodes of the DSC shell are constrained in axial direction and a node of the ITCP is constrained in vertical direction to aid in convergence. The insertion force is modeled through a uniform pressure applied within the inner diameter of the grapple support. Two load cases were considered for evaluation: one with a push load of 135 kips, and a second with an internal pressure of 30 psig and a push load of 135 kips. Table 2-5 lists the load conditions.

For grapple pull, symmetric boundary conditions are applied at the plane of symmetry of the model. Outer top nodes of the DSC shell are constrained in the axial direction and a node of the ITCP is constrained in the vertical direction to aid in convergence. The extraction force is modeled through nodal forces applied on selected nodes within the footprint of the grapple hook. Four load cases were considered for evaluation: one with pull load of 80 kips, a second with an internal pressure of 30 psig and a pull load of 80 kips, a third with a 135 kips pull load, and a fourth with a pull load of 135 kips and internal pressure of 30 psig. Refer to Table 2-5 for load condition cases.

3.9.1.2.4.5 Transfer/Handling Load

The same model described in Section 3.9.1.2.4.1 for dead weight in the EOS-TC is used and updated to reflect the effect of the vertical 1g load, transverse 1g load, axial 1g load and internal pressure of 30 psig.

Two runs were performed for this load:

1. Deadweight +1g vertical + 1g transverse + 1g axial with the weight of DSC internals modelled by equivalent pressure application on TSP with addition of internal pressure of 30 psig.

2. Deadweight +1g vertical + 1g transverse + 1g axial with the weight of DSC internals modelled by equivalent pressure application on IBCP with addition of internal pressure of 30 psig.

3.9.1.2.4.6 Seismic Load during Storage

The seismic criteria consist of the Enhanced Regulatory Guide 1.60 Response Spectra [3.9.1-8], anchored at 0.50g horizontal and 0.333g vertical peak ground accelerations.

The spectral seismic accelerations applicable to the evaluation of DSC corresponding to the 3% damped amplified spectrum (Section 2.3.4 of Chapter 2) and considering the frequency content of the loaded module in each orthogonal direction are 1.229g, 0.694g and 0.333g in the transverse, axial and vertical direction, respectively (See Table 3.9.4-3). However, the DSC shell assembly is conservatively evaluated for seismic acceleration of 3g in each orthogonal direction.

The same model described in Section 3.9.1.2.4.1.3 is used and updated to reflect effect of the vertical 3g load, transverse 3g load, axial 3g load and internal pressure of 30 psig.

Two runs are performed for this load:

1. 3g vertical + 3g transverse + 3g axial with the weight of DSC internals modelled by equivalent pressure application on TSP with addition of internal pressure of 30 psig.

2. 3g vertical + 3g transverse + 3g axial with the weight of DSC internals modelled by equivalent pressure application on IBS with addition of internal pressure of 30 psig.

The dead weight with 3g vertical and 3g transverse effect is modelled by multiplying the pressure projected at the EOS-HSM Support Rail through the DSC Shell by factor of 5 $\left[\sqrt{(3g+1g)^2+(3g)^2}\right]$.

DSC support within the EOS-HSM is provided by two, 3-inch wide rails at ± 30° from the bottom centerline. Seismic axial forces toward the EOS-HSM door are resisted by the DSC axial restraint. The DSC axial restraint is a 2-inch by 4-inch solid steel bar located on the vertical centerline, at the edge of the DSC shell below the center of the DSC. The DSC axial restraint bears against the edge of the DSC Shell and OBCP. The nodes of DSC shell and OBCP, which bears against the area of the DSC axial restraint, are restrained in the axial direction.

The DSC shell and the OBCP experiences compressive bearing stress in the close vicinity of the DSC axial restraint. The bearing stresses experienced by the DSC shell and OBCP do not need to be evaluated for Service Level D loads. For other service levels (excluding Level D loads), the bearing stress due to seismic load, 14.79 ksi, is less than allowable bearing stress 19.4ksi (Level A, 500 °F).

Seismic axial forces away from the EOS-HSM door are resisted by the DSC stop plates located at the end of the DSC support structure. Since the OTCP is recessed from the edge of the DSC shell, the stop plates bear against the bottom edge of the DSC shell only. The nodes of the top end of DSC shell that will come into contact with the DSC stop plate are restrained in axial direction. The bearing stress for loads excluding Level D loads is 12.77 ksi due to seismic load, which is less than allowable bearing stress 19.4ksi (Level A, 500 °F).

3.9.1.2.4.7 Cask Drop

The maximum deceleration of 53.4g and 16.0g is calculated for side and corner drop, respectively, in Appendix 3.9.3. Conservatively, 75g side and end drop accelerations are applied statically. Drops are only postulated for the DSC when positioned inside the TC135. The following accident onsite transfer drops scenarios are addressed:

- 65-in. side drop of the TC onto a concrete pad resting on a generic soil profile.

- An oblique corner drop from a height of 65 in. at an angle of 30° to the horizontal, onto the top or bottom corner of the TC (two cases) using a bounding deceleration based on a 65-inch drop.

Because the top end drop and bottom end drop are not credible events under 10 CFR Part 72, these drop analyses are not required. However, consideration of end drops and the 65-inch side drop is performed to conservatively envelop the effects of a corner drop.

In summary, three drop conditions are considered in the ANSYS analyses:

1. 75g bottom end drop
2. 75g top end drop
3. 75g side drop

3.9.1.2.4.7.1 Vertical Drop (End Drop)

For the bottom end drop, symmetric boundary conditions are applied at the plane of symmetry of the model. The interface between the bottom surface of the DSC shell and the OBCP (excluding the OBCP surface, which falls inside the grapple ring support) with the TC135 is modeled with CONTA178 node to node contact elements. The nodes of the TC135 are constrained in vertical direction representing TC as a rigid surface. The payload is conservatively taken as total load of 105 kips multiplied by 75. The inertia load of the basket assembly and fuel is applied as uniform pressure acting on the IBCP. Elastic material model is used in the analysis. In addition to pressure representing the payload inertia load, an additional case with an internal pressure of 30 psig is analyzed.

For the bottom end drop, the couplings (CP) representing welds between the lug plate to DSC shell and the weld between the OBCP to DSC shell are replaced with spring elements (COMBIN14).

For the top end drop, symmetric boundary conditions are applied at the plane of symmetry of the model. The interface between the top surface of the DSC shell and the OTCP with the TC135 is modeled with CONTA178 node to node contact elements. The nodes of the TC135 are constrained in all directions representing TC as a rigid surface. The payload is conservatively taken as total load of 105 kips multiplied by 75g. The inertia load of the basket assembly and fuel is applied as uniform pressure acting on the bottom side of the TSP. Elastic material model is used in the analysis. In addition to pressure representing the payload inertia load, an additional case with an internal pressure of 30 psig is analyzed.

Four load cases are analyzed for end drop:

- Bottom end drop without internal pressure

- Bottom end drop with internal pressure
- Top end drop without internal pressure
- Top end drop with Internal pressure

The maximum stresses from these load cases are reported in the stress results table.

3.9.1.2.4.7.2 Side Drop

3.9.1.2.4.7.2.1 Side Drop on Cask Rails

Two load cases are analyzed for side drop on cask rails, with and without internal pressure. Also the weight of the basket and fuel assemblies is applied as uniform pressure on the DSC inner surface from 0 to 45 degrees.

3.9.1.2.4.7.2.2 Side Drop Away From Cask Rails

Gaps between the DSC shell and the cask inner surface are set to gaps calculated by an ANSYS macro file, based on nodal coordinates of the contact element node at the DSC side and the cask side. So, at the point where the DSC drops on the rigid cask, the gap is zero, and circumferentially away from the drop point, the radial gap increases incrementally. The small radial gap between the shield plugs and the DSC shell is set to zero, because this gap is closed during a side drop event.

In addition to pressure representing the payload inertia load, an additional case with an internal pressure of 30 psig is analyzed.

Two load cases are analyzed for Side drop away cask rail:

- Side drop away cask rail without internal pressure
- Side drop away from cask rail with internal pressure

The maximum stress out of the four load cases, which include side drop on TC rails, as well as side drop away from the TC rails, is reported in stress result table.

3.9.1.2.4.8 Thermal Loads

Per Chapter 4, the thermal storage load cases have lower temperature gradients in the DSC shell compared to thermal transfer load cases. Therefore, only bounding off-normal thermal transfer load cases have been selected for thermal stress analysis of EOS-37PTH DSC.

For thermal stress analysis, temperature profiles and maximum component temperatures are based on the thermal analyses of EOS-37PTH DSC in TC125 for transfer conditions, which is discussed in Chapter 4. Only the off-normal load cases with higher temperature gradients in DSC shell are taken for thermal stress analysis.

Since the TC125 is shorter than TC135, there is a higher temperature distribution in TC125. Therefore, the thermal analysis of EOS-37PTH in TC125 bounds the thermal analysis of EOS-37PTH in TC135.

The thermal conditions have been evaluated separately to minimize the number of analyses to be performed. For all DSC components, the thermal stresses have been combined by adding the maximum stress intensities of components from thermal load runs to the primary membrane plus bending stresses of components from mechanical load runs.

Thermal stresses are classified as secondary stresses per the ASME Code, [3.9.1-3]. These secondary stresses are a result of dissimilar material properties, primarily differential thermal growth of a structure due to material, thermal expansion coefficient differences between different materials used for construction of the structure, or differential temperature distribution throughout the structure, or a combination of both.

Nodal temperature from thermal analyses is transferred to the structural model described in Section 3.9.1.2.3.

The structural model is solved and stresses of thermal load of each load step are post-processed and the largest stresses for all the transfer cases are selected. Only the largest selected stresses are used for further stress evaluation and stress combination.

3.9.1.2.5 Load Combinations

The bounding load combinations, along with the applicable ASME service level, are listed in Table 2-5 for the shell assembly. Stresses generated by applied loads described in Section 3.9.1.2.4 are combined in a manner that bounds all load conditions under consideration.

3.9.1.3 DSC Shell Buckling Evaluation

An FE plastic analysis with large displacement option is performed to monitor occurrence of canister shell buckling under the specified loads.

The bottom end drop envelopes the top end drop because the top end structure is heavier than the bottom end structure, which will impose a larger load on the DSC Shell. A drop on the bottom end is therefore chosen for buckling analysis.

The same model as used for bottom end drop in Section 3.9.1.2.4.7.1 is used for buckling analysis.

The inertia load of the basket assembly and fuel is applied as uniform pressure acting on the IBCP. Elastic-plastic bilinear kinematic hardening material model is used at a uniform temperature of 500 °F with a plastic tangent modulus conservatively taken at 1% of the elastic modulus for buckling. Conservatively, no internal pressure that could have a stabilizing effect is applied. Large deformation effect NLGEOM is enabled in the ANSYS model.

Uniform pressure at the IBCP that represents the payload is multiplied by acceleration as g-factor that is incrementally increased by 5g with every load step. 50 load steps are defined, which correspond to total load of 250g. The last converged load step represents the stability limit load.

Load step # 27 corresponding to 130g load is the last saved converged solution. Two thirds of the maximum compressive load of 130g is equal to 87g limit load per F-1331.5 of Appendix F, [3.9.1-3], which is higher than required load of 75g. It is therefore concluded that buckling of the DSC will not occur during a hypothetical accident end drop.

3.9.1.4 DSC Fatigue Analysis

Fatigue effects on the EOS-37PTH DSC is addressed using NB-3222.4 criteria of [3.9.1-3]. Fatigue effects need not be specifically evaluated, provided the criteria contained in NB-3222.4(d) are met. A summary of the six criteria and their application to the DSC is presented below:

A. The first criterion states that the DSC is adequate for fatigue effects, provided that the total number of atmospheric-to-operating pressure cycles during normal operation (including startup and shutdown) does not exceed the number of cycles on the applicable fatigue curve corresponding to a S_a value of three times the S_m value of the material at operating temperatures. This condition is satisfied for the DSC since the pressure is not cycled during its design life. The pressure established at the time that the DSC is sealed following fuel loading and DSC closure operations is maintained during normal storage in the EOS-HSM.

B. The second criterion states that DSC is adequate for fatigue effects, provided that the specified full range of pressure fluctuations during normal operation does not exceed the quantity (1/3) x design pressure x (S_a/S_m), where S_a is the value obtained from the applicable fatigue curve for the total specified number of significant pressure fluctuations, and S_m is the allowable stress intensity for the material at operating temperatures.

Significant pressure fluctuations are those for which the total excursion exceeds (1/3) x design pressure x (S/S_m), where S equals the value of S_a for 10^6 cycles. Using a design pressure of 20.0 psig, an S_m value of 17,500 psi, and an S value of 28,200 psi, the total range for a significant pressure fluctuation is 10.7 psig. This pressure fluctuation is not expected to occur during normal storage as a result of seasonal ambient temperature changes.

Ambient temperature cycles significant enough to cause a measurable pressure fluctuation are assumed to occur five times per year for 80 years. The number of fluctuations with this pressure range is expected to be 400 for the DSC. The value of S_a associated with this number of cycles is 170 ksi. Therefore, the value of (1/3) x design pressure x (S_a/S_m) is equal to 64.76 psig. Clearly, this value will not be exceeded during the pressure fluctuation of the DSC. Therefore, the second criterion is satisfied for the DSC.

C. The third criterion states that the DSC is adequate for fatigue effects, provided that the temperature differences between any two adjacent points on the DSC during normal operation do not exceed $S_a/2E\alpha$, where S_a is the value obtained from the applicable fatigue curve for the specified number of startup-shutdown cycles, α is the instantaneous coefficient of thermal expansion at the mean value of the temperatures at the two points, and E is the modulus of elasticity at the mean value of the temperatures at the two points.

   For an operational cycle of the DSC, thermal gradients occur during fuel loading, DSC closure, transport to the EOS-HSM, and transfer of the DSC to the EOS-HSM. This half-cycle is approximately reversed for DSC unloading operations. However, this normal operational cycle occurs only once in the design service life of a DSC. Since there is only one startup-shutdown cycle associated with the DSC, the value of S_a is very large (>800 ksi). Therefore, the value of $S_m/2E\alpha$ is very large (>1500°F). This is far greater than the temperature difference between any two adjacent points on the dry shielded canister. Therefore, the third criterion is satisfied for the DSC.

D. The fourth criterion states that the DSC is adequate for fatigue effects, provided that the temperature difference between any two adjacent points on the DSC does not change during normal operation by more than the quantity $S_a/2E\alpha$, where S_a is the value obtained from the applicable fatigue curve for the total specified number of significant temperature difference fluctuations.

   A temperature difference fluctuation is considered to be significant if its total algebraic range exceeds the quantity S/2Eα where S is value of S_a (28,200 psi) obtained from the applicable fatigue curve for 10^6 cycles if the number of cycles is 10^6 or less.

Small fluctuations in the DSC thermal gradients during normal storage in the EOS-HSM occur as a result of seasonal ambient temperature changes. Ambient temperature cycles significant enough to cause a measurable thermal gradient fluctuation are assumed to occur five times per year for 80 years. The temperature gradient fluctuation is 250 cycles. Since this is less than 10^6 cycles, the value of $S/2E\alpha$ at 10^6 cycles is 112.7 °F.

The most significant fluctuation in normal operating temperature occurs during a change in ambient temperature from -20° F to 100 °F. A review of thermal evaluation of EOS-HSM loaded with EOS-37PTH DSC storage load cases in Chapter 4 concluded that the temperature difference between adjacent points in the DSC does not exceed the quantity 112.7 °F, therefore the fourth condition is satisfied for the DSC.

E. The fifth criterion states that for components fabricated from materials of differing moduli of elasticity or coefficients of thermal expansion, the total algebraic range of temperature fluctuation experienced by the component during normal operation must not exceed the magnitude $S_a/2(E_1\alpha_1 - E_2\alpha_2)$, where S_a is the value obtained from the applicable fatigue curve for the total specified number of significant temperature fluctuations, E_1 and E_2 are the moduli of elasticity, and α_1 and α_2 are the values of the instantaneous coefficients of thermal expansion at the mean temperature value involved for the two materials of construction.

A temperature fluctuation is considered to be significant if its total excursion exceeds the quantity $S/2(E_1\alpha_1 - E_2\alpha_2)$, where S is the value of S_a obtained from the applicable fatigue curve for 10^6 cycles. If the two materials have different applicable design fatigue curves, the lower value of S_a has to be used. Since the structural material used to construct the DSC shell is 240 Type 304 and shield plug is A-36, therefore taking the values of $E_1 = 25.9 \times 10^6$ psi, $E_2 = 27.3 \times 10^6$, $\alpha_1 = 10.5 \times 10^{-6}$ and $\alpha_2 = 8.0 \times 10^{-6}$ (Section II, Part D, [3.9.1-2]), the quantity $S/2(E_1\alpha_1 - E_2\alpha_2) = 268.6$°F.

Since the DSC experiences temperature fluctuation from -20 °F to 100 °F, the range of temperature fluctuation is 120°F which is less than 268.6 °F. Therefore, the fifth criterion is satisfied for the DSC.

F. The sixth criterion states that the DSC is adequate for fatigue effects, provided that the specified full range of mechanical loads does not result in a stress range that exceeds the S_a value obtained from the applicable fatigue curve for the total specified number of significant load fluctuations. If the total specified number of significant load fluctuations exceeds 10^6, the S_a value at $N = 10^6$ can be used.

A load fluctuation is considered to be significant if the total excursion of stresses exceed the value of S_a obtained from the applicable fatigue curve for 10^6 cycles. The only mechanical loads that affect the DSC are those associated with handling loads and a seismic event. One handling load cycle and a major seismic event are postulated during the design life of the DSC. The DSC stresses resulting from these mechanical load fluctuations are small since the structural capacity of the DSC is designed for extreme accident loads such as a postulated cask drop.

The number of significant cycles associated with mechanical load fluctuations is conservatively assumed to be 1,000. The value of S_a associated with this number of cycles is 120 ksi. Since the maximum stress range intensity permitted by the code is 3.0 S_m, or 52.5 ksi for SA-240, Type 304 stainless steel at 500 °F, this sixth condition is satisfied for the DSC.

The evaluation presented in the preceding paragraphs demonstrates that the six criteria contained in NB-3222.4(d) are satisfied for all components of the EOS-37PTH DSC.

3.9.1.5 DSC Weld Flaw Size Evaluation

EOS-37PTH DSC is considered as the bounding DSC for weld flaw evaluation because the weight of EOS-37PTH DSC (long) is greater than the weight of EOS-89BTH DSC.

3.9.1.5.1 Methodology

It is stipulated that the critical flaw configuration is a circumferential weld flaw exposed to the tensile component radial stress. The determination of the allowable surface and sub-surface flaw depth is accomplished by means of the methodology outlined below.

- Loads and load combinations that can result in noticeable tensile radial component stresses at the OTCP weld are identified.
- Membrane radial stresses occurring at the weld between the OTCP and the DSC Shell are evaluated.
- Limiting membrane radial stresses in the OTCP weld for all load combinations, for Service Levels A, B, and D are determined and limiting stresses are multiplied by safety factors SF_m for the corresponding service levels.
- Since OTCP weld is gas tungsten arc welding (GTAW) (non-flux weld), according to ASME Code Sec XI, Division 1, Figure C-4210-1 [3.9.1-4], maximum allowable flaw depth is estimated using limit load criteria.

The allowable membrane stress, S_t, in the flawed section for each service level is determined from Article C-5322, Appendix C [3.9.1-4] where the relation between the applied membrane stress and flaw depth at incipient stress is given.

3.9.1.5.2 Flaw Size Calculation

For 3D, half-symmetric model, as described in Section 3.9.1.2.3, the OTCP weld is modeled by coupling the coincident nodes at the DSC shell and the OTCP. The nodal tensile forces at the weld location are post-processed for each load case.

Radial stresses for controlling load combination are calculated by adding individual load cases. Bounding radial tensile stresses in OTCP weld for all load combinations for Service Level A, B, and D are assessed. The allowable flaw depths, calculated by means of the methodology described in previous Section and are shown in Table 3.9.1-13.

Based on the evaluation, requirements for welding and weld inspections should be based on limiting the weld critical depth for surface and subsurface flaws to the following values:

- Surface Crack: 0.38 inch.
- Subsurface Crack: 0.38 inch.

3.9.1.6 Conclusions

Table 3.9.1-7 through Table 3.9.1-12 summarize the stress intensities in different components of DSC shell assembly and compared with ASME code stress intensity allowables.

Based on the results of these analyses, the design of the DSC shell assembly is structurally adequate under all normal (Service Level A), off-normal (Service Level B), hypothetical accident (Service Level D) conditions during storage and during transfer.

3.9.1.7 References

3.9.1-1 Title 10, Code of Federal Regulations, Part 72, “Licensing Requirements for the Independent Storage of Spent Nuclear Fuel, High-Level Radioactive Waste, and Reactor-Related Greater than Class C Waste.”

3.9.1-2 American Society of Mechanical Engineers, ASME Boiler and Pressure Vessel Code, Section II, Part D, 2010 Edition through 2011 Addenda.

3.9.1-3 American Society of Mechanical Engineers, ASME Boiler and Pressure Vessel Code, Section III, 2010 Edition through 2011 Addenda.

3.9.1-4 American Society of Mechanical Engineers, ASME Boiler and Pressure Vessel Code, Section XI, Division 1, Appendix C, 2010 Edition Addenda through 2011 Addenda.

3.9.1-5 ANSI N14.5, "Leakage Tests on Packages for Shipment of Radioactive Materials," 1997.

3.9.1-6 ANSI N14.6 – 1993, "American National Standard for Radioactive Materials – Special Lifting Devices for Shipping Containers Weighing 10000 pounds (4500 kg) or More," American National Standards Institute, Inc., New York.

3.9.1-7 NUREG-1536, "Standard Review Plan for Spent Fuel Dry Cask Storage Systems at a General License Facility," Revision 1, U.S. Nuclear Regulatory Commission, July 2010.

3.9.1-8 U.S. Nuclear Regulatory Commission, Regulatory Guide 1.60, "Design Response Spectra for Seismic Design of Nuclear Power Plants," Revision 1, 1973.

3.9.1-9 ANSYS Computer Code and User's Manual, Release 14.0.

Table 3.9.1-1
EOS37PTH DSC Major Dimensions

Component	Dimensions
Outer Diameter of DSC Shell	75.50 inches
DSC Shell Thickness	0.5 inch
DSC Length	219 inches(1)
OTCP Thickness	2 inches
ITCP Thickness	2 inches
TSP Thickness	6 inches
OBCP Thickness	2 inches
IBCP Thickness	2 inches
IBS	4 inches

(1) Indicated length is for longest EOS-37PTH DSC

Table 3.9.1-2
Material used in the Stress Evaluation of EOS-37PTH DSC Components

DSC Shell	ASME SA-240 TYPE 304
OTCP	ASTM A240 TYPE 304
ITCP	ASTM A240 TYPE 304
TSP	ASTM A36
OBCP	ASME SA-240 TYPE 304
IBCP	ASME SA-240 TYPE 304
IBS	ASTM A36
Grapple Ring Support	ASME SA-240 TYPE 304
Grapple Ring	ASME SA 240 TYPE 304
Lifting Lug plate	ASME SA 240 TYPE 304
Lifting Lug	ASME SA 240 TYPE 304

Table 3.9.1-3
Material Non-linearity for Side drop accident condition

Material Property	SA-240 Type 304 at 500 °F	SA-36 at 500 °F
Elastic Modulus (psi)	25.9×10^6	27.3×10^6
Yield Strength (psi)	19,400	29,300
Tangent Modulus, E_t (psi)	5% of $E = 1.295 \times 10^6$	5% of $E = 1.365 \times 10^6$

Table 3.9.1-4
Allowable Weld Stresses for Pressure Boundary Partial Penetration Welds, Material Type 304

Service Level	Stress Region / Category	Stress Criteria	Allowable Stress Value at 500 °F [ksi]
Level A / Level B	Primary Membrane + Bending Stress, Pm + Pb	Pm + Pb= 0.8 [1.5 Sm]	21.0
	Primary + Secondary Stress, P+Q	Pm + Pb + Q = 0.8 [3.0 Sm]	42.0
Level C	Primary Membrane Stress, Pm or Primary Local Stress, PL	0.8 [Max (1.8Sm, 1.5Sy)]	25.2
Level D (Elastic)	Primary/Local Membrane + Bending Stress, Pm/PL + Pb	0.8 [Min(3.6 Sm, Su)]	50.4
Level D (Elastic / Plastic)	Primary Stress Intensity, P	0.8 [0.9 Su]	45.7

Table 3.9.1-5
SA-240/SA-479 304 & SA-182 F304 -Stress Allowables

Temp (°F)	S_m (ksi)	S_y (ksi)	S_u (ksi)	Level A/B			Level D (Elastic)		Level D (Plastic)	
				P_m	$P_m + P_b$	$P_m + P_b + Q$	P_m	$P_m + P_b$	P_m	$P_m + P_b$
70	20	30	75	20.0	30.0	60.0	48.0	72.0	52.5	67.5
200	20	25	71	20.0	30.0	60.0	48.0	71.0	49.7	63.9
300	20	22.4	66.2	20.0	30.0	60.0	46.3	66.2	46.3	59.6
400	18.6	20.7	64	18.6	27.9	55.8	44.6	64.0	44.8	57.6
500	17.5	19.4	63.4	17.5	26.3	52.5	42.0	63.0	44.4	57.1
600	16.6	18.4	63.4	16.6	24.9	49.8	39.8	59.8	44.4	57.1
700	15.8	17.6	63.4	15.8	23.7	47.4	37.9	56.9	44.4	57.1

Table 3.9.1-6
Allowable Base Metal Stresses for Non Pressure Boundary Partial Penetration & Fillet Welds Type 304 Base Metal

Temp. (°F)	S_y (ksi)	Level A $F_W = .40S_y$	Level B $F_W = .53S_y$	Level C $F_W = .60S_y$	Level D $F_W = .80S_y$
100	30	12	15.9	18	24
200	25	10	13.3	15	20
300	22.4	8.96	11.9	13.4	17.9
400	20.7	8.28	11	12.4	16.6
500	19.4	7.76	10.3	11.6	15.5
600	18.4	7.36	9.75	11	14.7
650	18	7.2	9.54	10.8	14.4
700	17.6	7.04	9.33	10.6	14.1

Table 3.9.1-7
DSC Shell Stress Results – Load Combinations
2 Pages

Load Comb No.	Stress Category	Loads	Stress intensity (ksi)	Allowable Stress (ksi)	Stress Ratio
1	P_m	DW_v+ max($PI_{(30)}$,BD,VD)	5.46	17.50	0.31
	P_m+P_b	DW_v+ max($PI_{(30)}$,BD,VD)	7.08	26.25	0.27
	P_m+P_b+Q	DW_v+ max($PI_{(30)}$,BD,VD)+THTS6	37.21	52.50	0.71
2	P_m	DW_h+ 1g axial + 1g transverse + 1g Vertical + $PI_{(30)}$	5.12	17.50	0.29
	P_m+P_b	DW_h+ 1g axial + 1g transverse + 1g Vertical + $PI_{(30)}$	5.30	26.25	0.20
	P_m+P_b+Q	DW_h+ 1g axial + 1g transverse + 1g Vertical + $PI_{(30)}$ + $THT_{(117°F)}$	35.43	52.50	0.67
3	P_m	DW_h+ 1g axial + 1g transverse + 1g Vertical + $PI_{(30)}$	5.12	17.50	0.29
	P_m+P_b	DW_h+ 1g axial + 1g transverse + 1g Vertical + $PI_{(30)}$	5.30	26.25	0.20
	P_m+P_b+Q	DW_h+ 1g axial + 1g transverse + 1g Vertical + $PI_{(30)}$ + THTS6	35.43	52.50	0.67
4	P_m	DW_h+ 135kips + $PI_{(30)}$	6.85	17.50	0.39
	P_m+P_b	DW_h+ 135kips + $PI_{(30)}$	13.27	26.25	0.51
	P_m+P_b+Q	DW_h+ 135kips + THTS6	43.40	52.50	0.83
5	P_m	DW_h+ 80 kips + $PI_{(30)}$	5.41	17.50	0.31
	P_m+P_b	DW_h+ 80 kips + $PI_{(30)}$	7.21	26.25	0.27
	P_m+P_b+Q	DW_h+ 80 kips + THTS6	37.34	52.50	0.71
6	P_m	DW_h+ 135 kips + $PI_{(30)}$	8.50	42.00	0.20
	P_m+P_b	DW_h+ 135 kips + $PI_{(30)}$	11.11	63.00	0.18
7A	P_m	DW_h+ max.(SD_AWAY_EP, SD_RAIL_EP) + $PI_{(30)}$	30.34	44.38	0.68
	P_m+P_b	DW_h+ max.(SD_AWAY_EP, SD_RAIL_EP)+ $PI_{(30)}$	39.94	57.06	0.70
7B	P_m	DW_v+ max.(TOP_ED, BOT_ED)+ $PI_{(30)}$	23.09	42.00	0.55
	P_m+P_b	DW_v+ max.(TOP_ED, BOT_ED)+ $PI_{(30)}$	45.55	63.00	0.72

Table 3.9.1-7
DSC Shell Stress Results – Load Combinations
2 Pages

Load Comb No.	Stress Category	Loads	Stress intensity (ksi)	Allowable Stress (ksi)	Stress Ratio
8	P_m	DW_h+ $PI_{(130)}$	13.08	42.00	0.31
	P_m+P_b	DW_h+ $PI_{(130)}$	19.37	63.00	0.31
9	P_m	DW_h+ $PI_{(30)}$	6.84	17.50	0.39
	P_m+P_b	DW_h+ $PI_{(30)}$	8.79	26.25	0.33
	P_m+P_b+Q	DW_h+ $PI_{(30)}^{+}$ THTS6	38.92	52.50	0.74
10	P_m	DW_h+ max.(HS_TOP, HS_BOT)+$PI_{(30)}$	38.46	42.00	0.92
	P_m+P_b	DW_h+ max.(HS_TOP, HS_BOT)+$PI_{(30)}$	46.10	63.00	0.73
11	P_m	max. ($PI_{(23)}$+155 kips ,$PE_{(14.7)}$+155 kips)	5.72	45.7	0.13
	P_m+P_b	max. ($PI_{(23)}$+155 kips,$PE_{(14.7)}$+155 kips)	14.25	45.7	0.31

Table 3.9.1-8
OTCP Stress Results – Load Combinations
2 Pages

Load Comb No.	Stress Category	Loads	Stress intensity (ksi)	Allowable Stress (ksi)	Stress Ratio
1	P_m	DW_v+ max($PI_{(30)}$,BD,VD)	3.26	17.50	0.19
	P_m+P_b	DW_v+ max($PI_{(30)}$,BD,VD)	5.96	26.25	0.23
	P_m+P_b+Q	DW_v+ max($PI_{(30)}$,BD,VD)+ THTS6	12.59	52.50	0.24
2	P_m	DW_h+ 1g axial + 1g transverse + 1g Vertical + $PI_{(30)}$	3.04	17.50	0.17
	P_m+P_b	DW_h+ 1g axial + 1g transverse + 1g Vertical + $PI_{(30)}$	5.54	26.25	0.21
	P_m+P_b+Q	DW_h+ 1g axial + 1g transverse + 1g Vertical + $PI_{(30)}$ + $THT_{(117°F)}$	12.17	52.50	0.23
3	P_m	DW_h+ 1g axial + 1g transverse + 1g Vertical + $PI_{(30)}$	3.04	17.50	0.17
	P_m+P_b	DW_h+ 1g axial + 1g transverse + 1g Vertical + $PI_{(30)}$	5.54	26.25	0.21
	P_m+P_b+Q	DW_h+ 1g axial + 1g transverse + 1g Vertical + $PI_{(30)}$ + THTS6	12.17	52.50	0.23
4	P_m	DW_h+ 135kips + $PI_{(30)}$	3.43	17.50	0.20
	P_m+P_b	DW_h+ 135kips + $PI_{(30)}$	6.25	26.25	0.24
	P_m+P_b+Q	DW_h+ 135kips + THTS6	12.88	52.50	0.25
5	P_m	DW_h+ 80 kips + $PI_{(30)}$	3.44	17.50	0.20
	P_m+P_b	DW_h+ 80 kips + $PI_{(30)}$	6.28	26.25	0.24
	P_m+P_b+Q	DW_h+ 80 kips + THTS6	12.91	52.50	0.25
6	P_m	DW_h+ 135 kips + $PI_{(30)}$	3.44	42.00	0.08
	P_m+P_b	DW_h+ 135 kips + $PI_{(30)}$	6.29	63.00	0.10
7A	P_m	DW_h+ max.(SD_AWAY, SD_RAIL_EP,SD_TOP_RAIL_EP)+ $PI_{(30)}$	14.64	44.38	0.33
	P_m+P_b	DW_h+ max.(SD_AWAY_EP, SD_RAIL_EP)+ $PI_{(30)}$	25.78	57.06	0.45
7B	P_m	DW_v+ max.(TOP_ED, BOT_ED)+ $PI_{(30)}$	9.51	42.00	0.23

Table 3.9.1-8
OTCP Stress Results – Load Combinations
2 Pages

Load Comb No.	Stress Category	Loads	Stress intensity (ksi)	Allowable Stress (ksi)	Stress Ratio
	P_m+P_b	DW_v+ max.(TOP_ED, BOT_ED)+ $PI_{(30)}$	17.26	63.00	0.27
8	P_m	DW_h+ $PI_{(130)}$	14.19	42.00	0.34
	P_m+P_b	DW_h+ $PI_{(130)}$	25.87	63.00	0.41
9	P_m	DW_h+ $PI_{(30)}$	3.74	17.50	0.21
	P_m+P_b	DW_h+ $PI_{(30)}$	6.84	26.25	0.26
	P_m+P_b+Q	DW_h+ $PI_{(30)}$+ THTS6	13.47	52.50	0.26
10	P_m	DW_h+ max.(HS_TOP, HS_BOT)+$PI_{(30)}$	15.94	42.00	0.38
	P_m+P_b	DW_h+ max.(HS_TOP, HS_BOT)+$PI_{(30)}$	28.17	63.00	0.45
11	P_m	max. ($PI_{(23)}$+155 kips ,$PE_{(14.7)}$+155 kips)	NA		
	P_m+P_b	max. ($PI_{(23)}$+155 kips,$PE_{(14.7)}$+155 kips)	NA		

Table 3.9.1-9
ITCP Stress Results – Load Combinations
2 Pages

Load Comb. No.	Stress Category	Loads	Stress intensity (ksi)	Allowable Stress (ksi)	Stress Ratio
1	P_m	DW_v+ max($PI_{(30)}$,BD,VD)	4.78	17.50	0.27
	P_m+P_b	DW_v+ max($PI_{(30)}$,BD,VD)	8.78	26.25	0.33
	P_m+P_b+Q	DW_v+ max($PI_{(30)}$,BD,VD)+ THTS6	35.66	52.50	0.68
2	P_m	DW_h+ 1g axial + 1g transverse + 1g Vertical + $PI_{(30)}$	3.07	17.50	0.18
	P_m+P_b	DW_h+ 1g axial + 1g transverse + 1g Vertical + $PI_{(30)}$	5.61	26.25	0.21
	P_m+P_b+Q	DW_h+ 1g axial + 1g transverse + 1g Vertical + $PI_{(30)}$ + $THT_{(117°F)}$	32.50	52.50	0.62
3	P_m	DW_h+ 1g axial + 1g transverse + 1g Vertical + $PI_{(30)}$	3.07	17.50	0.18
	P_m+P_b	DW_h+ 1g axial + 1g transverse + 1g Vertical + $PI_{(30)}$	5.61	26.25	0.21
	P_m+P_b+Q	DW_h+ 1g axial + 1g transverse + 1g Vertical + $PI_{(30)}$ + THTS6	32.50	52.50	0.62
4	P_m	DW_h+ 135kips + $PI_{(30)}$	3.47	17.50	0.20
	P_m+P_b	DW_h+ 135kips + $PI_{(30)}$	6.38	26.25	0.24
	P_m+P_b+Q	DW_h+ 135kips + THTS6	33.26	52.50	0.63
5	P_m	DW_h+ 80 kips + $PI_{(30)}$	3.45	17.50	0.20
	P_m+P_b	DW_h+ 80 kips + $PI_{(30)}$	6.32	26.25	0.24
	P_m+P_b+Q	DW_h+ 80 kips + THTS6	33.21	52.50	0.63
6	P_m	DW_h+ 135 kips + $PI_{(30)}$	3.44	42.00	0.08
	P_m+P_b	DW_h+ 135 kips + $PI_{(30)}$	6.31	63.00	0.10
7A	P_m	DW_h+ max.(SD_AWAY_EP, SD_RAIL_EP)+ $PI_{(30)}$	14.35	44.38	0.32
	P_m+P_b	DW_h+ max.(SD_AWAY_EP, SD_RAIL_EP)+ $PI_{(30)}$	22.81	57.06	0.40
7B	P_m	DW_v+ max.(TOP_ED, BOT_ED)+ $PI_{(30)}$	9.75	42.00	0.23
	P_m+P_b	DW_v+ max.(TOP_ED, BOT_ED)+ $PI_{(30)}$	17.79	63.00	0.28

Table 3.9.1-9
ITCP Stress Results – Load Combinations
2 Pages

Load Comb. No.	Stress Category	Loads	Stress intensity (ksi)	Allowable Stress (ksi)	Stress Ratio
8	P_m	DW_h+ $PI_{(130)}$	14.33	42.00	0.34
	P_m+P_b	DW_h+ $PI_{(130)}$	26.22	63.00	0.42
9	P_m	DW_h+ $PI_{(30)}$	3.87	17.50	0.22
	P_m+P_b	DW_h+ $PI_{(30)}$	7.12	26.25	0.27
	P_m+P_b+Q	DW_h+ $PI_{(30)}$+ THTS6	34.00	52.50	0.65
10	P_m	DW_h+ max.(HS_TOP, HS_BOT)+$PI_{(30)}$	15.32	42.00	0.36
	P_m+P_b	DW_h+ max.(HS_TOP, HS_BOT)+$PI_{(30)}$	23.67	63.00	0.38
11	P_m	max. ($PI_{(23)}$+155 kips ,$PE_{(14.7)}$+155 kips)	NA		
	P_m+P_b	max. ($PI_{(23)}$+155 kips,$PE_{(14.7)}$+155 kips)	NA		

Table 3.9.1-10
IBCP Stress Results – Load Combinations
2 Pages

Load Comb. No.	Stress Category	Loads	Stress intensity (ksi)	Allowable Stress (ksi)	Stress Ratio
1	P_m	DW_v+ max($PI_{(30)}$,BD,VD)	0.54	17.50	0.03
	P_m+P_b	DW_v+ max($PI_{(30)}$,BD,VD)	1.53	26.25	0.06
	P_m+P_b+Q	DW_v+ max($PI_{(30)}$,BD,VD)+THTS6	21.76	52.50	0.41
2	P_m	DW_h+ 1g axial + 1g transverse + 1g Vertical + $PI_{(30)}$	0.42	17.50	0.02
	P_m+P_b	DW_h+ 1g axial + 1g transverse + 1g Vertical + $PI_{(30)}$	1.68	26.25	0.06
	P_m+P_b+Q	DW_h+ 1g axial + 1g transverse + 1g Vertical + $PI_{(30)}$ + THTS6	21.90	52.50	0.42
3	P_m	DW_h+ 1g axial + 1g transverse + 1g Vertical + $PI_{(30)}$	0.42	17.50	0.02
	P_m+P_b	DW_h+ 1g axial + 1g transverse + 1g Vertical + $PI_{(30)}$	1.68	26.25	0.06
	P_m+P_b+Q	DW_h+ 1g axial + 1g transverse + 1g Vertical + $PI_{(30)}$ + THTS6	21.90	52.50	0.42
4	P_m	DW_h+ 135kips + $PI_{(30)}$	1.61	17.50	0.09
	P_m+P_b	DW_h+ 135kips + $PI_{(30)}$	5.36	26.25	0.20
	P_m+P_b+Q	DW_h+ 135kips + THTS6	25.58	52.50	0.49
5	P_m	DW_h+ 80 kips + $PI_{(30)}$	0.75	17.50	0.04
	P_m+P_b	DW_h+ 80 kips + $PI_{(30)}$	1.86	26.25	0.07
	P_m+P_b+Q	DW_h+ 80 kips + THTS6	22.08	52.50	0.42
6	P_m	DW_h+ 135 kips + $PI_{(30)}$	0.75	42.00	0.02
	P_m+P_b	DW_h+ 135 kips + $PI_{(30)}$	1.90	63.00	0.03
7A	P_m	DW_h+ max.(SD_AWAY_EP, SD_RAIL_EP)+ $PI_{(30)}$	21.60	44.38	0.49
	P_m+P_b	DW_h+ max.(SD_AWAY_EP, SD_RAIL_EP)+ $PI_{(30)}$	28.79	57.06	0.50
7B	P_m	DW_v+ max.(TOP_ED, BOT_ED)+ $PI_{(30)}$	6.41	42.00	0.15
	P_m+P_b	DW_v+ max.(TOP_ED, BOT_ED)+ $PI_{(30)}$	14.53	63.00	0.23

Table 3.9.1-10
IBCP Stress Results – Load Combinations
2 Pages

Load Comb. No.	Stress Category	Loads	Stress intensity (ksi)	Allowable Stress (ksi)	Stress Ratio
8	P_m	DW_h+ $PI_{(130)}$	2.27	42.00	0.05
	P_m+P_b	DW_h+ $PI_{(130)}$	6.49	63.00	0.10
9	P_m	DW_h+ $PI_{(30)}$	1.24	17.50	0.07
	P_m+P_b	DW_h+ $PI_{(30)}$	2.72	26.25	0.10
	P_m+P_b+Q	DW_h+ $PI_{(30)}$+ THTS6	22.94	52.50	0.44
10	P_m	DW_h+ max.(HS_TOP, HS_BOT)+$PI_{(30)}$	8.80	42.00	0.21
	P_m+P_b	DW_h+ max.(HS_TOP, HS_BOT)+$PI_{(30)}$	23.38	63.00	0.37
11	P_m	max. ($PI_{(23)}$+155 kips ,$PE_{(14.7)}$+155 kips)	2.45	45.7	0.05
	P_m+P_b	max. ($PI_{(23)}$+155 kips,$PE_{(14.7)}$+155 kips)	5.85	45.7	0.13

Table 3.9.1-11
ITCP-DSC shell Weld Stress Results – Load Combinations

Load Comb. No.	Stress Category	Loads	Max Stress (ksi)	Allowable Stress (ksi)	Stress Ratio
1	P_m+P_b	DW_v+ max($PI_{(30)}$,BD,VD)	5.70	21.00	0.27
	P_m+P_b+Q	DW_v+ max($PI_{(30)}$,BD,VD)+THTS6	6.71	42.00	0.16
2	P_m+P_b	DW_h+ 1g axial + 1g transverse + 1g Vertical + $PI_{(30)}$	4.26	21.00	0.20
	P_m+P_b+Q	DW_h+ 1g axial + 1g transverse + 1g Vertical + $PI_{(30)}$ + THTS6	5.27	42.00	0.13
3	P_m+P_b	DW_h+ 1g axial + 1g transverse + 1g Vertical + $PI_{(30)}$	4.26	21.00	0.20
	P_m+P_b+Q	DW_h+ 1g axial + 1g transverse + 1g Vertical + $PI_{(30)}$ + THTS6	5.27	42.00	0.13
4	P_m+P_b	DWh+ 135kips + $PI_{(30)}$	4.94	21.00	0.24
	P_m+P_b+Q	DWh+ 135kips + THTS6	5.95	42.00	0.14
5	P_m+P_b	DWh+ 80 kips + $PI_{(30)}$	3.98	21.00	0.19
	P_m+P_b+Q	DWh+ 80 kips + THTS6	5.00	42.00	0.12
6	P_m+P_b	DWh+ 135 kips + $PI_{(30)}$	3.78	50.40	0.07
7A	P_m+P_b	DWh+ max.(SD_AWAY, SD_RAIL)+ $PI_{(30)}$	12.02	50.40	0.24
7B	P_m+P_b	DW_v+ max.(TOP_ED, BOT_ED)+ $PI_{(30)}$	16.50	50.40	0.33
8	P_m+P_b	DW_h+ $PI_{(130)}$	18.66	50.40	0.37
9	P_m+P_b	DW_h+ $PI_{(30)}$	4.70	21.00	0.22
	P_m+P_b+Q	DW_h+ $PI_{(30)}$+ THTS6	5.72	42.00	0.14
10	P_m+P_b	DWh+ max.(HS_TOP, HS_BOT)+ $PI_{(30)}$	15.38	50.40	0.31
11	P_m+P_b	max. ($PI_{(23)}$+155 kips,$PE_{(14.7)}$+155 kips)	NA		

Table 3.9.1-12
OTCP-DSC shell Weld Stress Results – Load Combinations

Load Comb. No.	Stress Category	Loads	Max Stress (ksi)	Allowable Stress (ksi)	Stress Ratio
1	P_m+P_b	DW_v+ max($PI_{(30)}$,BD,VD)	1.28	21.00	0.06
	P_m+P_b+Q	DW_v+ max($PI_{(30)}$,BD,VD)+ THTS6	1.92	42.00	0.05
2	P_m+P_b	DW_h+ 1g axial + 1g transverse + 1g Vertical + $PI_{(30)}$	1.12	21.00	0.05
	P_m+P_b+Q	DW_h+ 1g axial + 1g transverse + 1g Vertical + $PI_{(30)}$ + THTS6	1.76	42.00	0.04
3	P_m+P_b	DW_h+ 1g axial + 1g transverse + 1g Vertical + $PI_{(30)}$	1.12	21.00	0.05
	P_m+P_b+Q	DW_h+ 1g axial + 1g transverse + 1g Vertical + $PI_{(30)}$ + THTS6	1.76	42.00	0.04
4	P_m+P_b	DWh+ 135kips + $PI_{(30)}$	1.35	21.00	0.06
	P_m+P_b+Q	DWh+ 135kips + THTS6	1.99	42.00	0.05
5	P_m+P_b	DWh+ 80 kips + $PI_{(30)}$	1.28	21.00	0.06
	P_m+P_b+Q	DWh+ 80 kips + THTS6	1.92	42.00	0.05
6	P_m+P_b	DWh+ 135 kips + $PI_{(30)}$	1.37	50.40	0.03
7A	P_m+P_b	DWh+ max.(SD_AWAY, SD_RAIL)+ $PI_{(30)}$	3.99	50.40	0.08
7B	P_m+P_b	DW_v+ max.(TOP_ED, BOT_ED)+ $PI_{(30)}$	3.80	50.40	0.08
8	P_m+P_b	DW_h+ $PI_{(130)}$	5.58	50.40	0.11
9	P_m+P_b	DW_h+ $PI_{(30)}$	1.37	21.00	0.07
	P_m+P_b+Q	DW_h+ $PI_{(30)}$+ THTS6	2.01	42.00	0.05
10	P_m+P_b	DWh+ max.(HS_TOP, HS_BOT)+ $PI_{(30)}$	1.32	50.40	0.03
11	P_m+P_b	max. ($PI_{(23)}$+155 kips,$PE_{(14.7)}$+155 kips)	NA		

Table 3.9.1-13
Weld Flaw Depth for Controlling Load Combination

Service Level	Controlling Load Combination	Tensile Radial Stress SX (ksi)	Safety Factor SFm	Radial Stress including Safety Factor (Sx)x (SFm)	Allowable a/t [1]	Subsurface Flaws		Surface Flaws	
						Weld Thickness 2t [2] (inch)	Flaw Depth, 2a [2] (inch)	Weld Thickness t (inch)	Flaw Depth, a (inch)
A	4	0.33	2.7	0.89	(0.98) 0.75	0.50	0.38	0.50	0.38
B	4	0.33	2.4	0.79	(0.98) 0.75	0.50	0.38	0.50	0.38
D	7A	2.82	1.3	3.67	(0.91) 0.75	0.50	0.38	0.50	0.38

Notes:

(1) The limiting value of allowable a/t is 0.75 as per C-5322 of Ref. [3.9.1-4]. Thus, if calculated a/t > 0.75, allowable a/t = 0.75. The values in the parentheses show the calculated values.

(2) For subsurface flaws ‘t’ and ‘a’ are half-width and half-crack depth, respectively.

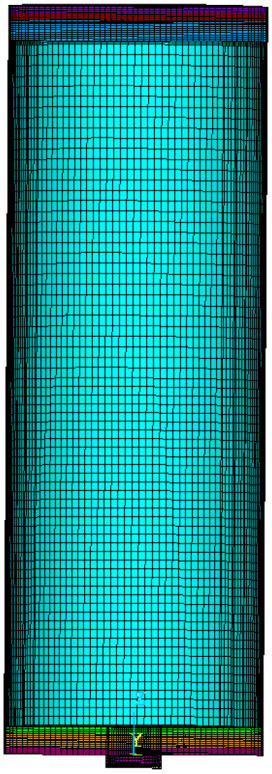

Figure 3.9.1-1
DSC FE Model

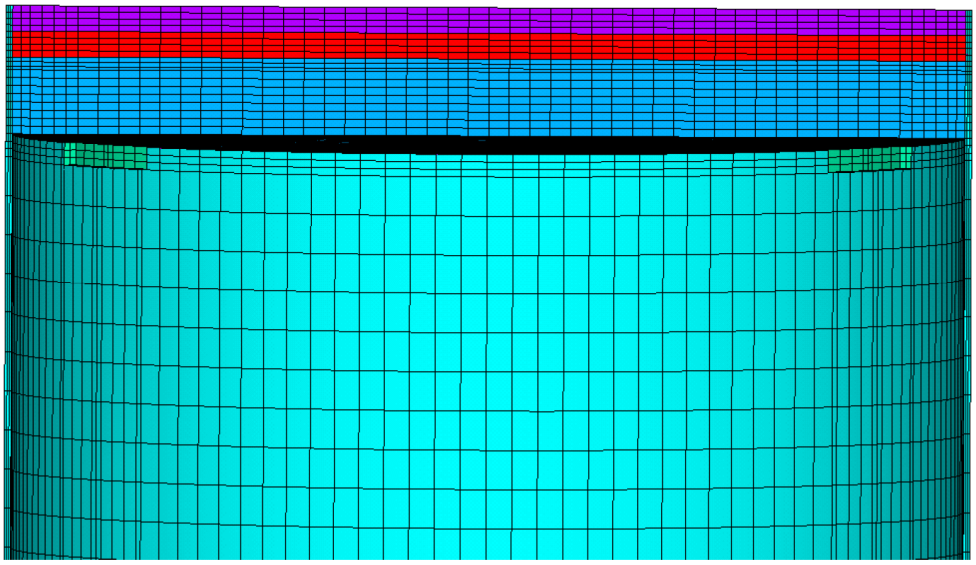

Figure 3.9.1-2
DSC FE Model-Top End

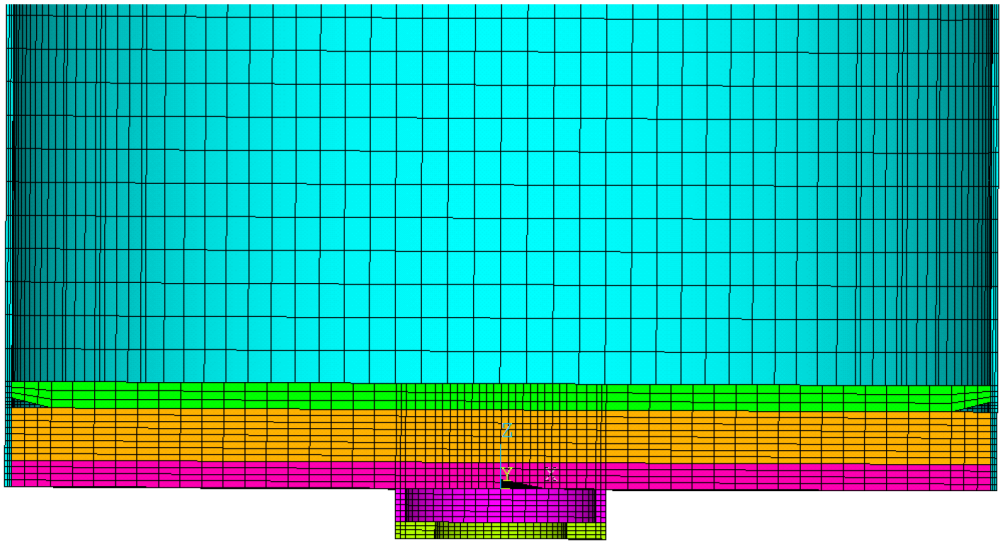

Figure 3.9.1-3
DSC FE Model-Bottom End

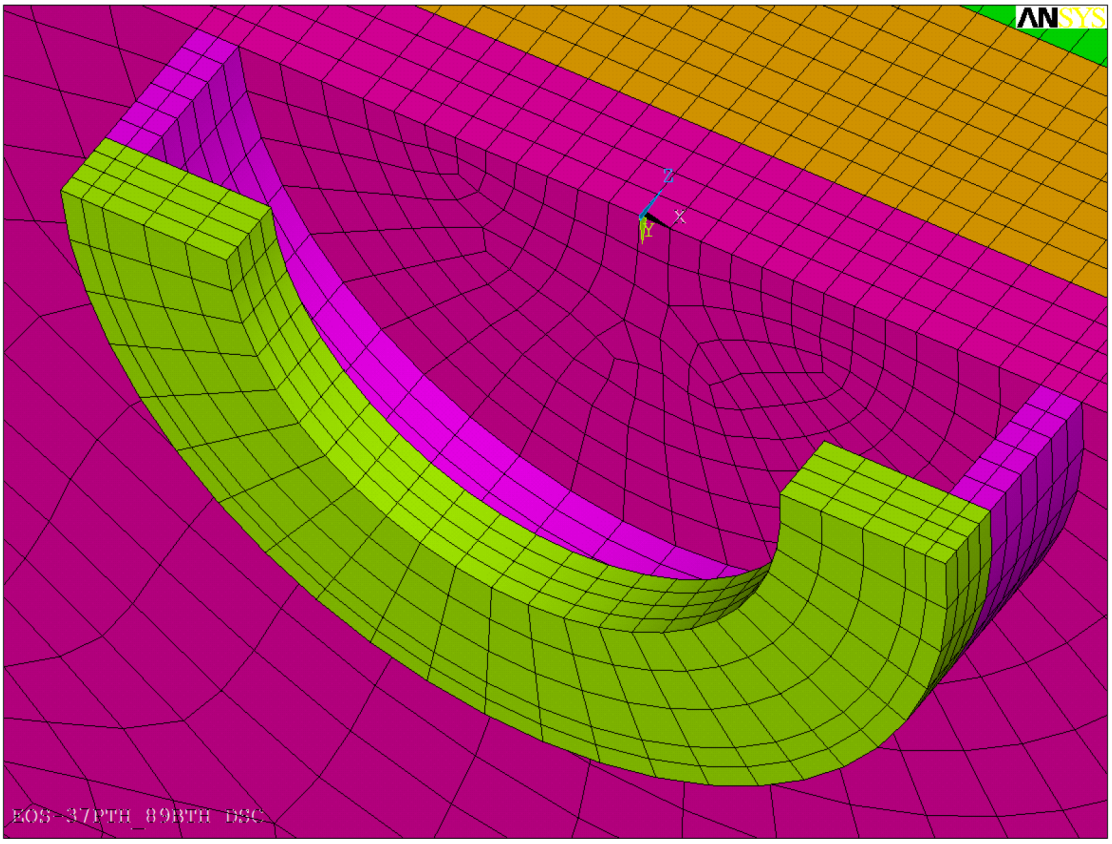

Figure 3.9.1-4
Mesh detail – Grapple Assembly

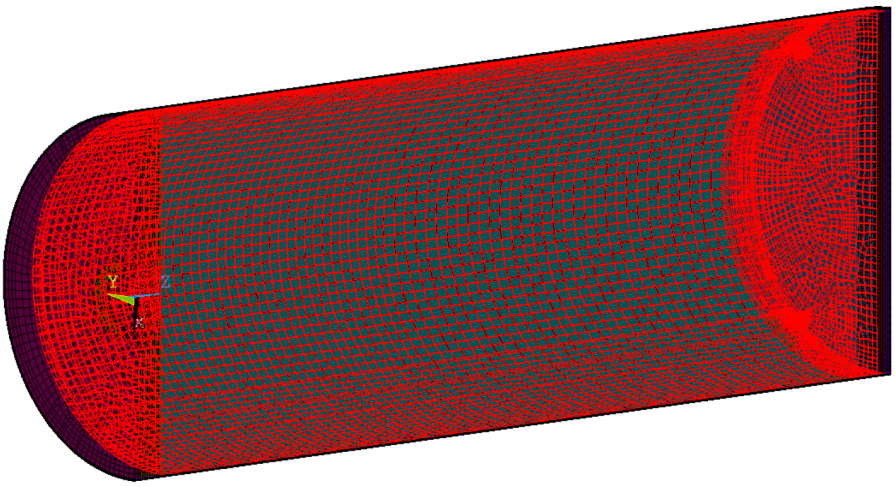

Figure 3.9.1-5
Internal Pressure – Load application

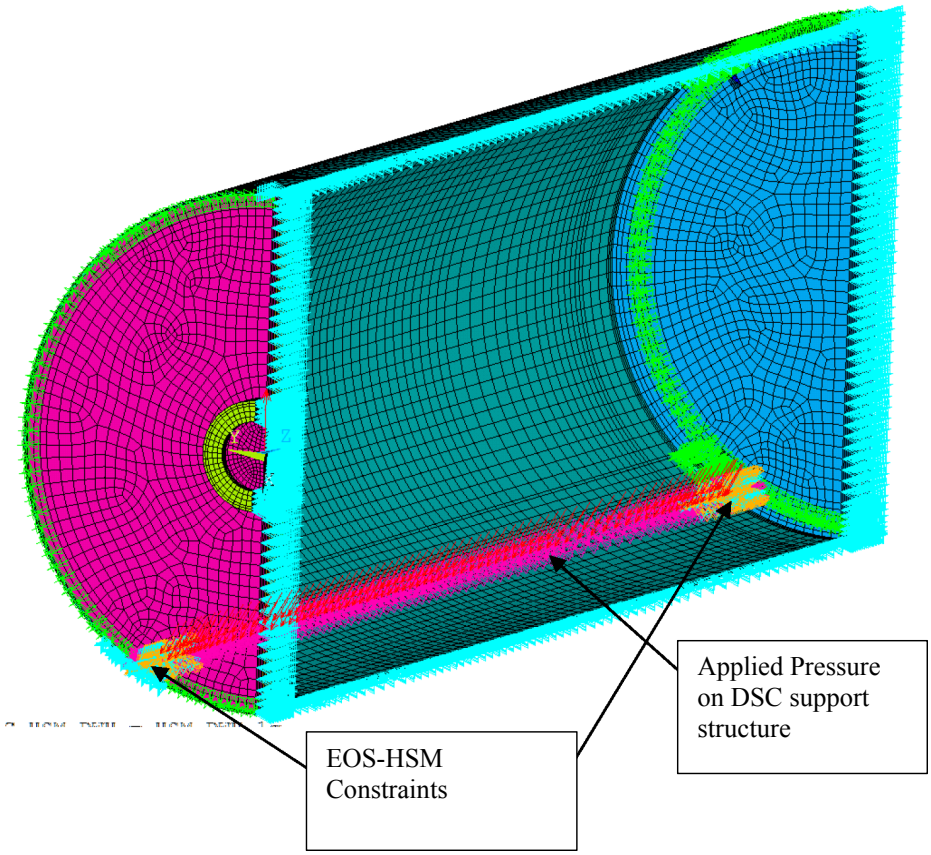

Figure 3.9.1-6
Dead Weight Simulation in EOS-HSM Detail

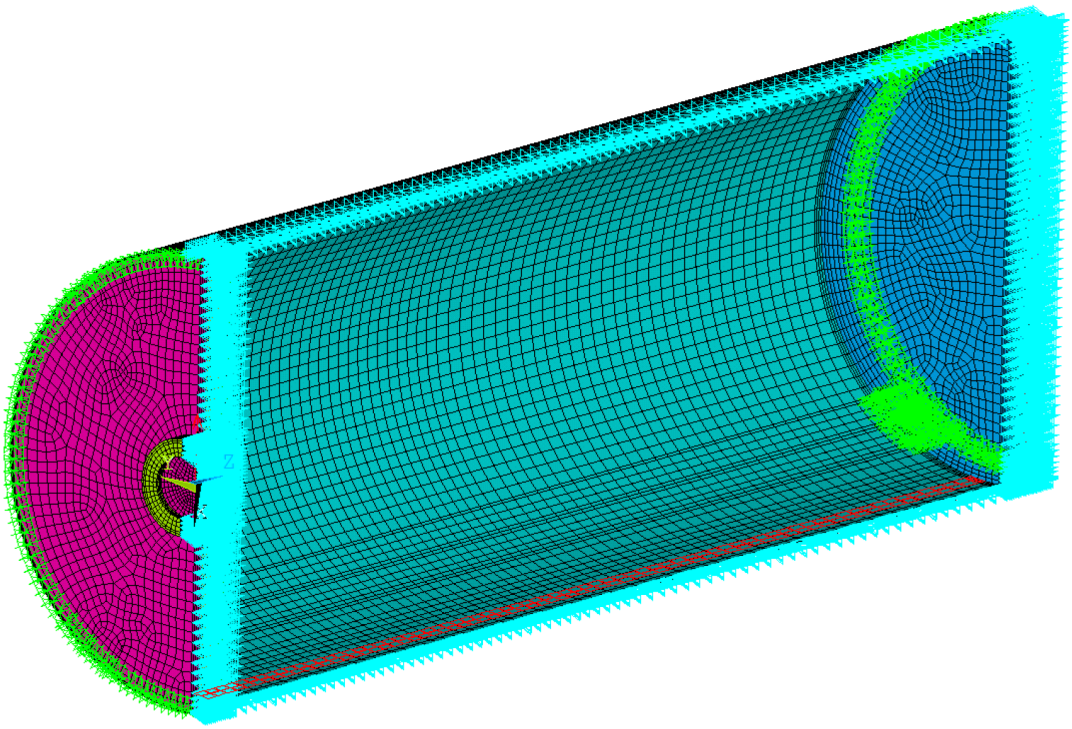

Figure 3.9.1-7
Dead Weight Simulation in EOS-TC

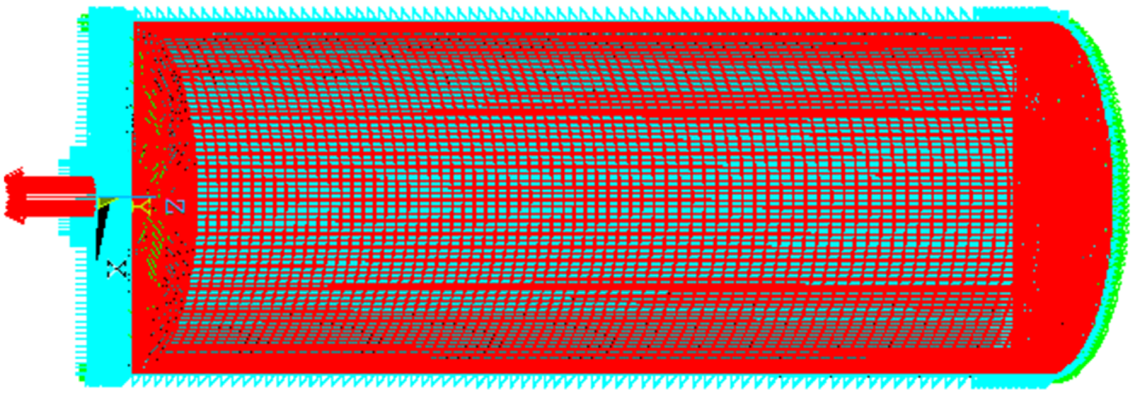

Figure 3.9.1-8
Pull Load with Internal Pressure

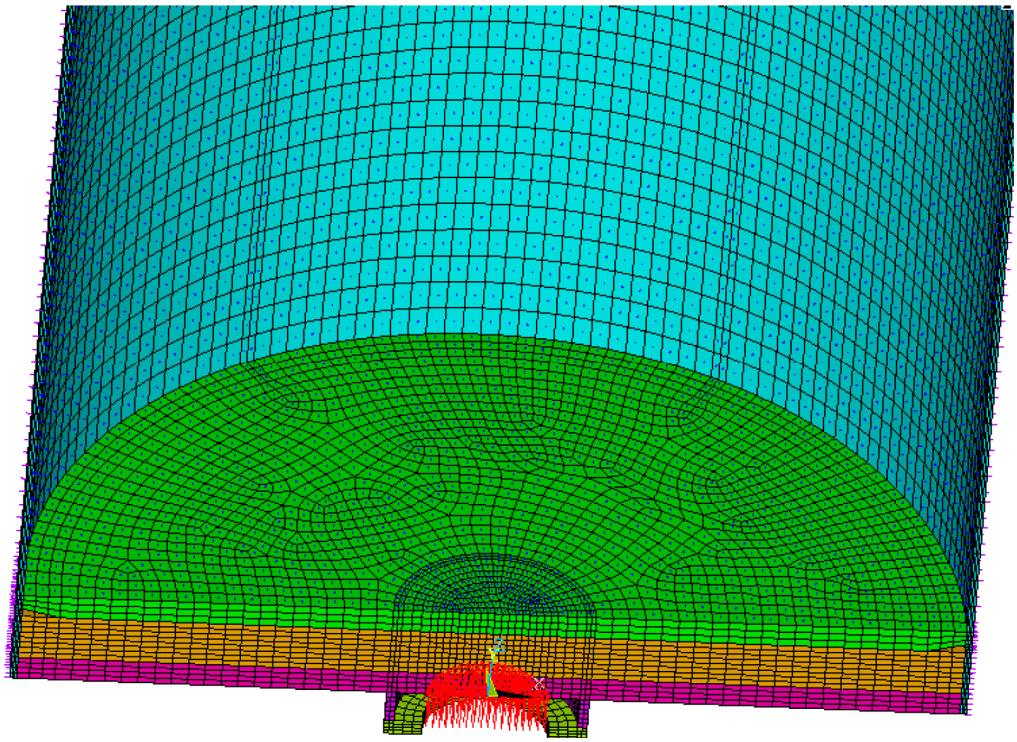

Figure 3.9.1-9
Push Load with Internal Pressure Detail

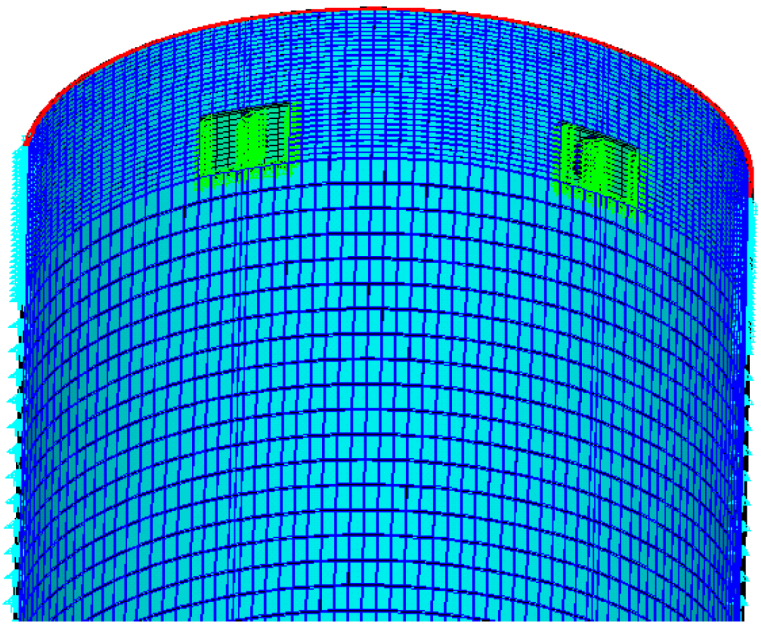

Figure 3.9.1-10
Leak Test with Internal Pressure Top detail

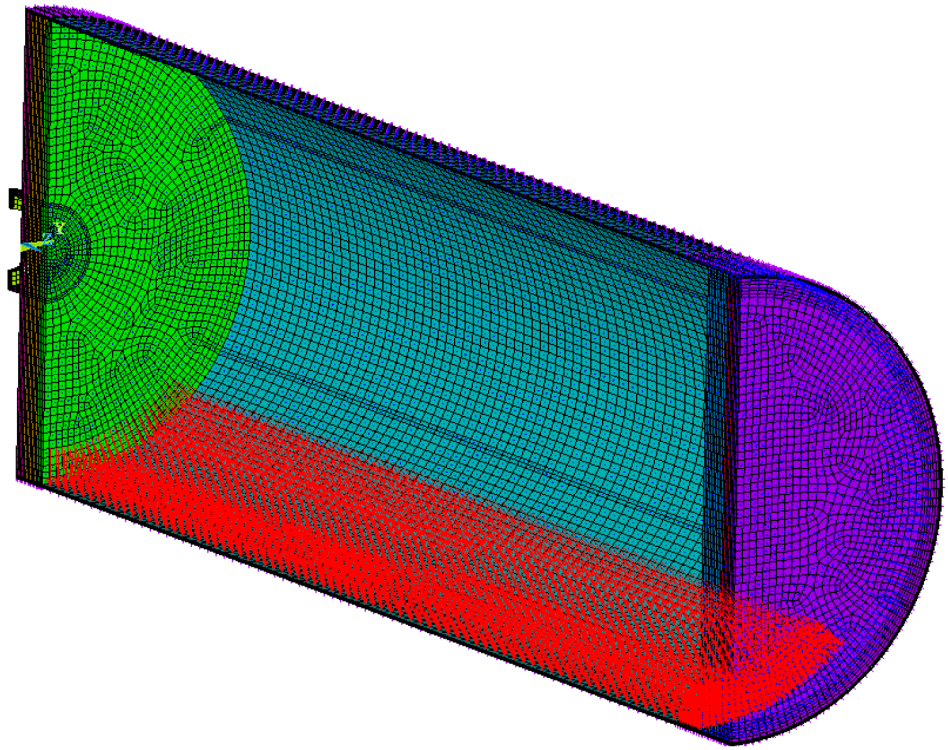

Figure 3.9.1-11
Side Drop on Cask Rail

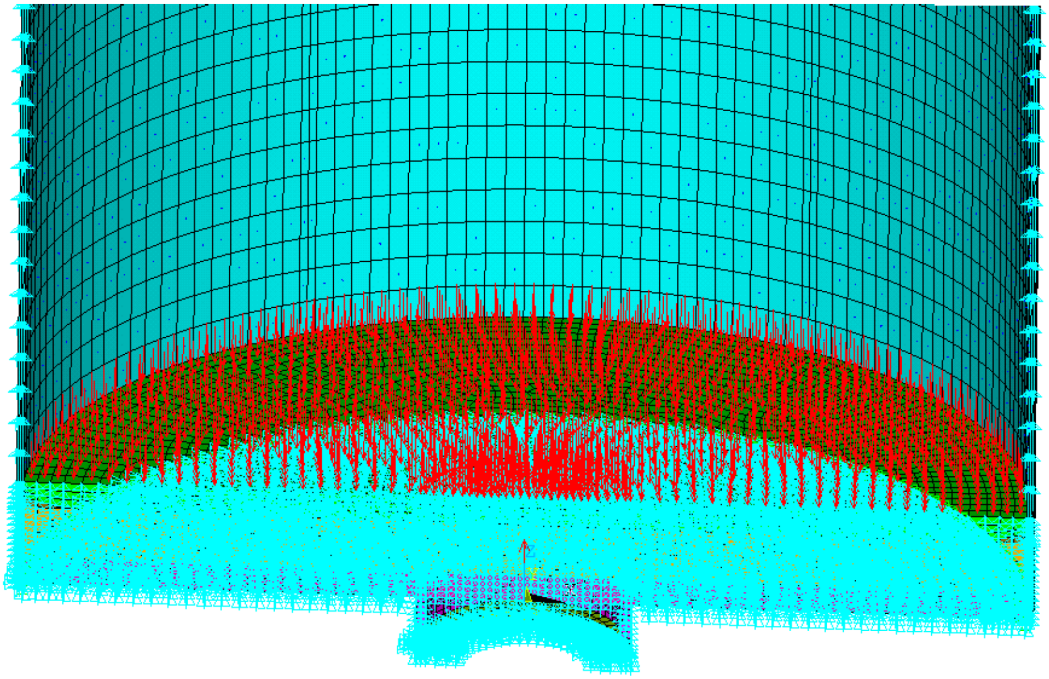

Figure 3.9.1-12
Bottom End Drop Simulation Detail

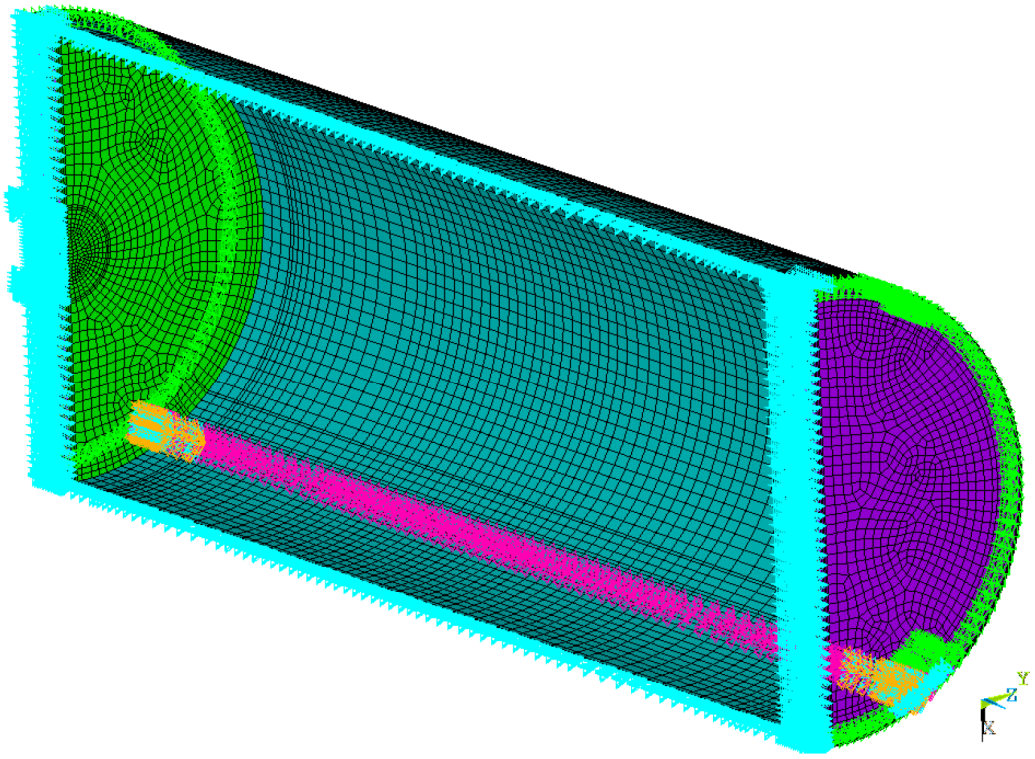

Figure 3.9.1-13
High Seismic in EOS-HSM Simulation

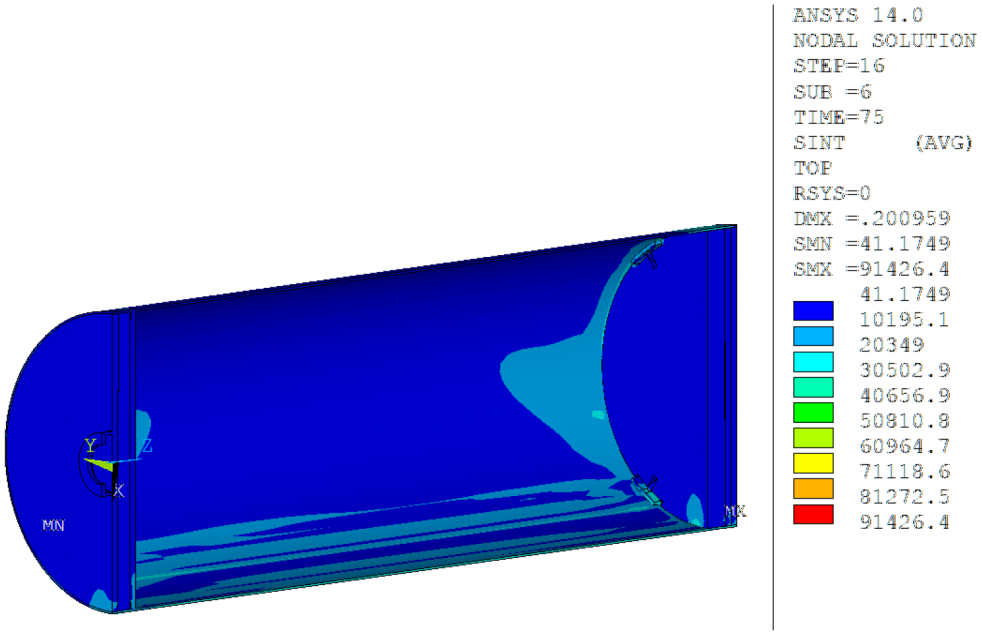

Figure 3.9.1-14
Side drop on cask rail (Elastic- Plastic analysis) – Stress Intensity (psi)

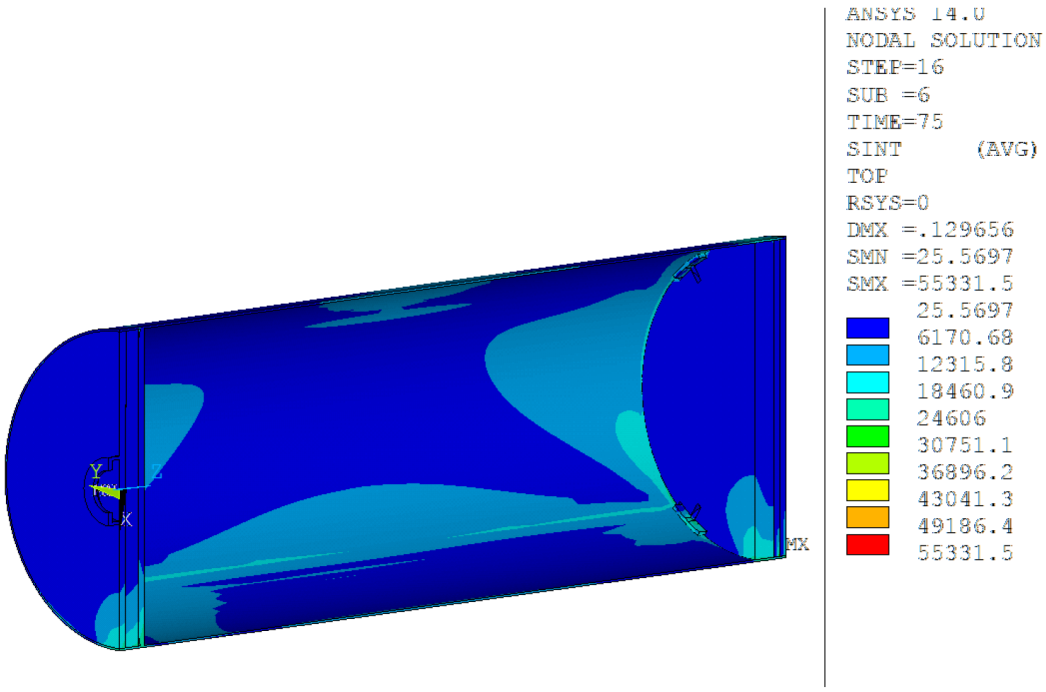

Figure 3.9.1-15
Side drop away from cask rail + 30 psig Internal Pressure – Stress Intensity (psi)

APPENDIX 3.9.2
EOS-37PTH AND EOS-89BTH BASKET STRUCTURAL ANALYSIS

Table of Contents

List of Tables

List of Figures

3.9.2 EOS-37PTH AND EOS-89BTH BASKET STRUCTURAL ANALYSIS

This appendix evaluates the structural integrity of the EOS-37PTH and EOS-89BTH DSC basket for normal, off-normal, *and side and end drop accident* loads.

3.9.2.1 EOS-37PTH Basket Structural Evaluation for Normal/Off-Normal Loads

This section evaluates the structural integrity of the EOS-37PTH DSC basket for normal and off-normal loads. Onsite transfer conditions in the TC108, TC125, and TC135 transfer cask (TC) and storage conditions in the EOS-HSM are considered.

3.9.2.1.1 General Description

The EOS-37PTH DSC consists of a shell assembly that provides confinement and shielding, and an internal basket assembly that locates and supports the FAs. The basket is made up of interlocking, slotted plates to form an egg-crate type structure. The egg-crate structure forms a grid of 37 fuel compartments that house PWR spent fuel assemblies (SFAs). A typical stack-up of grid plates is composed of a structural steel plate, an aluminum plate for heat transfer and a neutron absorber plate (neutron poison) for criticality.

[

]

The basket structure is open at each end and therefore, when the EOS-TC is oriented vertically, longitudinal FA loads are applied directly to the cover plates/shield plugs of the DSC shell assembly and not to the basket assembly. When the EOS-TC is oriented horizontally, longitudinal FA loads from handling may be at least partially transferred to the basket assembly due to friction. The FAs are laterally supported in the basket's fuel compartments. The basket is laterally supported by the basket transition rails and the DSC inner shell.

The minimum open dimension of each fuel compartment cell is sized to allow storage of the applicable fuel, which provides clearance around the FAs. The length of the DSC shell/basket assemblies can be customized to accommodate different FA lengths. The basket length is less than the DSC cavity length to allow for thermal expansion and tolerances.

[

]

The DSC shell and basket assemblies are detailed in Section 1.3.

3.9.2.1.2 Key Dimensions and Materials

The key basket dimensions and materials are per Drawings EOS01-1010-SAR and EOS01-1011-SAR (Section 1.3.1).

The key DSC dimensions and materials are per Drawing EOS01-1001-SAR (Section 1.3.1).

The key EOS-TC dimensions are per Drawings in Section 1.3.4.

3.9.2.1.3 Material Properties

The mechanical properties of structural materials used for the basket assembly as a function of temperature are shown in Chapter 8.

3.9.2.1.4 Temperature Data

Temperature data from the thermal analyses in Chapter 4 at the axial location of hottest temperatures are considered for the thermal stress analysis and component evaluations. A bounding temperature gradient is used in the thermal stress analysis.

3.9.2.1.5 Fuel Data

Chapter 2 provides design characteristics for the types of pressurized water reactor (PWR) FAs to be considered. A bounding distributed weight of 11.0 lbs/in. in the active fuel region is considered in the deadweight and handling analyses.

3.9.2.1.6 Methodology

ANSYS 10.0A1 [3.9.2-2] is used for the evaluation of side loads and thermal loads. Hand calculations are performed to conservatively calculate the stresses due to the axial handling loads. Axial loads are combined with the corresponding side loads, as applicable. Load conditions for the vertical orientation of the DSC/TC are not controlling. Therefore, only the horizontal orientation is evaluated. However, the temperature gradient applied in the thermal analysis bounds the gradients applicable to both the horizontal and vertical orientations (see Section 3.9.2.1.6.1.4).

3.9.2.1.6.1 Finite Element Model

3.9.2.1.6.1.1 Analysis Model Description for Side Loads

In consideration of continuous support of the basket grid structure by the transition rails along the entire length, a 6-inch slice of the basket assembly is modeled, consisting of one-half the widths (basket axial direction) of the basket plates. One end of the 6-inch long model is at the symmetry plane of the horizontal plates and is at the free edges of the vertical plates. The opposite end of the 6-inch long model is at the symmetry plane of the vertical plates and is at the free edges of the horizontal plates. Symmetry boundary conditions (UY = ROTX = ROTZ = 0) are defined at the symmetry planes of the grid plates and at both cut faces of the transition rails and steel angle plates. Geometry plots of the ANSYS model are shown in Figure 3.9.2-1 through Figure 3.9.2-7.

The top and bottom regions of the basket assembly use grid plates with widths as small as 6 inches. The resulting ligaments at the 3-inch deep slots are only 3 inches wide, which is one-half of 6-inch wide ligaments for grid plates in the middle region. However, the tributary width for loading from fuel is also one-half of the tributary width for plates in the middle region, and the fuel distributed load is smaller at the ends since it is away from the active fuel region. Furthermore, the temperatures are lower at the top and bottom of the basket assembly. Therefore, the top and bottom regions of the basket assembly are bounded by the analyzed middle region.

The steel grid plates and the DSC shell are modeled using ANSYS Shell181 elements. No structural credit is taken for the poison plates or for the aluminum plates. The mass of the poison plates and aluminum plates is accounted for by increasing the density of the adjacent steel grid plates. Reinforcing steel angle plates in the R45 transition rails are also modeled using ANSYS Shell181 elements. The aluminum transition rails are modeled using ANSYS Solid185 elements.

Contact between the grid plates at the slots is modeled using ANSYS Conta178 elements (without friction). Initial gaps are defined for the contact elements based on the thickness stack-up of the steel, poison, and aluminum plates in each slot. Similarly, contact between the grid plates and the aluminum transition rails are modeled using ANSYS Conta178 elements (without friction). The initial gaps between the plates and the transition rails are considered closed. This implies that the unmodeled "sandwiched" aluminum, and poison plates are assumed to transfer loads normal to the plates. For stability and convergence purposes, soft springs (Combin14) are modeled coincident with the contact elements.

Bolts connecting the transition rails to the grid plates are modeled using ANSYS Beam4 elements. Nodes on the bolt elements are coupled to nodes on the grid plates, aluminum transition rails, and reinforcing steel angle plates in the rails, as applicable. At one end of each bolt, a contact element (Conta178) is defined in the axial direction of the bolt. The couples and contact element are defined so that only tension loads are transferred through the bolts (due to oversized bolt holes).

Similarly, tie rods for the R90 transition rail assemblies are modeled using ANSYS Beam4 elements. For loading other than thermal, the ends of tie rods are connected to the transition rails in the same manner as for the bolts, so that only tension loads are transferred. One Belleville spring washer is used at each end of the tie rods to allow for thermal growth of the R90 aluminum rail assemblies. Therefore, nonlinear Combin39 spring elements are used in lieu of the contact elements only for the thermal analyses (see Section 3.9.2.1.6.1.2). The thermal loading basically compresses the washer, so *the tie rods* behave like tension-only for other loads.

The DSC shell, when fully welded with cover plates, is much stiffer than the basket and therefore, for static analyses of the basket for small load levels such as deadweight and on-site handling loads, the DSC shell is considered to be rigid. Gaps between the basket and the DSC cylindrical shell are modeled using ANSYS Conta178 elements (without friction). Each gap element contains two nodes; one on each surface of the structures. Initial gaps are based on a basket outside diameter of 74.10 inches and a DSC inside diameter of 74.50 inches, and the side load orientation. Initial gaps are adjusted in consideration of the radial thermal growth of the basket relative to the growth of the DSC shell.

To consider bounding conditions, two sets of analyses are performed. The first set of analyses defines nominal gaps for a basket thermal growth, relative to the DSC shell, approximated to be 0.05 inches. The second set of analyses adjusts the gaps for a basket minimum thermal growth, relative to the DSC shell, of 0.0158 inch, calculated based on average temperatures of the basket and DSC shell at the hottest cross-section per Chapter 4.

Side loads due to transfer handling bound the loads applicable to storage in the EOS-HSM for which only deadweight is applicable. As discussed earlier, the DSC shell, when fully welded with cover plates, is much stiffer than the basket and therefore, for static analyses of the basket for small load levels such as deadweight and on-site handling loads, the DSC shell is considered to be rigid. Therefore the impact of the rail location is insignificant and one model envelopes the configuration when the DSC is inside the EOS-TC and EOS-HSM.

3.9.2.1.6.1.2 Analysis Model Description for Thermal Loads

The basket assembly thermal stress model is similar to the side-loaded model except that it excludes the DSC cylindrical shell (which does not restrain the thermal growth of the basket). One Belleville spring washer is used at each end of the tie rods to allow for thermal growth of the R90 aluminum rail assemblies. Therefore, nonlinear Combin39 spring elements are used in lieu of contact elements at one end of each tie rod for the thermal analyses. The force-deflection input is determined using data associated with the spring washer.

Boundary conditions for the transition rails and rail angle plates are removed from one end of the model to avoid fictitious thermal stresses that would occur if both ends were restrained. Two thermal cases are considered in consideration of the boundary conditions for the transition rails and rail angle plates: restraint at y = 0 inch (near end restraint), and restraint at y = 6 inches(far end restraint). Although the maximum stress results from these two cases are effectively the same, the results are combined with the deadweight and handling cases using ANSYS load combinations to preclude the conservatism of adding maximum stresses regardless of location. The consideration of two sets of boundary conditions for thermal ensures that the correct maximum stress in combination with deadweight and handling stress is obtained.

3.9.2.1.6.1.3 Material Properties in Analyses

The modeled components of the basket and DSC are based on lower bound material properties. The material properties used for stress analyses (except thermal stress analyses) are based on bounding average temperature values at the hottest section for off-normal transfer in a horizontal EOS-TC. Elastic analyses are used for all normal and off-normal conditions.

3.9.2.1.6.1.4 Loads

Load cases are based on the loads described in Chapter 2.

For side loading, the fuel weight load is modeled conservatively using a pressure load equivalent to the applicable acceleration, or G-load, times the FA weight divided by the basket fuel compartment area associated with the active fuel region length and the fuel compartment width between slots (8.79 inches). A fuel load of 11.0 lbs/in acting on the fuel compartment width between slots is applied to bound the load distribution in the active fuel region for all PWR fuel types identified in Chapter 2. Figure 3.9.2-8 shows the application of fuel weight pressure loads to the model.

For 0° and 180° side load orientations, the equivalent fuel assembly pressure acts only on the horizontal plates. For 90° and 270° side load orientations, the equivalent fuel assembly pressure acts only on the vertical plates. For other orientations, the equivalent FA pressure acts perpendicular to the horizontal and vertical plates, proportioned based on the Cosine and Sine of the orientation angle.

Based on the handling load combination required per Chapter 2, the following bounding normal side load conditions (DSC and basket in horizontal position) are evaluated:

- DW + 1g Vertical = 2.0g Vertical at $\theta = 180°$
- DW + 0.5g Vert. + 0.5g Transverse = 1.58g at $\theta_{198} = 198.43°$ *
- DW + 1.0g Transverse = 1.414g at $\theta_{225} = 225.0°$ *

* $\theta_{198} = 180° + \text{Tan}^{-1}(0.5 / 1.5) = 198.43°$; $\theta_{225} = 180° + \text{Tan}^{-1}(1.0 / 1.0) = 225°$

Thermal stress analyses are based on a bounding temperature profile. The temperature profile used is represented by the following equation, labeled "EOS Basket Analysis" in Figure 3.9.2-9:

$$T(x) = -0.3952\ x^2 + 3.4661\ x + 790.29$$

Where,

T(x) = Basket temperature as a function of radius, x.

Figure 3.9.2-9 shows the raw temperature data (versus radius) for one load case from the thermal analyses, labeled "EOS-37PTH in EOS-TC125, Grid Plates, LC # 6" (worst-case temperature condition for steepness of radial temperature gradient). A comparison of the curves shows that the curve labeled as "EOS Basket Analysis," which gives the temperatures versus radius used in the basket thermal stress analysis herein, provides the bounding steeper gradient.

3.9.2.1.6.2 Criteria

The basis for allowable stresses is obtained from Chapter 8 and ASME Section III, Division 1, Subsection NG [3.9.2-1]. The criteria are summarized in Chapter 3, Table 3-2. Allowable stresses for the threaded fasteners, used to connect the transition rails to the basket grid structure, are from Chapter 8 and Section NG-3230 of [3.9.2-1]. The criteria are summarized in Table 3.9.2-1. The component allowable stress values are summarized in Table 3.9.2-2. The allowable stresses are based on material properties at 700 °F for the grid plates and 550 °F for the transition rails, angle plates, bolts and tie rods. These temperatures bound the average temperatures at the hottest section for the grid plates and transition rails, respectively, summarized in Chapter 4 for off-normal transfer in a horizontal EOS-TC.

3.9.2.1.6.3 Creep Evaluation for Long Term Storage

The aluminum R90 rails are designed to resist the bearing loads due to the deadweight of the loaded basket for 80 years while stored in the EOS-HSM. For long-term creep effects, where loading on the aluminum transition rail redistributes over time, an average bearing stress is an appropriate value to consider.

Conservatively, it is assumed that the entire weight of the basket is resisted by the three pieces of a single aluminum R90 rail. The 1g deadweight load from the entire weight of a 6-inch long portion of the basket is approximately 3,416 lb. The area of the corresponding 6-inch long portion of the R90 rail that resists the load is approximately = 156 in^2. However, credit for the outer portion of the width of the rail is excluded by conservatively considering only half of the rail width. The corresponding bearing stress is calculated as follows:

Basket 1g vertical bearing stress = Load / Area = 43.8 psi, or, 0.044 ksi.
(on aluminum R90 transition rail)

The individual compartment load at each SFA location on the supporting aluminum plate gives a much lower bearing stress. Using a conservative width of only 8 inches for a compartment gives:

SFA 1g vert. bearing stress = (Load / length) / Width = 1.375 psi, or, 0.0014 ksi.
(on aluminum plate)

The allowable bearing stresses are provided in Chapter 8, and based on Reference [3.9.2-3]; they represent the stress in Aluminum 1100 to produce a strain of 0.01 in 550,000 hours (approximately 63 years). However, the creep strain curve is so flat that the values at 80 years are approximately the same. The allowable bearing stress for Aluminum 1100 represents a conservative lower bound. The initial temperature values (time = 0) and the corresponding allowable bearing stresses in the basket aluminum components, to limit creep strain to 0.01, are as follows:

- 0.254 ksi in the hottest aluminum plate, with a starting temperature of 680 °F
- 0.758 ksi in the hottest R90 rail, with a starting temperature of 470 °F
- 0.876 ksi in a less than hottest R90 rail, based on a starting temperature of 440 °F

From Chapter 4 for normal conditions (applicable to long-term storage conditions) at the hottest cross-section of the basket, the average R90 transition rail temperature is not more than 469 °F, which is less than the above temperature of 470 °F for the hottest R90 rail. Similarly, from Chapter 4, for normal conditions, the hottest basket plate temperature is not more than 668 °F, which is less than the above temperature of 680 °F for the hottest aluminum plate. Based on this comparison of temperatures, and since the heat dissipation rate for the EOS-37PTH basket is better than that for the basket temperature data (temperature versus time) used in Reference [3.9.2-3], the allowable creep stresses given above are applicable to the aluminum components of the EOS-37PTH basket.

3.9.2.1.7 Results

3.9.2.1.7.1 Results for On-Site DW+Handling and Thermal Stress Analysis

Combined results for basket component stress results for normal condition deadweight + handling loads and thermal stress analysis are shown in Table 3.9.2-3. The tabulated results show that all stresses meet the corresponding Code limits.

ANSYS Force Summation Comparison

An ANSYS force summation for the basket components only, for the 2g deadweight plus handling load combination, is compared to the expected load as shown below:

Force Summation: F_z = -6,831.256 lb
(in vertical direction (z), length of model is 6 inches)
Expected Load:
Basket weight / length w/o spent fuel: = 167.2 lb/in
Basket wt. w/o spent fuel (6” long) = 1,003 lb.
Spent fuel weight (6” long) = (11 lb/in) (6” length of basket) (37 SFAs)
= 2,442 lb.
Total weight of the basket, with spent fuel (6” long) = 3,445 lb (for 1g)
Expected Load at 2g (in vertical direction) = 6,890 lb.

The ANSYS load of 6,831 is within 1% of the hand-calculated weight load and therefore, is acceptable.

Similarly, the ANSYS 1g load is 3,416 lb, or half of the ANSYS 2g load, as expected.

3.9.2.1.7.2 Aluminum Components – Long Term Storage Deadweight Bearing Stress

The aluminum R90 rails are designed to resist the bearing loads due to the deadweight of the loaded basket for 80 years while stored in the EOS-HSM. A review of the R90 transition rail stresses in Figure 3.9.2-11 shows that for the 1g deadweight loading, the R90 rail carries most of the loading. The aluminum R45 rails take some of the bearing load but are not controlling. The stresses shown in Figure 3.9.2-11 are unaveraged stresses that include local and peak effects. However, for long-term creep effects, where loading on the aluminum transition rail redistributes over time, an average bearing stress is a more appropriate value to consider. The stresses calculated in Section 3.9.2.1.6.3 are compared to allowable stress values that are reduced to limit the effect due to creep.

Comparison of Aluminum Bearing Stress to Allowable Creep Stress from Section 3.9.2.1.6.3:

Component	Bearing Stress	Allowable Creep Stress	Stress/Allowable Ratio
Alum. Rail	0.044 ksi	0.758 ksi	0.0580
Alum. Plate	0.0014 ksi	0.254 ksi	0.0055

3.9.2.1.8 Conclusions

Finite element analyses and hand calculations for the EOS-37PTH basket assembly are performed for all normal and off-normal on-site conditions. Controlling stress intensities are reported in Table 3.9.2-3. A comparison of stress intensities to the corresponding allowable values indicate that all load conditions and combinations show acceptable stress levels, as applicable.

3.9.2.2 EOS-89BTH Basket Structural Evaluation for Normal/Off-Normal Loads

The basis for the fuel compartment allowable stress values is the ASME Code, Section III, Subsection NG (Reference [3.9.2-1]), as given in Chapter 8.

3.9.2.2.1 General Description

The EOS-89BTH DSCs consists of a shell assembly that provides confinement and shielding, and an internal basket assembly that locates and supports the FAs. The basket is made up of interlocking slotted plates to form an egg-crate type structure. The egg-crate structure forms a grid of 89 fuel compartments that house boiling water reactor (BWR) SFAs. A typical stack-up of grid plates is composed of a structural steel plate, an aluminum plate for heat transfer and a neutron absorber plate (neutron poison) for criticality.

The DSC shell and basket assemblies are detailed in drawings in Section 1.3.2.

The descriptions in Section 3.9.2.1.1 of the transition rails and basket are also applicable to the EOS-89BTH DSC.

3.9.2.2.2 Key Dimensions and Materials

The key basket dimensions and materials are per Drawings EOS01-1020-SAR and EOS01-1021-SAR Section 1.3.2.

The key DSC dimensions and materials are per Drawing EOS01-1001-SAR (Section 1.3.2):

The key EOS-TC dimensions are per the drawings in Section 1.3.4.

3.9.2.2.3 Material Properties

The mechanical properties of structural materials used for the basket assembly and canister as a function of temperature are shown in Chapter 8.

3.9.2.2.4 Temperature Data

Temperature data from the EOS-89BTH thermal analyses and from the EOS-37PTH thermal analyses in Chapter 4, at the axial location of hottest temperatures, are considered herein for the thermal stress analysis and component evaluations. The conservative temperature gradient used herein for the thermal stress analysis bounds the gradients for the EOS-89BTH basket. See Section 3.9.2.1.6.1.4 for further discussion.

3.9.2.2.5 Fuel Data

Chapter 2 provides design characteristics for the types of BWR FAs to be considered. A maximum FA weight of 705 lbs is used. A distributed weight of 705 lbs / 150 in. = 4.7 lbs/in is considered to be bounding in the active fuel region for the deadweight and handling analyses.

3.9.2.2.6 Methodology

Same as Section 3.9.2.1.6.

3.9.2.2.6.1 Finite Element Model

3.9.2.2.6.1.1 Analysis Model Description for Side Loads

Geometry plots of the ANSYS model are shown in Figure 3.9.2-12 through Figure 3.9.2-18. All other details of the analysis model description are the same as Section 3.9.2.1.6.1.1.

3.9.2.2.6.1.2 Analysis Model Description for Thermal Loads

Same as Section 3.9.2.1.6.1.2.

3.9.2.2.6.1.3 Material Properties in Analyses

Same as Section 3.9.2.1.6.1.3.

3.9.2.2.6.1.4 Loads

Load cases are based on the loads described in Chapter 2.

For side loading, the fuel weight load is modeled conservatively using a pressure load equivalent to the applicable acceleration, or g-load, times the FA weight divided by the basket fuel compartment area associated with the active fuel region length and the fuel compartment width between slots (5.85 inches). A fuel load of 4.7 lbs/in acting on the fuel compartment width between slots is applied to bound the load distribution in the active fuel region for all BWR fuel types identified in Chapter 2. Figure 3.9.2-19 shows the application of fuel weight pressure loads to the model.

For 0° and 180° side load orientations, the equivalent FA pressure acts only on the horizontal plates. For 90° and 270° side load orientations, the equivalent fuel assembly pressure acts only on the vertical plates. For other orientations, the equivalent FA pressure acts perpendicular to the horizontal and vertical plates, proportioned based on the Cosine and Sine of the orientation angle.

Based on the handling load combination, the following bounding normal side load conditions (DSC and basket in horizontal position) are evaluated:

- - DW + 1g Vertical = 2.0g Vertical at $\theta = 180°$
- - DW + 0.5g Vert. + 0.5g Transverse = 1.58g at $\theta_{198} = 198.43°$ *
- - DW + 1.0g Transverse = 1.414g at $\theta_{225} = 225.0°$ *

* $\theta_{198} = 180° + \text{Tan-1}(0.5 / 1.5) = 198.43°$; $\theta_{225} = 180° + \text{Tan-1}(1.0 / 1.0) = 225°$

Thermal stress analyses are made based on a bounding temperature profile. The temperature profile used is represented by the following equation labeled "EOS Basket Analysis" in Figure 3.9.2-9:

$$T(x) = -0.3952\ x^2 + 3.4661\ x + 790.29$$

Where,

T(x) = Basket temperature as a function of radius, x.

Due to the lower heat load in the EOS-89BTH DSC compared to the EOS-37PTH DSC, limited analyses are run in Chapter 4 to demonstrate that the maximum fuel cladding temperatures for the EOS-89BTH will be bounded by those for the EOS-37PTH. However, resulting maximum EOS-89BTH basket component temperatures are in some cases shown to be greater than for the EOS-37PTH basket component temperatures.

Figure 3.9.2-20 shows that although the EOS-89BTH grid plate temperatures are slightly greater than the EOS-37PTH grid plate temperatures, the gradients are similar. As shown in these figures and in comparison plots for other thermal cases, the analyzed temperature profile has a steeper temperature gradient than that for the raw data. Therefore, it can be concluded that the conservative temperature gradient used herein for the thermal stress analysis will bound the gradients for the EOS-89BTH basket. Figure 3.9.2-21 shows the bounding temperature profile applied to the ANSYS model.

3.9.2.2.6.2 Criteria

The basis for allowable stresses is obtained from Chapter 8 and ASME Section III, Division 1, Subsection NG (Reference [3.9.2-1]). The criteria are summarized in Chapter 3, Table 3-2.

Allowable stresses for the threaded fasteners, used to connect the transition rails to the basket grid structure, are from Chapter 8 and Section NG-3230 of [3.9.2-1]. The criteria are summarized in Table 3.9.2-1. The component allowable stress values are summarized in Table 3.9.2-2. The allowable stresses are based on material properties at 700 °F for the grid plates (except where noted otherwise) and 550 °F for the transition rails, angle plates, bolts and tie rods. These temperatures bound the average temperatures at the hottest section for the grid plates and transition rails, respectively, summarized in Chapter 4 for transfer in a horizontal EOS-TC (non-accident).

3.9.2.2.6.3 Creep Evaluation for Long Term Storage

The aluminum R90 rails are designed to resist the bearing loads due to the deadweight of the loaded basket for 80 years while stored in the EOS-HSM. For long-term creep effects, where loading on the aluminum transition rail redistributes over time, an average bearing stress is an appropriate value to consider.

Conservatively assuming that the entire weight of the basket is resisted by the three pieces of a single aluminum R90 rail, the 1g deadweight load from the entire weight of a 6-inch long portion of the basket is approximately 3,462 lb. The area of the corresponding 6-inch long portion of the R90 rail that resists the load is approximately = 102 in^2. However, credit for the outer portion of the width of the rail is excluded by conservatively considering only half of the rail width. The corresponding bearing stress is calculated as follows:

Basket 1g vert. bearing stress = Load / Area = 67.9 psi, or, 0.068 ksi. (on aluminum R90 transition rail)

The individual compartment load at each SFA location on the supporting aluminum plate gives a much lower bearing stress. Using a conservative width of only 5 inches for a compartment gives:

SFA 1g vert. bearing stress = (Load / length) / Width = 0.940 psi, or, 0.00094 ksi. (on aluminum plate)

The allowable bearing stresses are provided in Section 3.9.2.1.6.3. The initial temperature values (time = 0) and the corresponding allowable bearing stresses in the basket aluminum components, to limit creep strain to 0.01, are as follows:

- 0.254 ksi in the hottest aluminum plate, with a starting temperature of 680 °F
- 0.758 ksi in the hottest R90 rail, with a starting temperature of 470 °F
- 0.876 ksi in a less than hottest R90 rail, based on a starting temperature of 440 °F

From Chapter 4, for normal conditions (applicable to long-term storage conditions) at the hottest cross-section of the basket, the average R90 transition rail temperature is not more than 446 °F, which is less than the above temperature of 470 °F for the hottest R90 rail. Similarly, from Chapter 4, for normal conditions, the hottest basket plate temperature is not more than 676 °F, which is less than the above temperature of 680 °F for the hottest aluminum plate. Based on this comparison of temperatures, and since the heat dissipation rate for the EOS-89BTH basket is better than that for the basket temperature data (temperature versus time) used in Reference [3.9.2-3], the allowable creep stresses given above are applicable to the aluminum components of the EOS-89BTH basket.

3.9.2.2.7 Results

3.9.2.2.7.1 Results for On-Site DW+Handling and Thermal Stress Analysis

Combined results with controlling stress ratios for normal condition deadweight + handling loads and thermal analysis are shown in Table 3.9.2-4. The tabulated results show that all stresses meet the corresponding Code limits.

ANSYS Force Summation Comparison

An ANSYS force summation for the basket components only, for the 2g deadweight plus handling load combination, is compared to the expected load as shown below:

Force Summation: F_z = -6,923.822 lb (in vertical direction (z), length of model is 6")
Expected Load:
Basket weight / length w/o spent fuel = (19,300 + 637 + 1,110 + 3,980) / 166.0 + 1,720 / 175.0
= 160.6 lb/in
Basket wt. w/o spent fuel (6" long) = (160.6) (6") = 964 lb.
Spent fuel weight (6" long) = (4.7 lb/in) (6" length of basket) (89 SFAs)
= 2,510 lb.

Total weight of the basket, with spent fuel (6" long) = 964 + 2,510 = 3,474 lb (for 1g)
Expected Load at 2g (in vertical direction) = 2 (3,474) = 6,948 lb.

The ANSYS load of 6,924 is within 0.4% of the hand-calculated weight load and therefore, is acceptable.

Similarly, the ANSYS 1g load is 3,462 lb, or half of the ANSYS 2g load, as expected.

3.9.2.2.7.2 Aluminum Components – Long Term Storage Deadweight Bearing Stress

The aluminum R90 rails are designed to resist the bearing loads due to the deadweight of the loaded basket for 80 years while stored in the EOS-HSM. A review of the R90 transition rail stresses in Figure 3.9.2-22 shows that for the 1g deadweight loading, the R90 rail carries most of the loading. The aluminum R45 rails take some of the bearing load but are not controlling. The stresses shown in Figure 3.9.2-22 are unaveraged stresses that include local and peak effects. However, for long-term creep effects, where loading on the aluminum transition rail redistributes over time, an average bearing stress is a more appropriate value to consider.

The stresses calculated in Section 3.9.2.2.6.3 are compared to allowable stress values that are reduced to limit the effect due to creep.

Comparison of Aluminum Bearing Stress to Allowable Creep Stress from Section 3.9.2.2.6.3:

Component	Bearing Stress	Allowable Creep Stress	Stress/Allowable Ratio
Alum. Rail	0.068 ksi	0.758 ksi	0.0897
Alum. Plate	0.00094 ksi	0.254 ksi	0.0037

3.9.2.2.7.3 Conclusions

Finite element analyses and hand calculations for the EOS-89BTH basket assembly are performed for all normal and off-normal on-site conditions. Controlling stress intensities are reported in Table 3.9.2-4. A comparison of stress intensities to the corresponding allowable values indicate that all load conditions show acceptable stress levels, as applicable.

3.9.2.3 EOS-37PTH Basket Structural Evaluation for On-Site Accident Drop Loads

This section evaluates the structural integrity of the EOS-37PTH DSC basket for on-site accident side and end drop loads. On-site transfer conditions in the EOS-TC108, EOS-TC125, or EOS-TC135 are considered for thermal properties used in the side drop load analyses.

3.9.2.3.1 General Description

Same as Section 3.9.2.1.1.

3.9.2.3.2 Key Dimensions and Materials

Same as Section 3.9.2.1.2.

3.9.2.3.3 Material Properties

Same as Section 3.9.2.1.3.

3.9.2.3.4 Temperature Data

Same as Section 3.9.2.1.4.

3.9.2.3.5 Fuel Data

Chapter 2 provides design characteristics for the types of pressurized water reactor (PWR) FAs to be considered. A bounding distributed weight of 11.0 lbs/in. in the active fuel region is considered for the on-site accident side drop analyses.

3.9.2.3.6 Methodology

ANSYS 10.0A1 [3.9.2-2] is used for the evaluation of on-site accident side drop loads. Hand calculations are performed to conservatively calculate the stresses due to the on-site axial end drop loads. Stresses due to the end drop loads are not controlling. Therefore, only the side drop load analysis results are presented.

3.9.2.3.6.1 Finite Element Model

3.9.2.3.6.1.1 Analysis Model Description for Side Loads

In consideration of continuous support of the basket grid structure by the transition rails along the entire length, a 6-inch slice of the basket assembly is modeled, consisting of one-half the widths of the basket plates. One end of the 6-inch long model is at the symmetry plane of the horizontal plates and is at the free edges of the vertical plates. The opposite end of the 6-inch long model is at the symmetry plane of the vertical plates and is at the free edges of the horizontal plates. Symmetry boundary conditions (UY = ROTX = ROTZ = 0) are defined at the symmetry planes of the grid plates and at both cut faces of the transition rails and steel angle plates. Geometry plots of the ANSYS model are shown in Figure 3.9.2-1 through Figure 3.9.2-8 (180 degree drop orientation shown).

The top and bottom regions of the basket assembly use grid plates with widths as small as 6 inches. The resulting ligaments at the 3-inch deep slots are only 3 inches wide, which is one-half of 6-inch wide ligaments for grid plates in the middle region. However, the tributary width for loading from fuel is also one-half of the tributary width for plates in the middle region, and the fuel distributed load is smaller at the ends since it is away from the active fuel region. Furthermore, the temperatures are lower at the top and bottom of the basket assembly. Therefore, the top and bottom regions of the basket assembly are bounded by the analyzed middle region.

The steel grid plates and the DSC shell are modeled using ANSYS Shell181 elements. No structural credit is taken for the poison plates or for the aluminum plates. The mass of the poison plates and aluminum plates is accounted for by increasing the density of the adjacent steel grid plates. Reinforcing steel angle plates in the R45 transition rails are also modeled using ANSYS Shell181 elements. The aluminum transition rails are modeled using ANSYS Solid185 elements.

Contact between the grid plates at the slots is modeled using ANSYS Conta178 elements (without friction). Initial gaps are defined for the contact elements based on the thickness stack-up of the steel, poison, and aluminum plates in each slot. Similarly, contact between the grid plates and the aluminum transition rails are modeled using ANSYS Conta178 elements (without friction). The initial gaps between the plates and the transition rails are considered closed. This implies that the unmodeled "sandwiched" aluminum and poison plates are assumed to transfer loads normal to the plates. For stability and convergence purposes, soft springs (Combin14) are modeled coincident with the contact elements.

Bolts connecting the transition rails to the grid plates are modeled using ANSYS Beam4 elements. Nodes on the bolt elements are coupled to nodes on the grid plates, aluminum transition rails, and reinforcing steel angle plates in the rails, as applicable. At one end of each bolt, a contact element (Conta178) is defined in the axial direction of the bolt. The couples and contact elements are defined such that only tension loads are transferred through the bolts (due to oversized bolt holes). Similarly, tie rods for the R90 transition rail assemblies are modeled using ANSYS Beam4 elements. The ends of tie rods are connected to the transition rails in the same manner as for the bolts, such that only tension loads are transferred. The Belleville spring washers used at the ends of the tie rods are considered to be compressed by thermal loading so the tie rods behave as tension-only for other loads. Additional side drop analyses are performed without the connection bolts and tie rods (assumed to fail) to demonstrate that they are not needed for an accident drop.

Gaps between the basket and the DSC cylindrical shell are modeled using ANSYS Conta178 elements (without friction). Initial gaps are based on a basket outside diameter of 74.10 inches and a DSC inside diameter of 74.50 inches, and the side load orientation. Initial gaps are adjusted in consideration of the radial thermal growth of the basket relative to the growth of the DSC shell. Each gap element contains two nodes; one on each surface of the structures. The flexibility of the DSC shell is considered. Therefore, additional gap elements (ANSYS Conta178) are modeled between the DSC and the EOS-TC cask, where the gap nodes specified at the inner side of the cask are restrained in the three translational directions. Initial gaps are based on a DSC outside diameter of 75.50 inches and an EOS-TC inner shell diameter of 76.25 inches, and the side load orientation. Initial gaps are adjusted in consideration of the radial thermal growth of the DSC shell relative to the growth of the cask. Cask rails are simulated by using the difference between cask and DSC radii, combined with the rail thickness, as applicable, and using zero gap contact elements at the rails in initial contact with the DSC and non-zero gap contact elements elsewhere between the DSC and the cask.

To consider the stiffening effect of the DSC end plates on the cylindrical shell, a simplified, half-length model of the DSC shell was used to get more realistic cylindrical shell side drop deformations for gap calculations. The model includes a thick cover plate representing the two cover plates, and contact elements to the nodes at the inner diameter of the cask and cask rails are modeled as described above for the basket model. Symmetry boundary conditions (UY = ROTX = ROTZ = 0) are defined at the end of the model opposite of the cover plate (mid-length of the DSC shell). Elastic-plastic material properties at 400 °F are defined for the shell, based on a bilinear material stress-strain curve with a 1% tangent modulus. The average shell temperature of a horizontally oriented DSC in an EOS-TC for off-normal conditions is less than 435 °F so an approximate value of 400 °F was used. A uniform pressure is applied to a range +/-45 degrees from the bottom to represent the basket and fuel load. Internal pressure and the associated stress stiffening effects are conservatively not modeled. The resulting shell displacements at the symmetry plane of the cylindrical shell, for the upper 140 degrees (+/-70 degrees) opposite from the point of drop, are applied for 180° and 270° side drop load analyses. For the 225° side drop load analyses, the shell displacements at the upper 60 degrees (+/-30 degrees) opposite from the point of drop are applied. This credits the stiffening effect of the DSC end plates while allowing the shell to locally displace around the cask rails based on interaction with loading from the basket components.

3.9.2.3.6.1.2 Material Properties in Analyses

The modeled components of the basket and DSC are based on lower bound material properties. The material properties used for stress/strain analyses are based on representative average temperature values.

For elastic-plastic strain and buckling analyses, bilinear material stress-strain curves are used with a 1% tangent modulus for all materials except the bolts and tie rods. This is consistent with previous licensed basket designs.

3.9.2.3.6.1.3 *Loads*

Load cases are based on the loads described in Chapter 2.

A 65 inch side drop is considered in various orientations to ensure the adequacy of the design under on-site accident side drop conditions. A side drop load of 60g is evaluated to bound the acceleration predicted in Appendix 3.9.3. A 75g end drop is also considered to conservatively envelop the effects of a 65-inch corner drop.

For side loading, the fuel weight load is modeled conservatively using a pressure load equivalent to the applicable acceleration, or G-load, times the fuel assembly weight divided by the basket fuel compartment area associated with the active fuel region length and the fuel compartment width between slots (8.79 inches). A fuel load of 11.0 lbs/in. acting on the fuel compartment width between slots is applied to bound the load distribution in the active fuel region for all PWR fuel types. Figure 3.9.2-8 shows the application of fuel weight pressure loads to the model (for a 180° side drop orientation).

For 0° and 180° side load orientations, the equivalent fuel assembly pressure acts only on the horizontal plates. For 90° and 270° side load orientations, the equivalent fuel assembly pressure acts only on the vertical plates. For other orientations, the equivalent fuel assembly pressure acts perpendicular to the horizontal and vertical plates, proportioned based on the Cosine and Sine of the orientation angle.

The following accident side drop load conditions (DSC and basket in horizontal position) are evaluated:

- *180° Side Drop on Rails*
  (due to symmetry, this also covers the 0° Side Drop)
- *270° Side Drop away from Rails*
  (due to symmetry, this also covers the 90° Side Drop)
- *225° Side Drop on Rails*
  (due to symmetry, this also covers other multiples of 45° Side Drop)

3.9.2.3.6.2 *Criteria*

The basis for allowable strains is obtained from Chapter 8. The strain criteria are discussed and summarized in Section 3.1.1.1.1.

The basket grid plate strain criteria are summarized in Table 3.9.2-5. The threaded fasteners, used to connect the transition rails to the basket grid structure, are not required to be evaluated because they are considered to fail (with analyses and calculations confirming that they are not needed for accident condition drops).

Section 3.9.3.3.2 demonstrates that uncontrolled crack propagation in the basket plates is not an issue for the AISI 4130 material.

3.9.2.3.7 Results

3.9.2.3.7.1 Results for Analysis of 60g Accident Side Loading

60g accident side drop loads are analyzed using the ANSYS model described in Section 3.9.2.3.6.1.1. Accident condition equivalent static elastic-plastic analyses are performed for computing the strains.

The fuel weight load is modeled conservatively using a pressure load equivalent to the applicable acceleration, or G-load, times the maximum fuel assembly weight per length (11.0 lbs/in) divided by the fuel compartment width (8.79 inches).

At the 180° side load orientation, the equivalent 1g fuel assembly pressure, acting only on the horizontal plates, P_{180h}, is calculated as follows:

$$P_{180h} = 11.0 \text{ lbs/in} / (8.79") = 1.2514 \text{ psi}$$

At the 270° side load orientation, 1g acting only on the vertical plates:

$$P_{270v} = 11.0 \text{ lbs/in} / (8.79") = 1.2514 \text{ psi}$$

At 225° (45 degrees from bottom), 1g acting on the horizontal and vertical plates:

$$P_{225h} = P_{225v} = P_{180h} \sin(45°) = 0.8849 \text{ psi}$$

The ANSYS unit (1g) accelerations, indicating direction of load, are:

180-degree	*acel, 0, 0, 1*
270-degree	*acel, 1, 0, 0*
225-degree	*acel, 0.7071, 0, 0.7071*

For side load analyses, the equivalent fuel assembly pressure loads and accelerations above are multiplied by the corresponding side load acceleration value (e.g., 60g).

Displacements, stresses, strains and forces for each converged load step are saved to ANSYS files.

Basket grid plate strain results for accident condition 60g side drop loads are shown in Table 3.9.2-6. Results with controlling strain ratios are shown in Table 3.9.2-7. An ANSYS strain contour plot corresponding to the bounding strain values is shown in Figure 3.9.2-23. The tabulated results show that all strains meet the corresponding allowable strain limits. As demonstrated in Section 3.9.3.3.2, uncontrolled crack propagation in the grid plates is not an issue for the 4130 material.

Analyses are run to 75g. The program stops at the load substep that fails to result in a converged solution, if convergence to 75g does not occur. The last converged load step is considered the buckling load. The buckling load values are compared with 60g, the required g-load for accident conditions, with results shown in Table 3.9.2-8. All analyses complete the 75g load step.

Stresses and strains in the aluminum basket transition rails are not explicitly evaluated. All analyzed drop conditions include the case where the connecting bolts and tie rods are assumed to fail, to demonstrate that the connection to the aluminum is not needed to maintain basket strains within the allowable strain limits. Therefore, the only significant stress in the basket aluminum rails is a bearing type stress where the transition rail is compressed between the basket grid plates and the inside surface of the EOS-DSC. Since bearing stresses are not required to be evaluated for accident conditions, no further evaluation of the basket transition rails is required.

ANSYS Force Summation Comparison

An ANSYS force summation for the basket components only, for the 60g side drop, is compared to the expected load as shown below:

From the ANSYS results for the 60g load step:

Force Summation: Fz = -204,896.4 lb
(in vertical direction (z), length of model is 6 inches)

Expected Load:

Basket weight / length w/o spent fuel:

= (18,900 + 1,080) / (181.5 - 0.9) + (983 + 4,790 + 4,370) / (181.5 - 1.25 - 0.9)

= 167.2 lb/in.

Basket wt. w/o spent fuel (6 inches long) = (167.2) (6 inches) = 1,003 lb.

Spent fuel weight (6" long) = (11 lb/in) (6-inch length of basket) (37 SFAs) = 2,442 lb.

Total weight of the basket, with spent fuel (6 incheslong) = 1,003 + 2,442 = 3,445 lb (for 1g)

Expected Load at 60g (in vertical direction) = 60 (3,445) = 206,700 lb.

The ANSYS load of 204,896 is very similar to the hand-calculated weight load (within 1%) and therefore, is acceptable.

3.9.2.3.7.2 75g Accident End Drop Loading Calculations

Compressive stress associated with the 75g end drop condition is calculated using conservative loads and geometry. For the 75g end drop load condition, the steel grid plates are assumed to carry their own weight plus the weight of all of the aluminum components. The fuel assembly loads are applied directly to the cover plates/shield plugs of the DSC shell assembly and not to the basket assembly. The basket weight considered below bounds the weight summarized in Chapter 3, Table 3-6. The axial stress calculated below represents the general membrane stress in the steel grid plates. The local bearing and peak stresses at the intersections of the slots are not required to be evaluated for accident conditions. There is no significant out-of-plane bending in the grid plates for the 75g end drop condition.

75g axial load:

$\sigma_{Axial\text{-}75g} = 75 (W_{basket}) / A_S$ *(conservative to use full basket weight)*

$W_{basket} = 36.0$ *kips (conservative)*

Section Area, A_S *= summation of plate lengths and thicknesses (from plate details), conservatively excluding slot widths and extensions beyond the last slot of each plate.*

$A_S = 4[\ 0.281"(7)(8.80") + 0.281"(7)(8.80") + 0.281"(5)(8.80") + 0.313"(3)(8.80")]$

$= 221.0\ in^2$

Therefore,

$\sigma_{Axial\text{-}75g} = 75 (36.0) / 221.0$

$= 12.22$ *ksi*

This stress value is low (below yield), such that the 75g end drop load condition strains do not control and no further evaluation is required.

3.9.2.3.7.3 Adjacent Fuel Compartment Relative Displacements

Maximum relative perpendicular displacement from one fuel compartment plate to another is determined from the ANSYS results for the accident side drops. These differences are addressed in the criticality evaluations to ensure that the fuel assembly array pitch does not significantly change due to the accident side drop. The sketch below indicates the sign convention and typical locations where displacements are extracted.

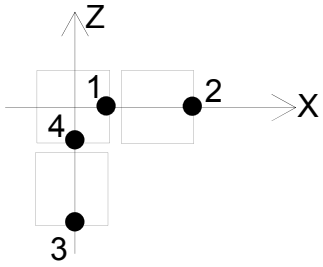

The relative displacements are calculated as follows:

$\Delta_{UX} = UX_2 - UX_1$

$\Delta_{UZ} = UZ_4 - UZ_3$

Maximum relative displacements for those adjacent compartments that have moved closer together are tabulated in Table 3.9.2-9. Relative displacements that indicate fuel compartments have moved away from one another are ignored. The summary table includes results for analyses with bolts and tie rods modeled and for analyses without bolts and tie rods modeled.

3.9.2.3.7.4 Conclusions

Finite element analyses and hand calculations for the EOS-37PTH basket assembly are performed for all accident side and end drop on-site conditions. Controlling strains are reported in Table 3.9.2-7. A comparison of strains to the corresponding allowable values indicates that all load conditions show acceptable results.

As demonstrated in Section 3.9.3.3.2, uncontrolled crack propagation in the grid plates is not an issue for the 4130 material.

3.9.2.4 EOS-89BTH Basket Structural Evaluation for On-Site Accident Drop Loads

This section evaluates the structural integrity of the EOS-89BTH DSC basket for on-site accident side and end drop loads. On-site transfer conditions in the EOS-TC108, EOS-TC125, or EOS-TC135 are considered for thermal properties used in the side drop load analyses.

3.9.2.4.1 General Description

Same as Section3.9.2.2.1.

3.9.2.4.2 Key Dimensions and Materials

Same as Section3.9.2.2.2.

3.9.2.4.3 Material Properties

Same as Section 3.9.2.2.3.

3.9.2.4.4 Temperature Data

Same as Section3.9.2.2.4.

3.9.2.4.5 Fuel Data

Chapter 2 provides design characteristics for the types of BWR FAs to be considered. A maximum FA weight of 705 lbs is used. A distributed weight of 705 lbs / 150 in. = 4.7 lbs/in is considered to be bounding in the active fuel region for the on-site accident side drop analyses.

3.9.2.4.6 Methodology

ANSYS 10.0A1 [3.9.2-2] is used for the evaluation of on-site accident side drop loads. Hand calculations are performed to conservatively calculate the stresses due to the on-site axial end drop loads. Stresses due to the end drop loads are not controlling. Therefore, only the side drop load analysis results are presented.

3.9.2.4.6.1 Finite Element Model

3.9.2.4.6.1.1 Analysis Model Description for Side Loads

Geometry plots of the ANSYS model are shown in Figure 3.9.2-12 through Figure 3.9.2-18. All other details of the analysis model description are the same as Section 3.9.2.3.6.1.1.

3.9.2.4.6.1.2 Material Properties in Analyses

Same as Section 3.9.2.3.6.1.2.

3.9.2.4.6.1.3 Loads

Load cases are based on the loads described in Chapter 2.

A 65 inch side drop is considered in various orientations to ensure the adequacy of the design under on-site accident side drop conditions. A side drop load of 60g is evaluated to bound the acceleration predicted in Appendix 3.9.3. A 75g end drop is also considered to conservatively envelop the effects of a 65 inch corner drop.

For side loading, the fuel weight load is modeled conservatively using a pressure load equivalent to the applicable acceleration, or G-load, times the fuel assembly weight divided by the basket fuel compartment area associated with the active fuel region length and the fuel compartment width between slots (5.85 inches). A fuel load of 4.7 lbs/in acting on the fuel compartment width between slots is applied to bound the load distribution in the active fuel region for all BWR fuel types. Figure 3.9.2-19 shows the application of fuel weight pressure loads to the model (for a 180° side drop orientation).

For 0° and 180° side load orientations, the equivalent fuel assembly pressure acts only on the horizontal plates. For 90° and 270° side load orientations, the equivalent fuel assembly pressure acts only on the vertical plates. For other orientations, the equivalent fuel assembly pressure acts perpendicular to the horizontal and vertical plates, proportioned based on the Cosine and Sine of the orientation angle.

The following accident side drop load conditions (DSC and basket in horizontal position) are evaluated:

- *180° Side Drop on Rails*
  (due to symmetry, this also covers the 0° Side Drop)
- *270° Side Drop away from Rails*
  (due to symmetry, this also covers the 90° Side Drop)
- *225° Side Drop on Rails*
  (due to symmetry, this also covers other multiples of 45° Side Drop)

3.9.2.4.6.2 Criteria

The basis for allowable strains is obtained from Chapter 8. The strain criteria are discussed and summarized in Section 3.1.1.1.1.

The basket grid plate strain criteria are summarized in Table 3.9.2-5. The threaded fasteners, used to connect the transition rails to the basket grid structure, are not required to be evaluated because they are considered to fail (with analyses and calculations confirming that they are not needed for accident condition drops).

Section 3.9.3.3.2 demonstrates that uncontrolled crack propagation in the basket plates is not an issue for the AISI 4130 material.

3.9.2.4.7 Results

3.9.2.4.7.1 Results for Analysis of 60g Accident Side Loading

60g accident side drop loads are analyzed using the ANSYS model described in Section 3.9.2.4.6.1.1. Accident condition equivalent static elastic-plastic analyses are performed for computing the strains.

The fuel weight load is modeled conservatively using a pressure load equivalent to the applicable acceleration, or G-load, times the maximum fuel assembly weight per length (4.7 lbs/in) divided by the fuel compartment width (5.85 inches).

At the 180° side load orientation, the equivalent 1g fuel assembly pressure, acting only on the horizontal plates, P_{180h}, is calculated as follows:

$$P_{180h} = 4.7 \text{ lbs/in} / (5.85 \text{ inches}) = 0.8034 \text{ psi}$$

At the 270° side load orientation, 1g acting only on the vertical plates:

$$P_{270v} = 4.7 \text{ lbs/in} / (5.85 \text{ inches}) = 0.8034 \text{ psi}$$

At 225° (45 degrees from bottom), 1g acting on the horizontal and vertical plates:

$$P_{225h} = P_{225v} = P_{180h} \sin(45°) = 0.5681 \text{ psi}$$

The ANSYS unit (1g) accelerations, indicating direction of load, are:

180-degree	*acel, 0, 0, 1*
270-degree	*acel, 1, 0, 0*
225-degree	*acel, 0.7071, 0, 0.7071*

For side load analyses, the equivalent fuel assembly pressure loads and accelerations above are multiplied by the corresponding side load acceleration value (e.g., 60g).

Displacements, stresses, strains and forces for each converged load step are saved to ANSYS files.

Basket grid plate strain results for accident condition 60g side drop loads are shown in Table 3.9.2-10. Results with controlling strain ratios are shown in Table 3.9.2-11. ANSYS strain contour plots corresponding to the bounding strain values are shown in Figure 3.9.2-24 and Figure 3.9.2-25. The tabulated results show that all strains meet the corresponding allowable strain limits. As demonstrated in Section 3.9.3.3.2, uncontrolled crack propagation in the grid plates is not an issue for the 4130 material.

Analyses are run to 75g. The program stops at the load substep that fails to result in a converged solution, if convergence to 75g does not occur. The last converged load step is considered the buckling load. The buckling load values are compared with 60g, the required g-load for accident conditions, with results shown in Table 3.9.2-8. All analyses complete the 75g load step.

Stresses and strains in the aluminum basket transition rails are not explicitly evaluated. All analyzed drop conditions include the case where the connecting bolts and tie rods are assumed to fail, to demonstrate that the connection to the aluminum is not needed to maintain basket strains within the allowable strain limits. Therefore, the only significant stress in the basket aluminum rails is a bearing type stress where the transition rail is compressed between the basket grid plates and the inside surface of the EOS-DSC. Since bearing stresses are not required to be evaluated for accident conditions, no further evaluation of the basket transition rails is required.

ANSYS Force Summation Comparison

An ANSYS force summation for the basket components only, for the 60g side drop, is compared to the expected load as shown below:

From the ANSYS results for the 60g load step:

Force Summation: Fz = -207,687.2 lb
(in vertical direction (z), length of model is 6 inches)

Expected Load:

Basket weight / length w/o spent fuel:

= (19,300 + 637 + 1,110 + 3,980) / 166.0 + 1,720 / 175.0

= 160.6 lb/in

Basket wt. w/o spent fuel (6 inches long) = (160.6) (6 inches) = 964 lb.

Spent fuel weight (6 inches long) = (4.7 lb/in) (6-inch length of basket) (89 SFAs) = 2,510 lb.

Total weight of the basket, with spent fuel (6 inches long) = 964 + 2,510 = 3,474 lb (for 1g)

Expected Load at 60g (in vertical direction) = 60 (3,474) = 208,440 lb.

The ANSYS load of 207,687 is very similar to the hand-calculated weight load (within 0.4%) and therefore, is acceptable.

3.9.2.4.7.2 75g Accident End Drop Loading Calculations

Compressive stress associated with the 75g end drop condition is calculated using conservative loads and geometry. For the 75g end drop load condition, the steel grid plates are assumed to carry their own weight plus the weight of all of the aluminum components. The fuel assembly loads are applied directly to the cover plates/shield plugs of the DSC shell assembly and not to the basket assembly. The basket weight considered below bounds the weight summarized in Chapter 3, Table 3-7. The axial stress calculated below represents the general membrane stress in the steel grid plates of the holddown ring, for which the plate cross-sectional area is less than other sections of the basket. The local bearing and peak stresses at the intersections of the slots are not required to be evaluated for accident conditions. There is no significant out-of-plane bending in the grid plates for the 75g end drop condition.

75g axial load:

$\sigma_{Axial\text{-}75g} = 75 (W_{basket}) / A_S$ *(conservative to use full basket weight)*

$W_{basket} = 32.0$ *kips (conservative)*

Section Area, A_S *= summation of plate lengths and thicknesses*

The shortest length (top or bottom) of each holddown ring plate is considered, rounded down to the nearest tenth of an inch. The area is reduced by 10% to conservatively account for slots.

$A_S = 0.90(2)[0.250"(69.9") + 0.1875"(46.7") + 0.250"(69.9") + 0.250"(44.8") + 0.250"(19.1") + 0.250"(19.1")]$

$= 116.0\ in^2$

Therefore,

$\sigma_{Axial\text{-}75g} = 75 (32.0) / 116.0$

$= 20.69$ *ksi*

This stress value is low (below yield), such that the 75g end drop load condition strains do not control and no further evaluation is required.

3.9.2.4.7.3 *Adjacent Fuel Compartment Relative Displacements*

Maximum relative perpendicular displacement from one fuel compartment plate to another is determined from the ANSYS results for the accident side drops. These differences are addressed in the criticality evaluations to ensure that the fuel assembly array pitch does not significantly change due to the accident side drop. The sketch below indicates the sign convention and typical locations where displacements are extracted.

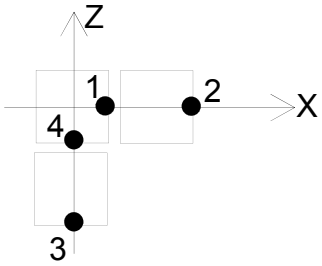

The relative displacements are calculated as follows:

$\Delta_{UX} = UX_2 - UX_1$

$\Delta_{UZ} = UZ_4 - UZ_3$

Maximum relative displacements for those adjacent compartments that have moved closer together are tabulated in Table 3.9.2-13. Relative displacements that indicate fuel compartments have moved away from one another are ignored. The summary table includes results for analyses with bolts and tie rods modeled and for analyses without bolts and tie rods modeled.

3.9.2.4.7.4 *Conclusions*

Finite element analyses and hand calculations for the EOS-89BTH basket assembly are performed for all accident side and end drop on-site conditions. Controlling strains are reported in Table 3.9.2-11. A comparison of strains to the corresponding allowable values indicates that all load conditions show acceptable results.

As demonstrated in Section 3.9.3.3.2, uncontrolled crack propagation in the grid plates is not an issue for the 4130 material.

3.9.2.5 References

3.9.2-1 American Society of Mechanical Engineers, "ASME Boiler and Pressure Vessel Code," Section III, Division 1, Subsection NG, 2010 Edition thru 2011 Addenda.

3.9.2-2 ANSYS Computer Code and User's Manual, Release 10.0.

3.9.2-3 AREVA TN Technical Report, "Evaluation of Creep of NUHOMS® Basket Aluminum Components under Long Term Storage Conditions", E-25768, Rev. 0 (Structural Integrity Associates, Inc. File No. TNI-20Q-302, Rev. 0).

Table 3.9.2-1
Threaded Fastener Stress Design Criteria *(Normal / Off-Normal)*

Stress Category	Allowable Stresses Normal / Off-Normal (1)
Primary + Secondary Membrane $P_m + Q_m$ (2)	min(0.9 S_y, 2/3 S_u)
Primary + Secondary Shear $P_m + Q_m$ (3)(6)	0.6 S_y
Primary + Secondary Bearing $P_m + Q_m$ (4)	2.7 S_y
Primary Membrane P_m (2)	S_m
Primary Shear P_m (3)	0.6 S_m
Primary + Secondary Membrane + Bending $P_m + Q_m + P_b + Q_b$ (5)(6)	min(1.2 S_y, 8/9 S_u)

(1) Classification and stress limits are as defined in ASME Code, Section III, Subsection NG [3.9.2-1].

(2) Averaged stress intensity on tensile stress area at threaded section.

(3) Averaged stress across shear area of threaded section.

(4) Averaged bearing stress under the fastener head.

(5) Stress intensity, excluding effects of stress concentrations.

(6) Not applicable to this evaluation; no significant thermal shear due to oversized/slotted holes, and no significant bending.

Table 3.9.2-2
Component Allowable Stresses *(Normal / Off-Normal)*

Component	Material	Temp. (°F)	Stress Category	Allowable Stress (ksi)
Steel Grid Plates	AISI 4130	700	P_m	24.96
			$P_m + P_b$	37.43
			$P_m + P_b + Q$	74.87
Rail Angle Plates	SA-516 Grade 70	550	P_m	20.00
			$P_m + P_b$	30.00
			$P_m + P_b + Q$	60.00
Transition Rails	Aluminum 6061	550	$P_m + P_b$	4.85
			$P_m + P_b + Q$	9.70
Bolts (1)	SA-193 Grade B7	550	Tension, P_m	28.95
			Tension, $P_m + Q_m$	78.21
			Shear, P_m	17.37
Tie Rods	SA-193 Grade B7	550	Tension, P_m	28.95
			Tension, $P_m + Q_m$	78.21

(1) For basket side loading, only tension loads are transferred through the bolts and tie rods due to oversized/slotted bolts holes that allow for thermal expansion.

Table 3.9.2-3
EOS-37PTH Basket Stress Summary – Enveloped DW + Handling + Thermal

Load Combination	Component	Stress Category	Maximum Stress (ksi) (1)	Allowable Stress (ksi)	Stress Ratio
Enveloping Results for Normal Conditions in the EOS-TC	Grid Plates (3)	P_m	4.61+0.25= 4.86	24.96	0.195
		$P_m + P_b$	23.95+0.25= 24.20	37.43	0.647
		$P_m + P_b + Q$	31.94	74.87	0.427
	Angle Plates	P_m	3.56	20.00	0.178
		$P_m + P_b$	4.63	30.00	0.154
		$P_m + P_b + Q$	12.75	60.00	0.213
	Transition Rails	$P_m + P_b$	2.72	4.85	0.560
		$P_m + P_b + Q$	8.57	9.70	0.883
	Bolts (2)(4)	P_m	12.24	28.95	0.423
		$P_m + Q_m$	44.61	78.21	0.570
	Tie Rods (2)	P_m	7.32	28.95	0.253
		$P_m + Q_m$	14.87	78.21	0.190

(1) $P_m + P_b + Q$ values are determined using ANSYS load combinations.

(2) Bolt and tie rod stresses listed are increased for the reduced area at the threads.

(3) Grid plate stresses include hand calculated stresses for 0.5g axial, where controlled by the DW + (0.5g Vert., 0.5g Trans., 0.5g Ax.) Handling load combination.

(4) Bolt maximum shear stress is 14.84 < 17.37, with a stress ratio of 0.854 per conservative hand calculation for axial handling.

Table 3.9.2-4
EOS-89BTH Basket Stress Summary – Enveloped DW + Handling + Thermal

Load Combination	Component	Stress Category	Maximum Stress (ksi) (1)	Allowable Stress (ksi)	Stress Ratio
Enveloping Results for Normal Conditions in the EOS-TC	Grid Plates (3)	P_m	4.30	24.96	0.172
		$P_m + P_b$	17.11+0.42 =17.53	37.43	0.468
		$P_m + P_b + Q$	23.23+0.42= 23.65	74.87	0.316
	Angle Plates	P_m	1.77	20.00	0.088
		$P_m + P_b$	2.58	30.00	0.086
		$P_m + P_b + Q$	12.52	60.00	0.209
	Transition Rails	$P_m + P_b$	4.47	4.85	0.921
		$P_m + P_b + Q$	11.77	9.70	1.214 (4)
	Bolts (2)(5)	P_m	6.15	28.95	0.212
		$P_m + Q_m$	24.47	78.21	0.313
	Tie Rods (2)	P_m	2.99	28.95	0.103
		$P_m + Q_m$	8.59	78.21	0.110

(1) $P_m + P_b + Q$ values are determined using ANSYS load combinations.

(2) Bolt and tie rod stresses listed are increased for the reduced area at the threads.

(3) Grid plate stresses include hand calculated stresses for 0.5g axial, where controlled by the DW + (0.5g Vert., 0.5g Trans., 0.5g Ax.) Handling load combination.

(4) This level of stress occurs only at very small locations at locations of bolts, and they are considered to be peak stresses. In addition, most of this stress is due to thermal, occurs during initial heat-up, is not cyclic and therefore, is not a fatigue concern. Stresses away from these small areas are significantly lower and well within the allowable stress.

(5) Bolt maximum shear stress is 14.92 < 17.37, with a stress ratio of 0.859 per conservative hand calculation for axial handling.

Table 3.9.2-5
Basket Grid Plate Accident Drop Strain Design Criteria

Strain Category	***Allowable Strains*** [2]
	Accident [1]
Primary Membrane ε_m	*1.0%*
Primary Membrane + Bending $\varepsilon_m + \varepsilon_b$	*3.0%*
Primary + Peak $\varepsilon_m + \varepsilon_b + \varepsilon_F$	*10.0%* [3]
Compression or Buckling	*Note 4*

(1) Basket strain limits are described in Chapter 3.

(2) Plastic strain limits.

(3) Membrane + bending strains determined from the analyses conservatively include peak strain, such that the limit on primary + peak does not need to be evaluated.

(4) Determine the buckling load for each postulated drop orientation to demonstrate that the basket does not buckle within maximum drop load of 60g. Report the safety margin.

Table 3.9.2-6
EOS-37PTH Basket Grid Plate Strain Summary – Side Drops with and without Bolts and Tie Rods

Side Drop Load Case	***Fastener Status***	***Strain (1) Category***	***Maximum Strain/Stress (in/in / ksi)***	***Allowable Strain/Stress (in/in / ksi)***
60g, 180 deg. Side Drop	*with Bolts/Tie Rods*	ε_m	*0.00000*	*0.01*
		$\varepsilon_m + \varepsilon_b$	*0.00797*	*0.03*
	without (2) Bolts/Tie Rods	ε_m	*0.00000*	*0.01*
		$\varepsilon_m + \varepsilon_b$	*0.00834*	*0.03*
60g, 270 deg. Side Drop	*with Bolts/Tie Rods*	ε_m	*0.00000*	*0.01*
		$\varepsilon_m + \varepsilon_b$	*0.00770*	*0.03*
	without (2) Bolts/Tie Rods	ε_m	*0.00000*	*0.01*
		$\varepsilon_m + \varepsilon_b$	*0.00807*	*0.03*
60g, 225 deg. Side Drop	*with Bolts/Tie Rods*	ε_m	*0.00000*	*0.01*
		$\varepsilon_m + \varepsilon_b$	*0.00400*	*0.03*
	without (2) Bolts/Tie Rods	ε_m	*0.00000*	*0.01*
		$\varepsilon_m + \varepsilon_b$	*0.00376*	*0.03*

(1) Von Mises plastic strain.

(2) Bolts and tie rods are removed from the model for this analysis, assuming that they fail.

Table 3.9.2-7
EOS-37PTH Basket Grid Plate Strain Summary – Enveloped Accident Conditions

Load Combination	***Strain (1) Category***	***Maximum Strain/Stress (in/in / ksi)***	***Allowable Strain/Stress (in/in / ksi)***	***Strain Ratio***
Enveloping Results for Accident Conditions in the EOS-TC	ε_m	*0.00000*	*0.01*	*0.000*
	$\varepsilon_m + \varepsilon_b$	*0.00834*	*0.03*	*0.278*

(1) Von Mises plastic strain.

Table 3.9.2-8
EOS-37PTH Basket Buckling Analysis Results Summary

Load Condition	*Last Converged Load (G)*	*Actual Max. Load (G)*	*Factor of Safety*
60g 180 deg. drop, with bolts & tie rods	*75.0 (1)*	*60.0*	*1.25*
60g 270 deg. drop, with bolts & tie rods	*75.0 (1)*	*60.0*	*1.25*
60g 225 deg. drop, with bolts & tie rods	*75.0 (1)*	*60.0*	*1.25*
60g 180 deg. drop, without bolts & tie rods	*75.0 (1)*	*60.0*	*1.25*
60g 270 deg. drop, without bolts & tie rods	*75.0 (1)*	*60.0*	*1.25*
60g 225 deg. drop, without bolts & tie rods	*75.0 (1)*	*60.0*	*1.25*

(1) A maximum load of 75g was applied. Therefore, the buckling load and factor of safety may be greater.

Table 3.9.2-9
EOS-37PTH Basket Maximum Adjacent Fuel Compartment Relative Displacements

Load Condition	***Drop Orientation***	***Maximum Absolute Relative Displacement (in)[1]***			
		With Bolts & Tie Rods		***Without Bolts & Tie Rods***	
		Δ_{UX}	Δ_{UZ}	Δ_{UX}	Δ_{UZ}
60g Accident Side Drop	*180°*	*0.039726*	*0.078975*	*0.062991*	*0.083127*
	270°	*0.075675*	*0.056695*	*0.077194*	*0.046207*
	225°	*0.069254*	*0.077784*	*0.069877*	*0.078839*

(1) For displacements that indicate fuel compartments have moved closer together. Obtained from results for the 60g load step.

Table 3.9.2-10
EOS-89BTH Basket Grid Plate Strain Summary – Side Drops with and without Bolts and Tie Rods

Side Drop Load Case	*Fastener Status*	*Strain (1) Category*	*Maximum Strain/Stress (in/in / ksi)*	*Allowable Strain/Stress (in/in / ksi)*
60g, 180 deg. Side Drop	*with Bolts/Tie Rods*	ε_m	*0.00000*	*0.01*
		$\varepsilon_m + \varepsilon_b$	*0.00595*	*0.03*
	without (2) Bolts/Tie Rods	ε_m	*0.00000*	*0.01*
		$\varepsilon_m + \varepsilon_b$	*0.00611*	*0.03*
60g, 270 deg. Side Drop	*with Bolts/Tie Rods*	ε_m	*0.00049*	*0.01*
		$\varepsilon_m + \varepsilon_b$	*0.00498*	*0.03*
	without (2) Bolts/Tie Rods	ε_m	*0.00000*	*0.01*
		$\varepsilon_m + \varepsilon_b$	*0.00491*	*0.03*
60g, 225 deg. Side Drop	*with Bolts/Tie Rods*	ε_m	*0.00000*	*0.01*
		$\varepsilon_m + \varepsilon_b$	*0.00264*	*0.03*
	without (2) Bolts/Tie Rods	ε_m	*0.00000*	*0.01*
		$\varepsilon_m + \varepsilon_b$	*0.00229*	*0.03*

(1) Von Mises plastic strain.

(2) Bolts and tie rods are removed from the model for this analysis, assuming that they fail.

Table 3.9.2-11
EOS-89BTH Basket Grid Plate Strain Summary – Enveloped Accident Conditions

Load Combination	***Strain (1) Category***	***Maximum Strain/Stress (in/in / ksi)***	***Allowable Strain/Stress (in/in / ksi)***	***Strain Ratio***
Enveloping Results for Accident Conditions in the EOS-TC	ε_m	*0.00049*	*0.01*	*0.049*
	$\varepsilon_m + \varepsilon_b$	*0.00611*	*0.03*	*0.204*

(1) Von Mises plastic strain.

Table 3.9.2-12
EOS-89BTH Basket Buckling Analysis Results Summary

Load Condition	*Last Converged Load (G)*	*Actual Max. Load (G)*	*Factor of Safety*
60g 180 deg. drop, with bolts & tie rods	*75.0 (1)*	*60.0*	*1.25*
60g 270 deg. drop, with bolts & tie rods	*75.0 (1)*	*60.0*	*1.25*
60g 225 deg. drop, with bolts & tie rods	*75.0 (1)*	*60.0*	*1.25*
60g 180 deg. drop, without bolts & tie rods	*66.975*	*60.0*	*1.12*
60g 270 deg. drop, without bolts & tie rods	*75.0 (1)*	*60.0*	*1.25*
60g 225 deg. drop, without bolts & tie rods	*75.0 (1)*	*60.0*	*1.25*

(1) A maximum load of 75g was applied. Therefore, the buckling load and factor of safety may be greater.

Table 3.9.2-13
EOS-89BTH Basket Maximum Adjacent Fuel Compartment Relative Displacements

Load Condition	***Drop Orientation***	***Maximum Absolute Relative Displacement (in)[1]***			
		With Bolts & Tie Rods		***Without Bolts & Tie Rods***	
		Δ_{UX}	Δ_{UZ}	Δ_{UX}	Δ_{UZ}
60g Accident Side Drop	*180°*	*0.021608*	*0.045477*	*0.022232*	*0.056033*
	270°	*0.032627*	*0.040907*	*0.040814*	*0.022854*
	225°	*0.031594*	*0.041521*	*0.027013*	*0.042423*

(1) For displacements that indicate fuel compartments have moved closer together. Obtained from results for the 60g load step.

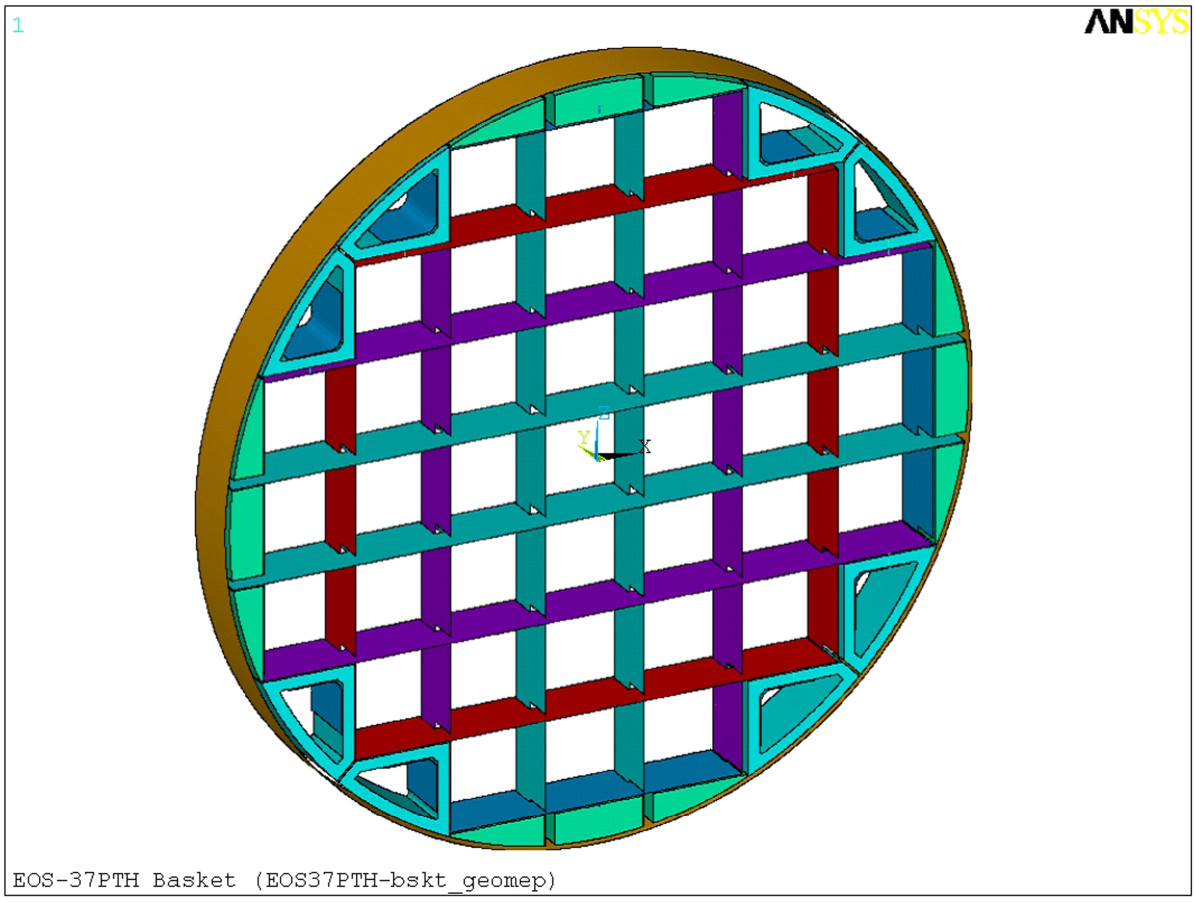

Figure 3.9.2-1
EOS-37PTH Basket Assembly ANSYS .Model (Components Only)
– Isometric View

Figure 3.9.2-2
EOS-37PTH Basket Assembly ANSYS Model (Components Only)
– Isometric View
Upper-Left Quadrant

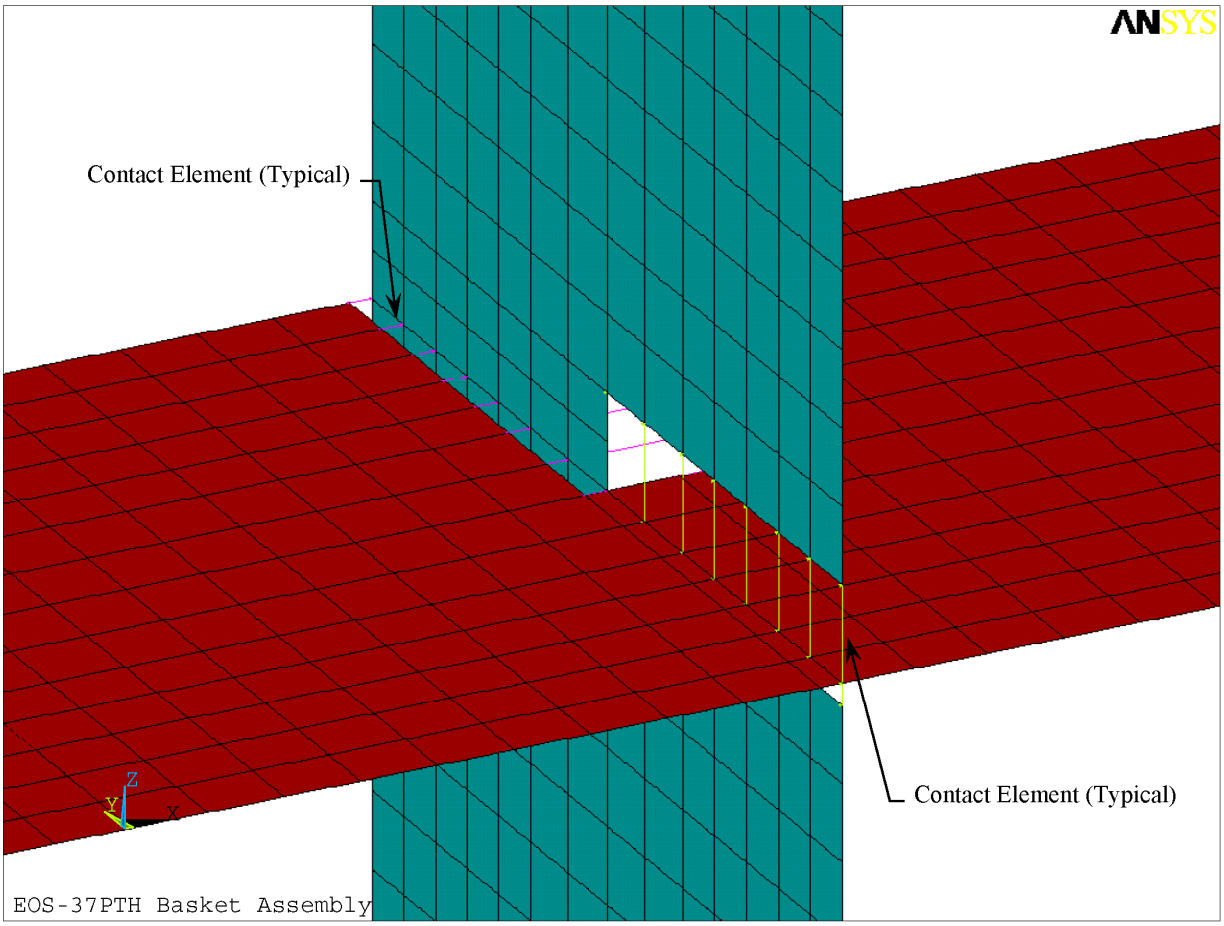

Figure 3.9.2-3
EOS-37PTH Basket Assembly Typical Grid Plate Intersection

Figure 3.9.2-4
EOS-37PTH Basket Assembly ANSYS Model (Components Only) – Front View

Figure 3.9.2-5
EOS-37PTH Basket Assembly ANSYS Model (Plate Thicknesses)
Lower Right Quadrant

Figure 3.9.2-6
EOS-37PTH Basket Assembly ANSYS Model (with Contact Elements) – Lower Right Quadrant

Figure 3.9.2-7
EOS-37PTH Basket Assembly ANSYS Model
−Transition Rail Bolt and Tie Rod Locations

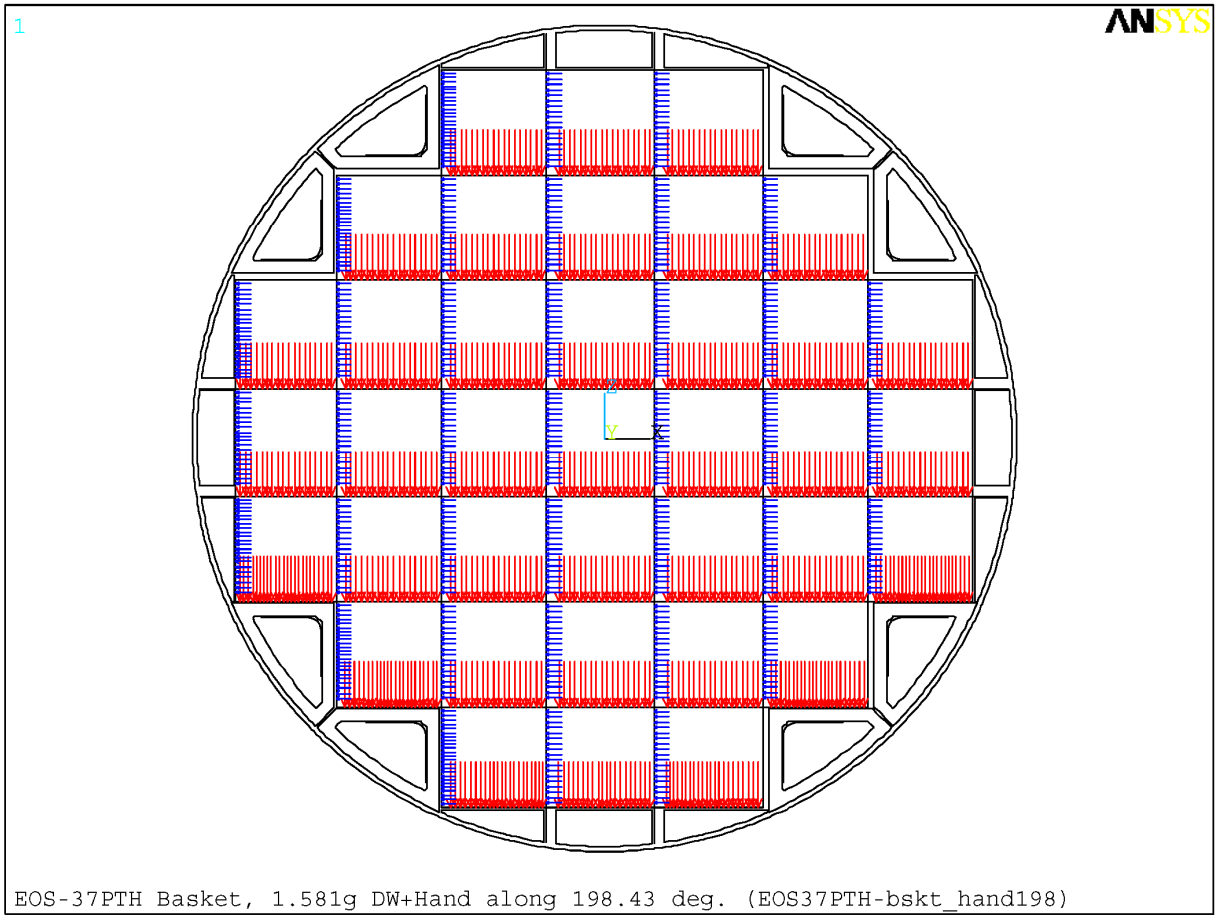

Figure 3.9.2-8
EOS-37PTH Basket Assembly ANSYS Model – Fuel Load Applied as Pressure

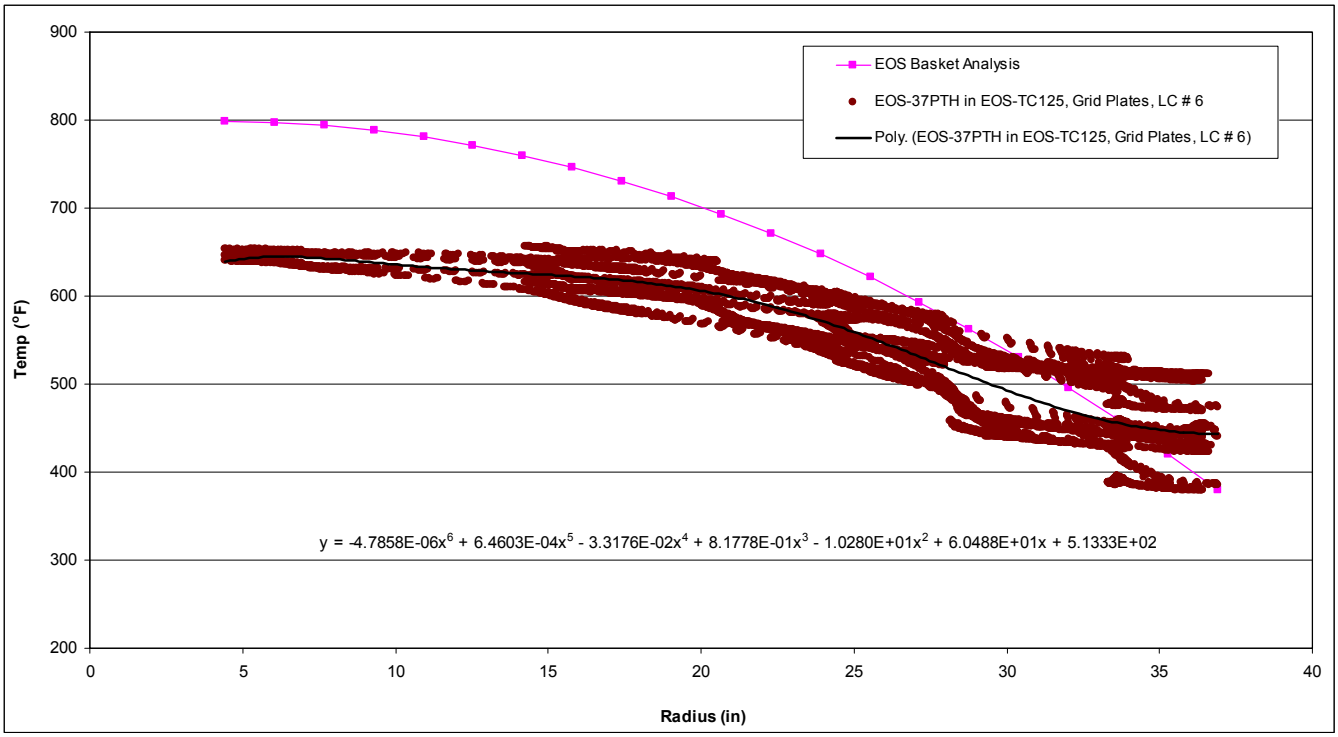

Figure 3.9.2-9
Comparison of Applied Temperature Profile to Data from Thermal Analysis for EOS-37PTH Basket Plates – Hottest Cross-Section, LC # 6, Horizontal, Off-Normal Hot Transfer in EOS-TC125, Outdoor

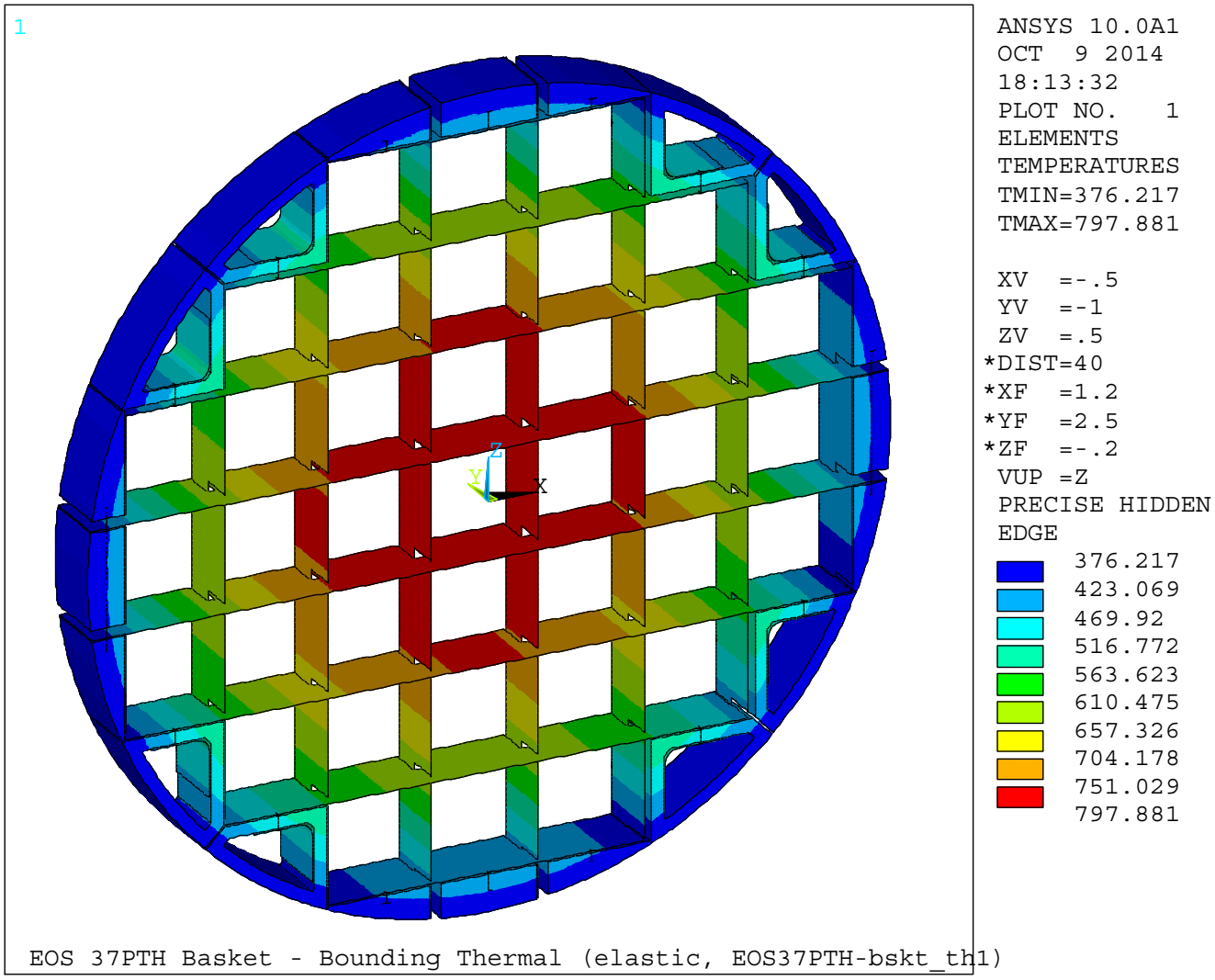

Figure 3.9.2-10
EOS-37PTH Basket Assembly ANSYS Model – Applied Bounding Thermal Profile

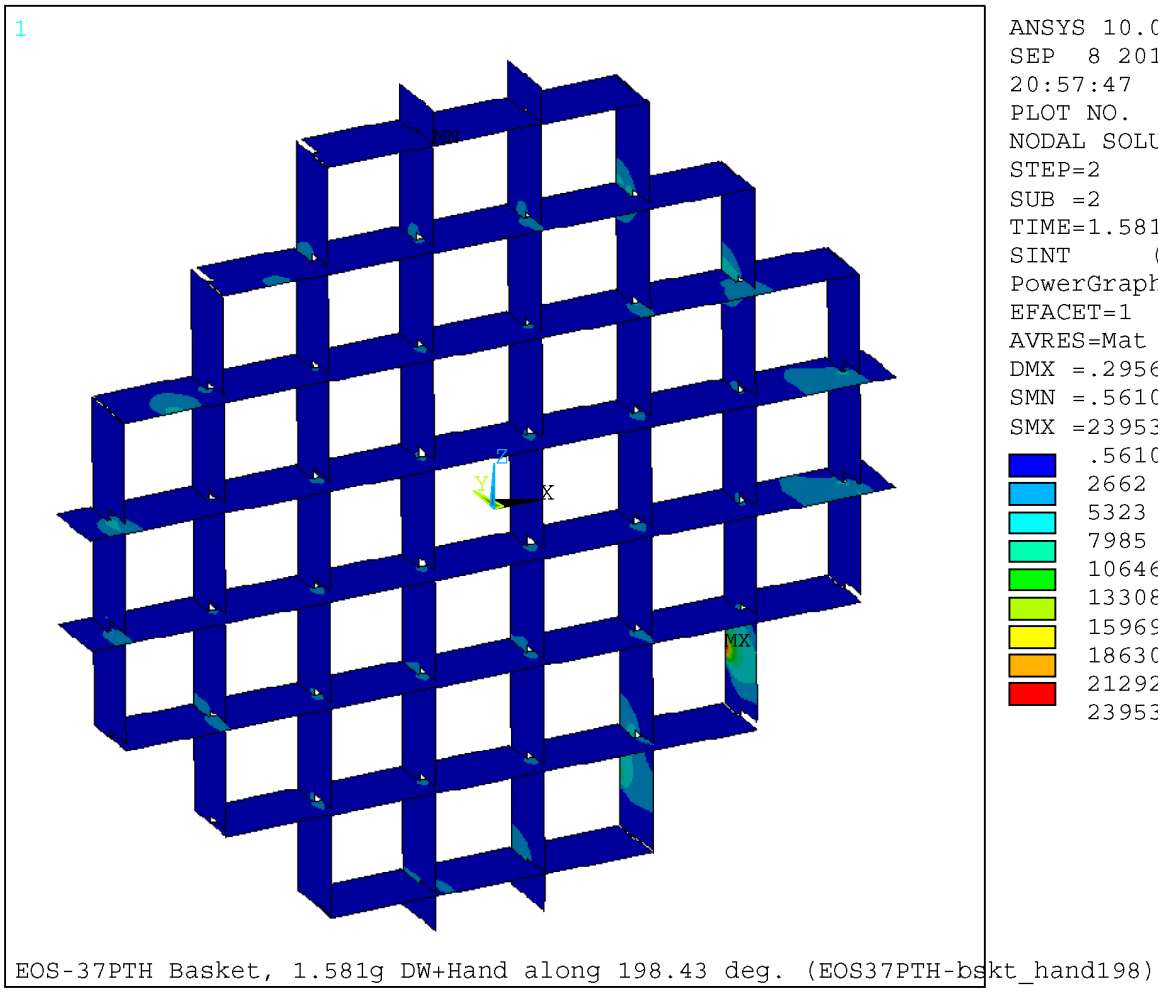

Figure 3.9.2-11
EOS-37PTH Basket 198.43 Degree 1.581g, DW + Handling
– Grid Plates, $P_m + P_b$ (stress intensity, psi)

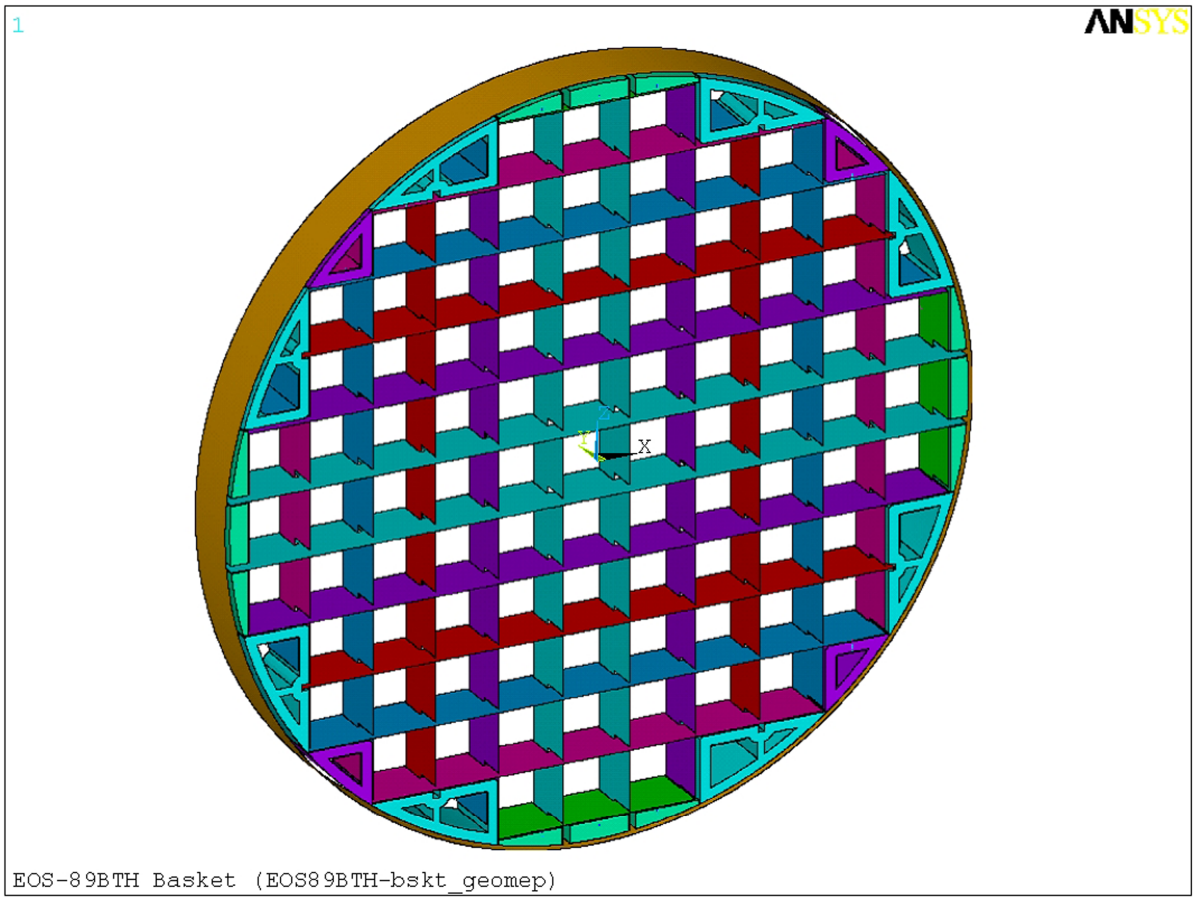

Figure 3.9.2-12
EOS-89BTH Basket Assembly ANSYS Model (Components Only) – Isometric View

Figure 3.9.2-13
EOS-89BTH Basket Assembly ANSYS Model (Components Only) –
Isometric View –
Upper-Left Quadrant

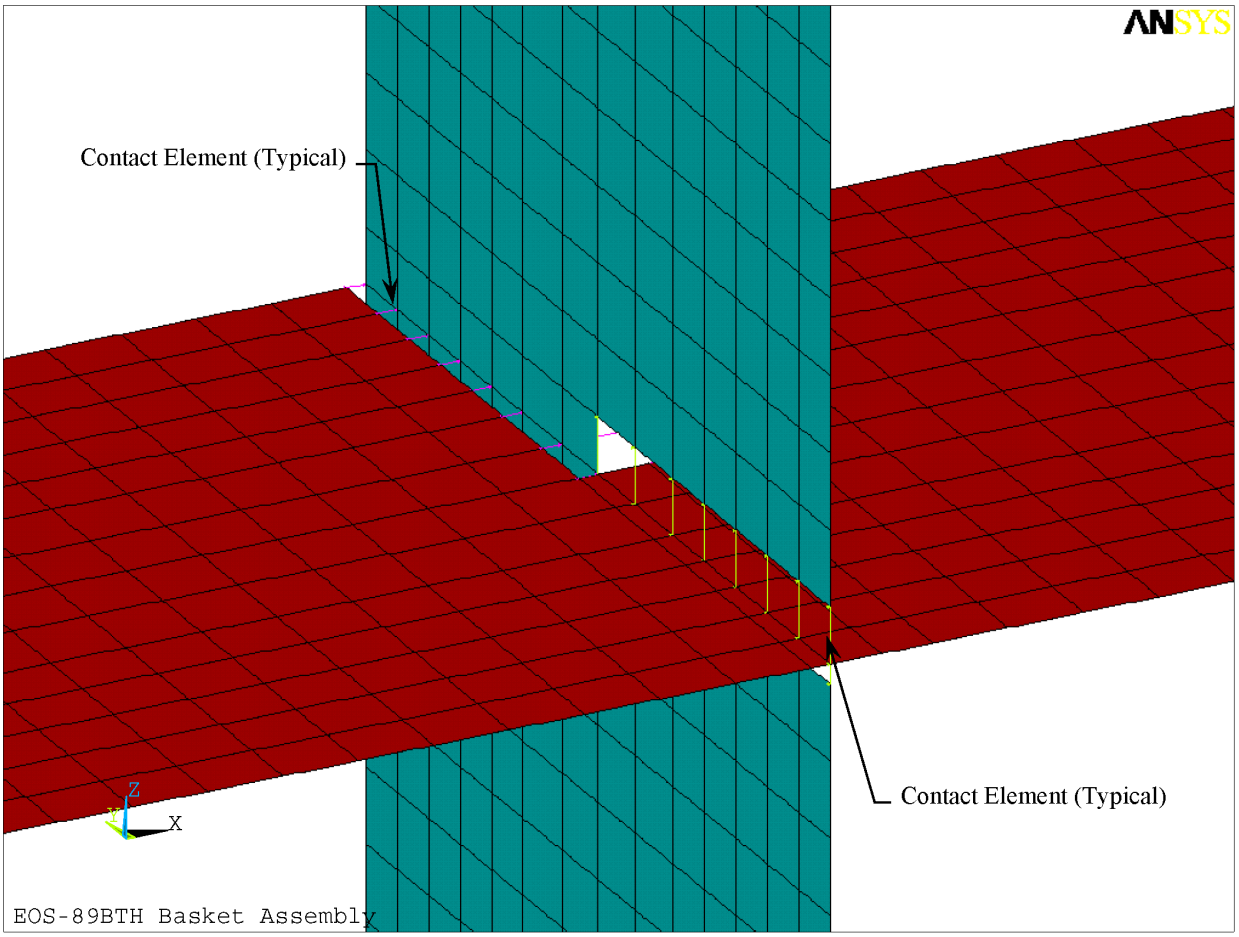

Figure 3.9.2-14
EOS-89BTH Basket Assembly Typical Grid Plate Intersection

Figure 3.9.2-15
EOS-89BTH Basket Assembly ANSYS Model (Components Only) – Front View

Figure 3.9.2-16
EOS-89BTH Basket Assembly ANSYS Model (Plate Thicknesses) –
Lower Right Quadrant

Figure 3.9.2-17
EOS-89BTH Basket Assembly ANSYS Model (with Contact Elements) – Lower Right Quadrant

Figure 3.9.2-18
EOS-89BTH Basket Assembly ANSYS Model –
Transition Rail Bolt and Tie Rod Locations

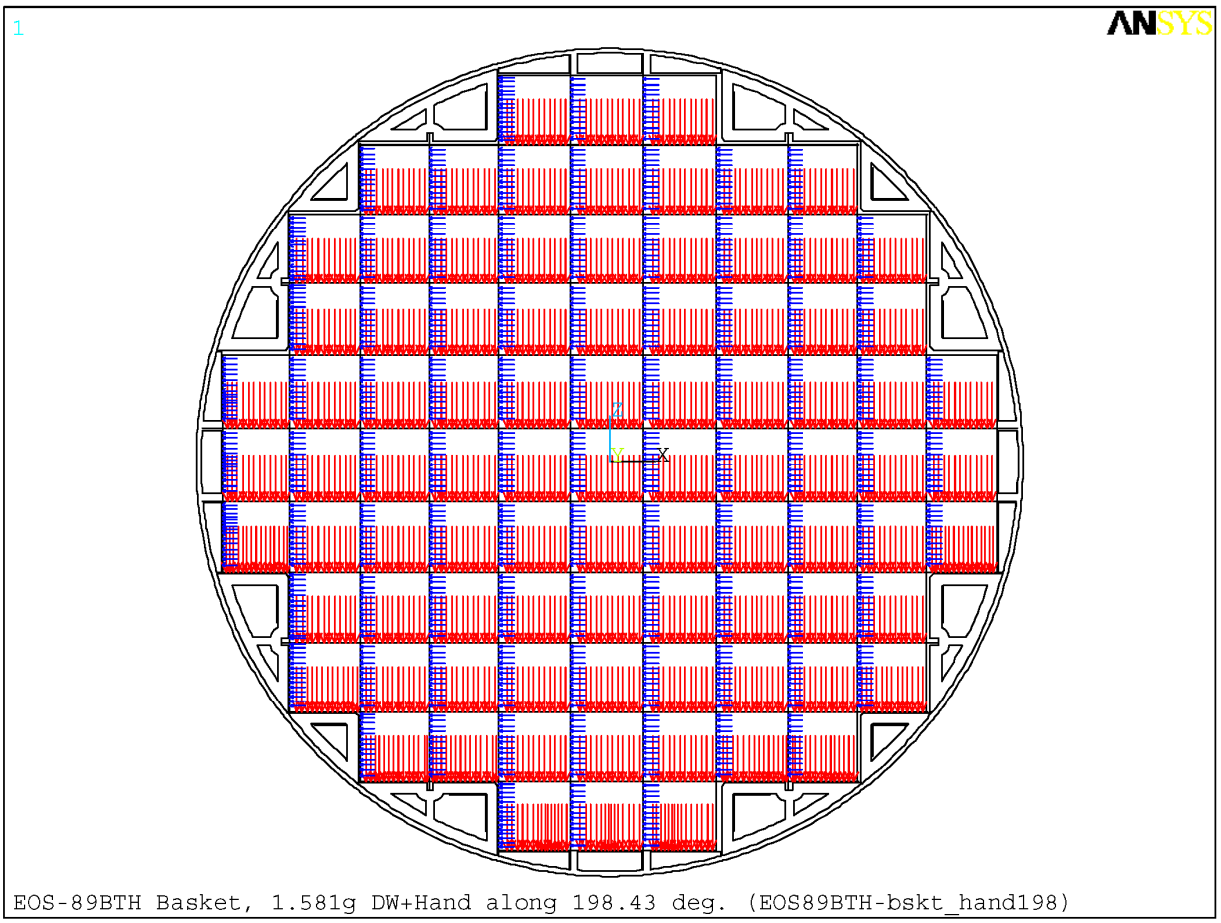

Figure 3.9.2-19
EOS-89BTH Basket Assembly ANSYS Model – Fuel Load Applied as Pressure

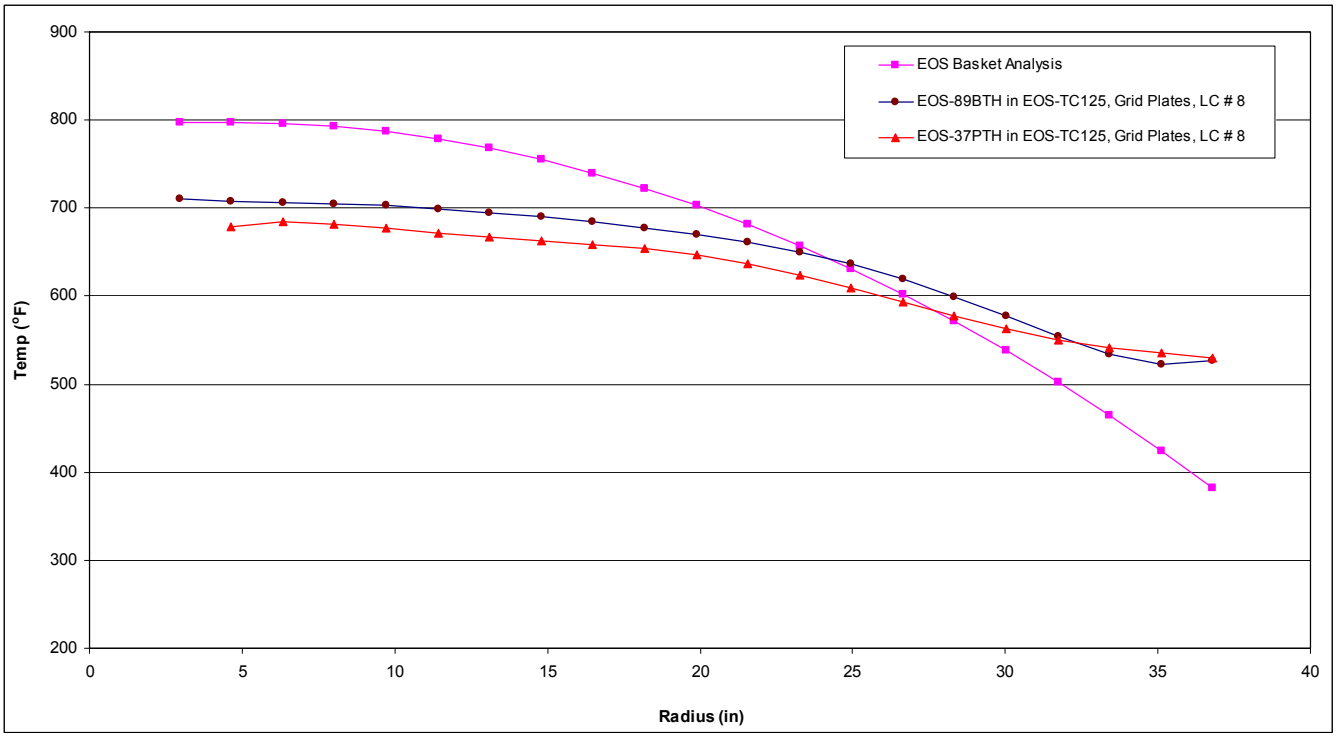

Figure 3.9.2-20
Comparison of EOS-89BTH and EOS-37PTH Temperatures (Curve Fits)
LC # 8, Vertical, Normal Hot Transfer in EOS-TC125, Indoor

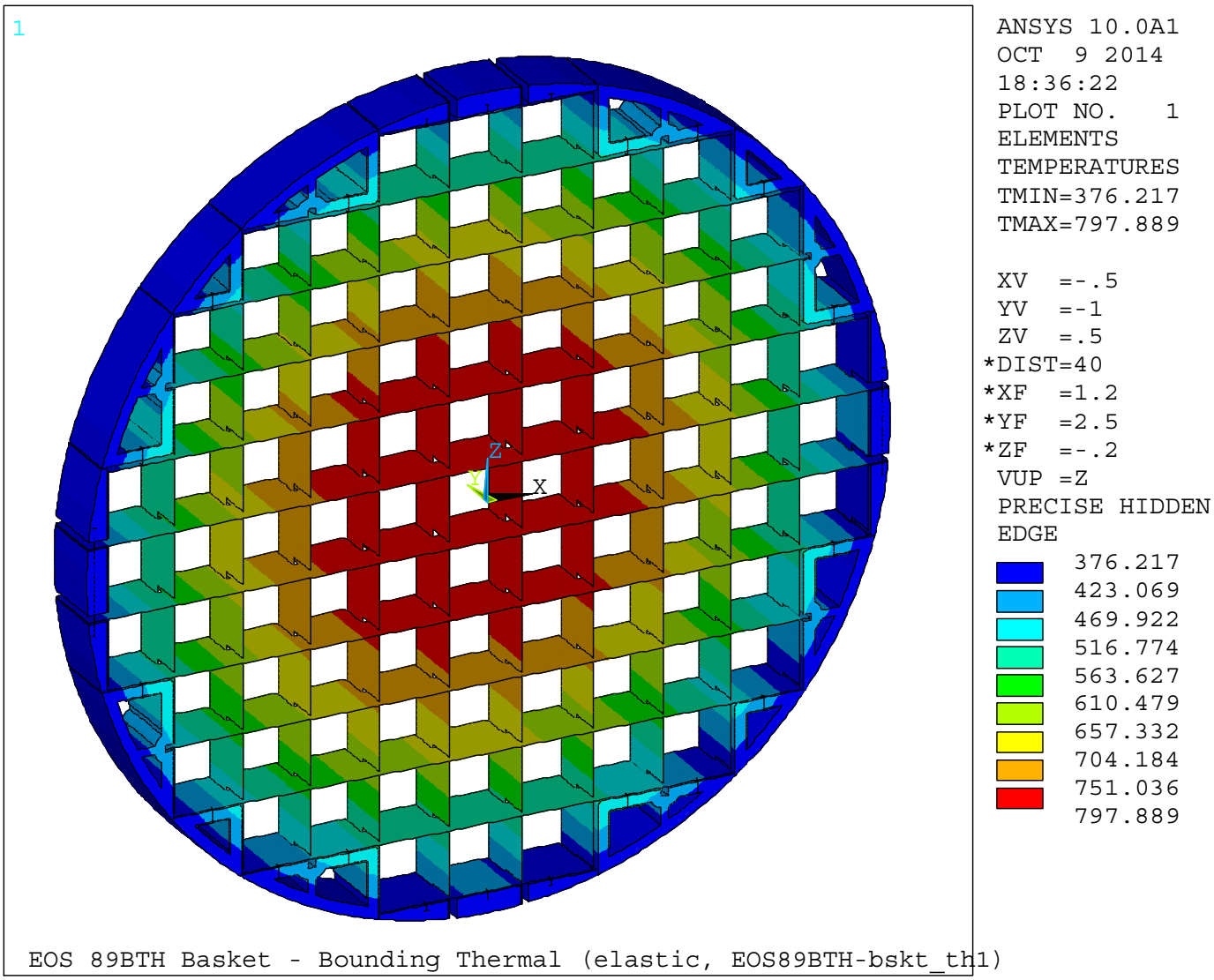

Figure 3.9.2-21
EOS-89BTH Basket Assembly ANSYS Model – Applied Bounding Thermal Profile

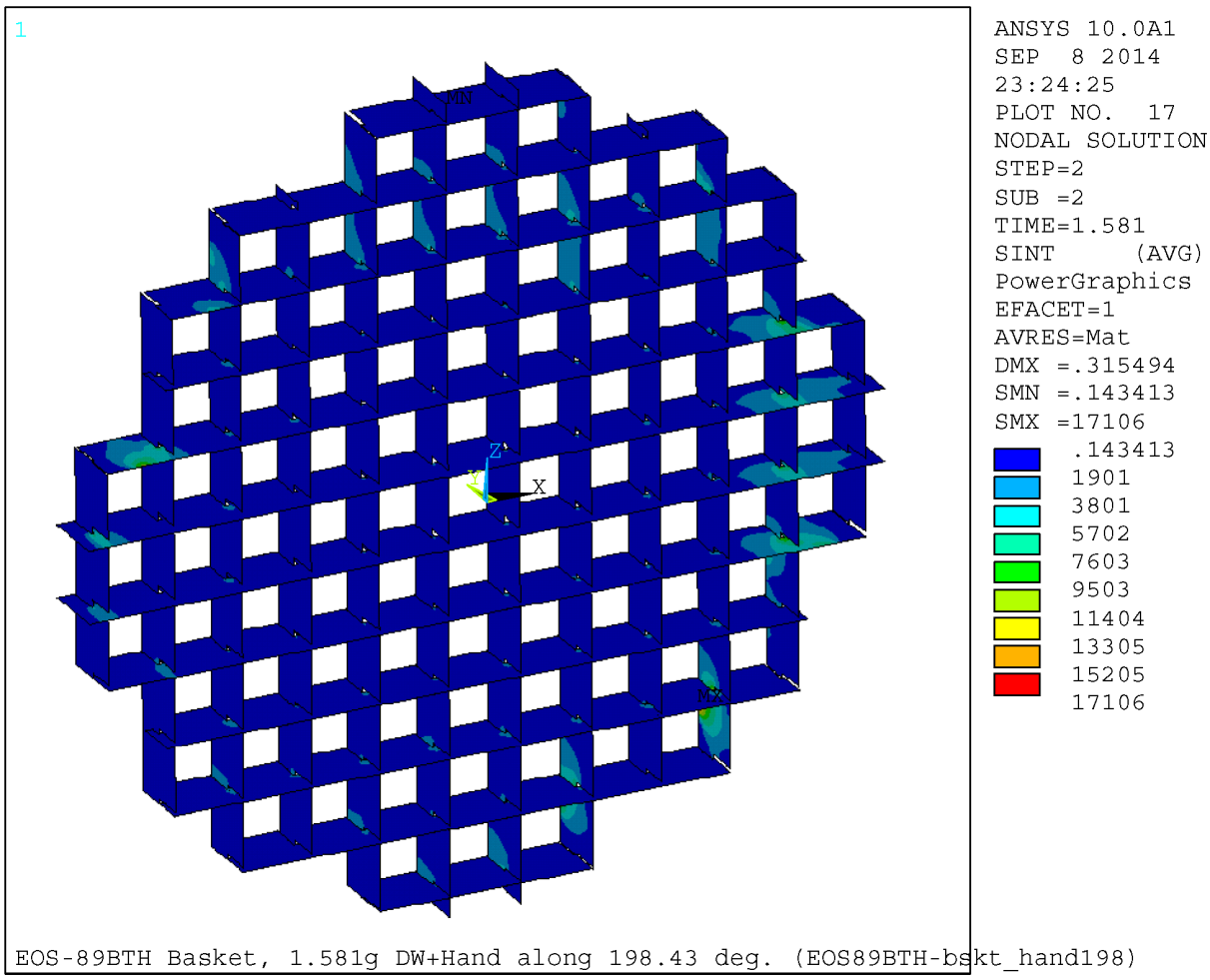

Figure 3.9.2-22
EOS-89BTH Basket 198.43 Degree 1.581g, DW + Handling
– Grid Plates, $P_m + P_b$ (stress intensity, psi)

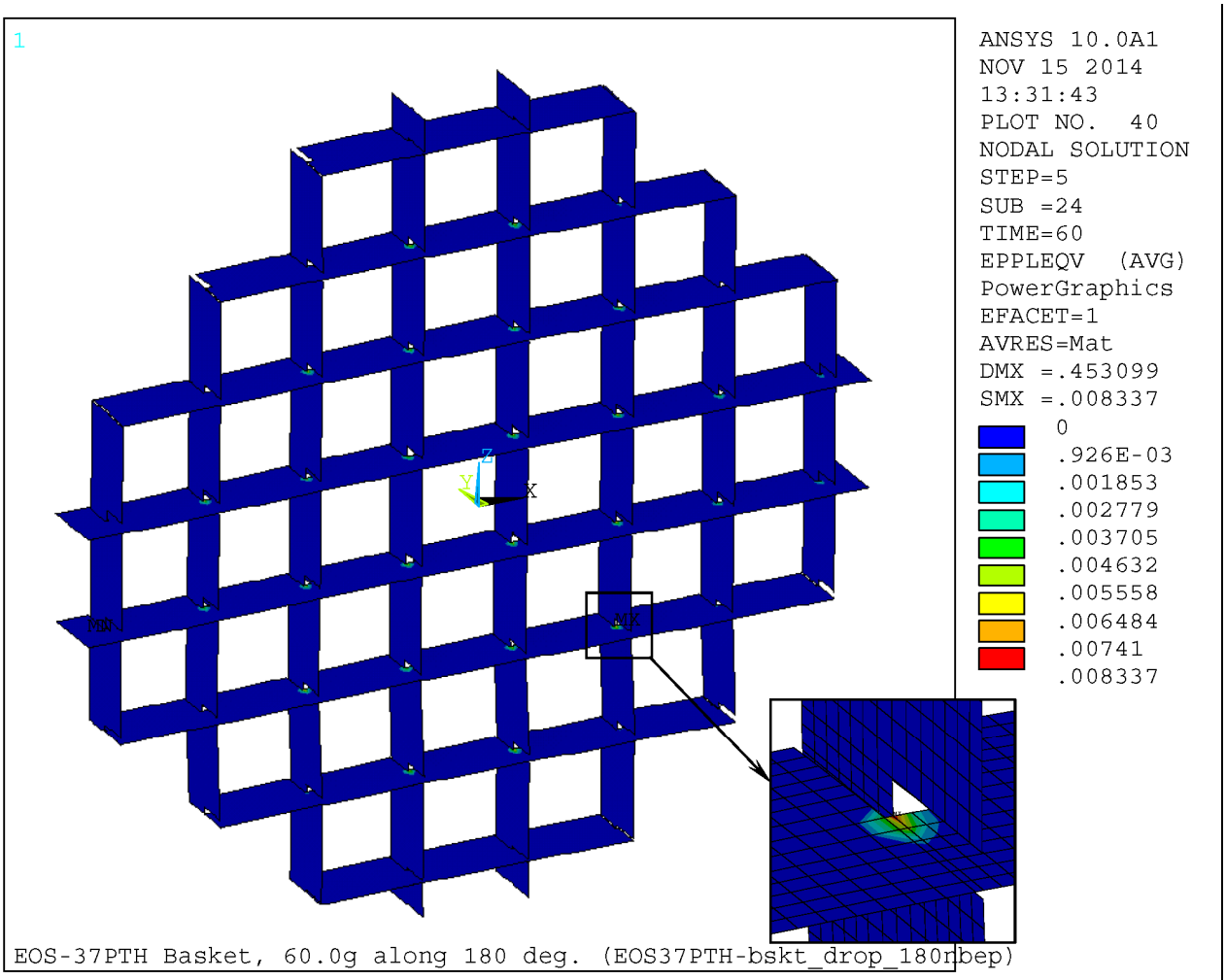

Figure 3.9.2-23
EOS-37PTH Basket 180 Degree 60g Side Drop (without bolts / tie rods) – Grid Plates, $\varepsilon_m + \varepsilon_b$ (von Mises Plastic Strain, in/in)

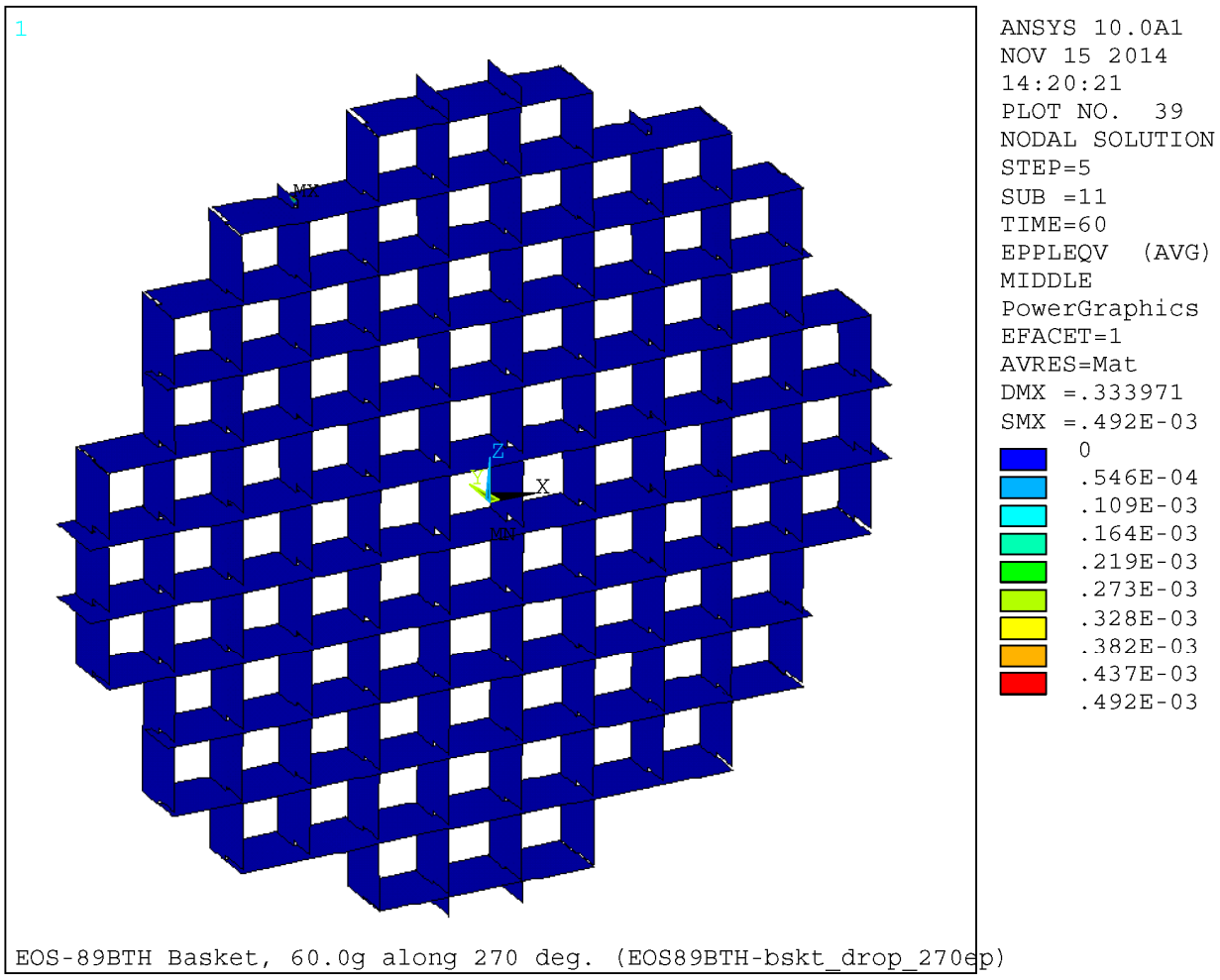

Figure 3.9.2-24
EOS-89BTH Basket 270 Degree 60g Side Drop (with bolts / tie rods) – Grid Plates, ε_m (von Mises Plastic Strain, in/in)

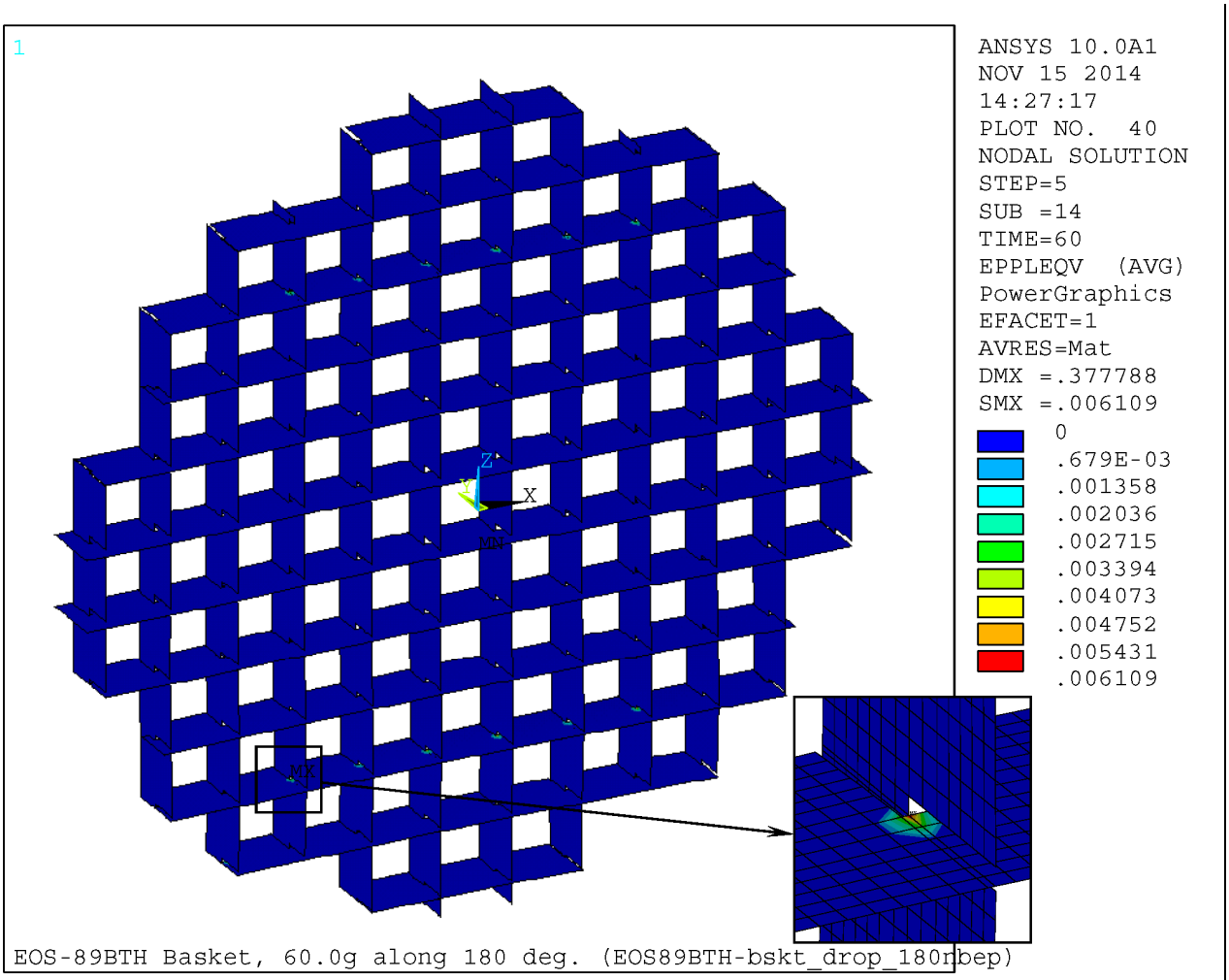

Figure 3.9.2-25
EOS-89BTH Basket 180 Degree 60g Side Drop (without bolts / tie rods) – Grid Plates, $\varepsilon_m + \varepsilon_b$ (von Mises Plastic Strain, in/in)

Proprietary Information on Pages 3.9.3-i through 3.9.3-iii and 3.9.3-1 through 3.9.6-38
Withheld Pursuant to 10 CFR 2.390

APPENDIX 3.9.4
EOS-HSM STRUCTURAL ANALYSIS

Table of Contents

List of Tables

List of Figures

3.9.4 EOS-HSM STRUCTURAL ANALYSIS

The purpose of this appendix is to present the structural evaluation of the EOS-HSM due to all applied loads during storage, loading and unloading operation. The NUHOMS® EOS System consists of the dual-purpose (transportation and storage) EOS-37PTH and EOS-89BTH dry shielded canister (DSC), a horizontal storage module (EOS-HSM), an onsite transfer cask (EOS-TC), and associated ancillary equipment.

3.9.4.1 General Description

General description and operational features for the NUHOMS® EOS System is provided in Chapter 1. The EOS-HSM is a freestanding, reinforced concrete structure, designed to provide environmental protection and radiological shielding for the EOS-37PTH DSC or EOS-89BTH DSC. The drawings of the EOS-HSM, showing different components and overall dimensions, are provided in Chapter 1.

The EOS-HSM consists of a base unit and a roof unit. The roof unit rests mainly on the front and rear walls, and partly on the side walls of the base unit. The roof and the base are connected by bolts/embedments to form a single module via four steel brackets located at each of the interior upper corners of base unit.

An alternate multi-segment design of horizontal storage module, the EOS-HSMS, may also be used in lieu of EOS-HSM as a part of NUHOMS® EOS System. The EOS-HSMS consists of two segments of the base unit and a roof unit. The two segments of base unit of EOS-HSMS are connected by grouted, high-strength, threaded bars/embedments, and the base and roof are connected in a similar way to that of EOS-HSM. EOS-HSM is used herein for both EOS-HSM and EOS-HSMS, unless a unique situation is presented.

The EOS-HSM storage modules can be arranged either in a single-row array, or in back-to-back double-row arrays by placing a module next to, and in contact with, adjacent module(s) with thick end shield walls connected to the EOS-HSM at the end of the arrays. The thick rear shield walls are also connected to the back wall of the EOS-HSM, if the modules are placed in a single-row array.

The EOS-37PTH DSC or EOS-89BTH DSC is supported inside the EOS-HSM by DSC support structure. The DSC support structure is comprised of two main support beams, two extension plates and two nitronic sliding rails and it spans between the front wall and the rear wall of the base unit. The web of the main support beams has openings to allow the air flow around the DSC. The DSC support structure provides support for the DSC during storage and also acts as a sliding surface during the insertion and retrieval of DSC.

The width of EOS-HSM is 116 inches. The overall height of EOS-HSM is 240 inches including the outlet vent cover. Three different EOS-HSM lengths are available in order to accommodate DSCs of different lengths. The internal cavity of the EOS-HSM accommodates DSCs of variable length by varying the location of the axial retainer and by variation of gap between the DSC and the EOS-HSM back wall.

The air inlet vents located at the front lower corners of base unit extend through the bottom of side wall on both sides, which ultimately lead to the cavity of base unit. The air outlet vents are provided in the roof at both sides of the module.

The front wall of EOS-HSM base unit has round access door opening provided for transferring EOS-37PTH DSC or EOS-89BTH DSC into the module or retrieving it from the module. The door opening is closed by a shield door after the insertion of EOS-37PTH DSC or EOS-89BTH DSC. The EOS-HSM shield door is a combination of rectangular and cylindrical concrete block with steel backing plate on the inside face. The shield door provides environmental protection, including missile and shielding protection.

End shield walls are installed at each end of a module array to provide the required missile and shielding protection. Similarly, a rear shield wall is installed at the rear of each module of the single row module array for same purpose.

For thermal protection of the EOS-HSM concrete, a thin stainless steel heat shield is installed inside the EOS-HSM. The interior surface of the upper part of the side wall is protected with side heat shields, and the underside of the roof unit is protected with a roof heat shield. The roof heat shield has an upward slope at 10 degrees from center towards outlet vent. The heat shield guides the cooling air flow through the EOS-HSM.

During DSC insertion and retrieval operations, the EOS-TC is docked with the EOS-HSM docking surface and mechanically secured to the cask restraint embedments provided in the front wall of the base unit. These embedments are equally spaced on either side of the door opening and located near the lower embedment for door attachment.

3.9.4.2 Material Properties

The material properties used in the analysis and design of EOS-HSM and its components are discussed in detail in Chapter 8.

3.9.4.3 Design Criteria

The reinforced concrete EOS-HSM and the DSC support structure are important to safety components of NUHOMS® EOS System. Consequently, they are designed and analyzed to perform their intended functions under the extreme environmental and natural phenomena specified in 10 CFR 72.122 [3.9.4-1] and American National Standards Institute (ANSI) 57.9 [3.9.4-10]. These include tornado and wind, seismic, and flood design criteria. The design wind pressure is determined as per American Society of Civil Engineers (ASCE) 7-10 [3.9.4-15].

The concrete EOS-HSM and steel DSC support structures are designed to the requirements of American Concrete Institute (ACI) 349-06 [3.9.4-12] and the American Institute of Steel Construction (AISC) Manual of Steel Construction [3.9.4-14], respectively, using the load combinations prescribed by ANSI 57.9 [3.9.4-10]. When ACI-349-06 does not have enough information, ACI-318-08 [3.9.4-11] is used as supplement. The following table summarizes the Codes and Standards for design and fabrication of these components.

Component	Material	Applicable Code
EOS-HSM Concrete Components	Concrete	ACI 349-06 (Design) ACI 318-08 (Fabrication) ASCE 7-10 (Loads) ANSI/ANS 57.9-84 (Loads & Load Combination)
DSC Support Structure, Heat Shields and other Steel Components	Steel	AISC Manual of Steel Construction,13th Edition (Structural Steel) AWS D1.1, March 2010 (Structural Weld) ASCE 7-10 (Loads) ANSI/ANS 57.9-84 (Loads & Load Combination)

The ultimate strength method of ACI 349-06 [3.9.4-12] is used for the design of the EOS-HSM reinforced concrete structural components. The reinforcement is provided to meet the minimum flexural and shear reinforcement requirement of ACI 349-06 and to ensure that the provided design strength exceeds the required strength. Alternatively, for some cases, the minimum reinforcement area requirement can be waived for components with a flexural stress ratio of less than 0.66 as per Section 10.5.3 of ACI 349-06 [3.9.4-12].

The axial, shear and moment capacities for all the concrete components of the EOS-HSM calculated based on ACI 349-06 are provided in Table 3.9.4-11 and Table 3.9.4-12. The capacities for blocked vent accident condition consider the strength reduction at elevated temperature.

The required steel strength, S, and required steel shear strength, S_v, for critical section of steel structure are calculated in accordance with the requirements of AISC Steel Construction Manual [3.9.4-14] using the Allowable Strength Design (ASD) method.

3.9.4.4 Load Cases

A summary of the design loads for EOS-HSM concrete component evaluation is provided in Table 3.9.4-4. This table also presents the applicable codes and standards for specific load. A summary of the design loads for DSC support structure is provided in Table 3.9.4-15.

3.9.4.5 Load Combination

The load combinations used in the structural analysis of EOS-HSM and DSC support structure comply with the requirement of 10 CFR 72.122 [3.9.4-1] and ANSI 57.9-84 [3.9.4-10]. Table 3.9.4-5 and Table 3.9.4-16 summarize the load combination requirement of EOS-HSM and DSC support structure, respectively.

3.9.4.6 Finite Element Models

EOS-HSM has variable length to store the DSCs of different lengths, however, only the longest module (EOS-HSM Long) is analyzed since it governs the structural design.

3.9.4.6.1 Finite Element Model to Evaluate EOS-HSM Concrete Components for Mechanical Loads

The structural analysis of an individual module provides a conservative estimate of the response of the EOS-HSM structural elements under the postulated static and dynamic loads for any EOS-HSM array configuration. The frame and shear wall action of the EOS-HSM concrete components are considered to be the primary structural system resisting the loads. The analytical model is evaluated for normal operating, off-normal, and postulated accident loads acting on the EOS-HSM.

A three-dimensional (3D) ANSYS finite element model (FEM) of the EOS-HSM, including all the concrete components, is developed. The eight-node brick element (ANSYS element type SOLID185) is used to model the concrete structure. Each node of the eight-node brick element has three translational degrees of freedom. The DSC is modeled using beam elements (ANSYS element type BEAM4). The DSC main support beam, W12x136 and the brace, C3x5 are also modelled using beam elements with appropriate section properties. The mass of the DSC is lumped at eleven discrete nodes of the beam using lumped mass elements (ANSYS element type MASS21). A plot of the ANSYS model of EOS-HSM and EOS-HSMS is shown in Figure 3.9.4-1 and Figure 3.9.4-2, respectively.

The DSC support structure is incorporated into the EOS-HSM analytical model to transfer the load to concrete components. The connections of the support structure to the concrete structure are modeled using rigid beam elements. The various normal, off-normal and accident loads are applied to the analytical model and internal forces and moments are computed by performing a linear elastic finite element analysis.

The node coupling option of ANSYS is used to represent the appropriate connection between the base and roof of the EOS-HSM model. For EOS-HSMS, the node to node contact element (ANSYS element type CONTA178) is used across the interface of the upper and lower segment to transfer the load from the roof and upper segment to the lower segment. The counter bore and rail extension baseplate groove at the door opening are not included in the FEM. Conservatively, the nodes at the bottom of EOS-HSM are constrained in all three translational degree of freedom, thus maximizing the EOS-HSM design forces and moments.

3.9.4.6.2 Finite Element Model of the EOS-HSM Concrete Structure for Thermal Stress Analysis

Thermal stress analyses of the EOS-HSM were performed using a 3D FEM, which includes only the concrete components. The connections of the door and the support structure rails to the EOS-HSM concrete structure are designed so that free thermal growth is permitted in these members when the EOS-HSM is subjected to thermal loads. Because of their free thermal growth, the door and the support structure do not induce thermal stresses in the concrete components of the EOS-HSM. Therefore, the analytical model of the EOS-HSM for thermal stress analysis of the concrete components does not include the DSC support structure and the door. The ANSYS models with temperature profile, which is used to perform thermal stress analysis of the concrete components, are shown in Figure 3.9.4-3 and Figure 3.9.4-4.

For the thermal load analysis, the bottom of the EOS-HSM (y=0 in ANSYS model) was restrained at one set of edge nodes (in axial and lateral directions) and friction forces were applied at the bottom of EOS-HSM base in the axial and lateral directions. One node in the front wall and two nodes in the back wall at y=0 are also restrained in vertical direction.

3.9.4.6.3 Finite Element Model for Structural Analysis of DSC Support Structure

A 3D FEM of the DSC main support beam with stiffener plates and rail extension baseplate is developed for the computer program ANSYS [3.9.4-19]. The web of the DSC main support beam has triangular openings resulting in vertical and diagonal web elements. The flanges and web elements of the support beam are modeled using BEAM189 element. Each element has three nodes with six degrees of freedom (three translational and three rotational) per node. The model is inclined by 30 degrees from the vertical. A plot of a partial model (front end) of the DSC main support beam model is shown in Figure 3.9.4-6.

The model is completely restrained at the bottom end of the rail extension baseplate. The ends of the DSC main support beam at the bottom are restrained for vertical displacement and rotation about longitudinal axis to simulate the simple support condition of the concrete pedestals at the front and rear walls. The support beam is also restrained laterally at the location of lateral braces.

The ETAB command of ANSYS is used to extract the beam element results due to individual load cases which then combined to determine the combined load results.

3.9.4.6.4 Finite Element Model for Structural Analysis of Heat Shield Panels and Connection Studs

The heat shields (coupled panel-stud system) are subjected to two loads: a combination of 1g dead load due to its own weight, and a seismic load that is dependent upon its natural frequency as well as the in-structure response spectra (ISRS) at the supports of the plate-stud system.

Modal time-history analysis of the EOS-HSM is performed using ANSYS computer code to determine the ISRS at the nodes at which the studs are supported.

ANSYS is also used to determine the natural vibration frequencies of the coupled panel-stud system. Shell elements (ANSYS element type SHELL63) are used to model the heat shield panel and beam elements (ANSYS element type BEAM4) are used for the studs. The FEM of the coupled panel-stud system is shown in Figure 3.9.4-8 and Figure 3.9.4-9.

The natural frequency of the plate-stud system is used to determine the appropriate g load from the ISRS. It is assumed that the heat shields are dynamically decoupled from the EOS-HSM because the concrete EOS-HSM is much more rigid than the heat shields and the weight of the heat shield is small as compared to the total weight of loaded EOS-HSM. Accordingly, the heat shields are not accounted for in the modal time-history analysis of the EOS-HSM, and the EOS-HSM is not considered in modal analysis of the heat shields.

3.9.4.7 Normal Operation Structural Analysis

The evaluation of the EOS-HSM is performed at normal operating condition. The following table shows the normal operating loads for which the EOS-HSM components are designed. The table also lists the individual EOS-HSM components that are affected by each loading.

Load Type	Components	
	EOS-HSM	**DSC Support Structure**
Dead Load	X	X
Live Load	X	X
Normal Handling	X	X
Normal Thermal	X	X
Wind Load	X	

The reinforced concrete and the steel DSC support structure of the EOS-HSM are analyzed for the normal, off-normal, and postulated accident conditions using FEMs described in Section 3.9.4.6. These models are used to evaluate concrete and support structure forces and moments due to dead load, live load, normal handling loads, normal thermal loads, and wind load. The methodology used to evaluate the effects of these normal loads is addressed in the following paragraphs.

3.9.4.7.1 EOS-HSM Dead Load (DL) Analysis

Dead loads are applied to the analytical model by application of 1g acceleration in the vertical direction where g is the gravitational acceleration (386.4 in/sec2). The 5% variation of dead load as indicated in ANSI/ANS 57.9 is not used because the heaviest design weight is used for analysis.

3.9.4.7.2 EOS-HSM Live load (LL) Analysis

Live load analysis is performed by applying 200 psf pressure on the roof. The DSC weight is also applied on the DSC support structure as a live load.

3.9.4.7.3 EOS-HSM Normal Operational Handling Load (R_o) Analysis

Normal operation assumes the canister is sliding over the DSC support structure due to a hydraulic ram force of up to 135,000 lbs (insertion) and 80,000 lbs (extraction) applied at the grapple ring. The normal operation handling load of 70,000 lbs is applied to each DSC main support beam in the axial direction resulting in a total applied load of 140,000 lbs on both beams which conservatively envelopes the total insertion/extraction force. The same magnitude of load of 70,000 lbs is also applied at each of the cask restraint embedment in opposite direction. In addition, the DSC weight is applied as a distributed load on both DSC support beam of the EOS-HSM.

3.9.4.7.4 EOS-HSM Normal Operating Thermal (T_o) Stress Analysis

The normal operating thermal (T_o) loads on EOS-HSM include the effect of design basis heat load up to 50 kW generated by DSC, plus the effect of normal ambient temperature range. To evaluate the effects of normal thermal loads on the EOS-HSM, heat transfer analyses for a range of normal ambient temperatures (-20 °F and 100 °F) are performed with DSC heat load of 50 kW. The normal thermal cold condition (-20 °F) is bounded by off-normal thermal cold condition (-40 °F). Therefore, off-normal thermal cold condition is used in place of normal thermal cold condition. The ambient condition that causes maximum temperature and maximum gradients in the concrete components is used in the analysis. The normal thermal hot condition is the governing case for this load case. The EOS-HSM thermal stress analysis was performed using thermal profiles and maximum temperatures that bounds those reported in Chapter 4.

3.9.4.7.5 EOS-HSM Design Basis Wind Load (W) Analysis

The DSC support structure and DSC inside the EOS-HSM are not affected by wind load. The concrete structure forces and moments due to design basis wind load (W) are bounded by the result of tornado generated wind load discussed in Section 3.9.4.9.1. Therefore, no separate analysis is performed for this case.

3.9.4.8 Off-Normal Operation Structural Analysis

This section describes the design basis off-normal events for the EOS-HSM components and presents analyses that demonstrate the adequacy of the design safety features of the EOS-HSM.

The following table shows the off-normal operating loads for which the EOS-HSM components are designed.

	Components	
Load Type	**EOS-HSM**	**DSC Support Structure**
Off-Normal Handling	X	X
Off-Normal Thermal	X	X

For an operating NUHOMS® EOS System, off-normal events could occur during fuel loading, TC handling, canister transfer, trailer towing, and other operational events. Two credible off-normal events as listed in the above table are defined that bound the range of off-normal conditions for EOS-HSM. The limiting off-normal events are defined as a jammed DSC during loading or unloading from the EOS-HSM and the extreme ambient temperatures of -40 °F (winter) and +117 °F (summer). These events bound the range of expected off-normal structural loads and off-normal temperatures range acting on the EOS-HSM. ANSYS FEMs described in Section 3.9.4.6 are used to evaluate concrete and support structure forces and moments due to these loads.

3.9.4.8.1 EOS-HSM Off-Normal Handling Loads (Ra) Analysis

This load case assumes that the EOS-TC is not accurately aligned with respect to the EOS-HSM resulting in binding of the DSC during a transfer operation causing the hydraulic pressure in the ram to increase. The ram force is limited to a maximum load of 135,000 lbs during insertion, as well as during retrieval. Therefore, for the DSC support structure, the off-normal jammed canister load (R_a) is defined as an axial load of 135 kips on one DSC support beam, plus a vertical load of one half the DSC weight (on both rails) at the most critical location.

3.9.4.8.2 EOS-HSM Off-Normal Thermal Loads Analysis

This load case is the same as the normal thermal load, but with an ambient temperature range from -40 °F to 117 °F. The temperature distributions for the extreme ambient conditions are used in the analysis for the concrete component evaluation.

3.9.4.9 Accident Condition Structural Analysis

The design basis accident events specified by ANSI/ANS 57.9-1984, and other credible accidents postulated to affect the normal safe operation of the EOS-HSM are addressed in this section.

Each accident condition is analyzed to demonstrate that the requirements of 10 CFR 72.122 are met and that adequate safety margins exist for the EOS-HSM design. The resulting accident condition stresses in the EOS-HSM components are evaluated and compared with the applicable code limits. The postulated accident conditions addressed in this section include:

- Tornado winds and tornado generated missiles (W_t, W_m)
- Design basis earthquake (E)
- Design basis flood (FL)
- Blocked Vent Accident Thermal (T_a)

ANSYS FEMs described in Section 3.9.4.6 are used to evaluate concrete and support structure forces and moments due to these loads.

3.9.4.9.1 Tornado Winds/Tornado Missile Load (W_t, W_m) Analysis

Stability and stress analyses are performed to determine the response of the EOS-HSM to tornado wind pressure loads. The stability analyses are discussed in detail in Appendix 3.9.7. The stress analyses are performed using the ANSYS FEM of a single EOS-HSM to determine design forces and moments. These conservative analyses envelope the effects of wind pressures on the EOS-HSM array. Thus, the requirements of 10 CFR 72.122 are met.

The EOS-HSM is qualified for maximum design basis tornado (DBT) generated design wind loads of 218 psf and 154 psf on the windward and leeward EOS-HSM walls (See Table 3.9.4-1 and Table 3.9.4-2), and a pressure drop of 3 psi.

A single, stand-alone EOS-HSM is protected by shield walls, or an adjacent module on either side and at the rear. For an EOS-HSM array, the critical module is on the windward end of the array. This module has an end shield wall to protect the module from tornado missile impacts. The shield wall is also subjected to the 218 psf windward pressure load. The leeward side of the same end module in the array has no appreciable suction load due to the presence of the adjacent module. The 154 psf suction load is applicable to the end shield wall on the opposite end module in the array. A suction of 326 psf is also applied to the roof of each EOS-HSM in the array.

For the stress analyses, the DBT wind pressures are applied to the EOS-HSM as uniformly distributed loads. The rigidity of the EOS-HSM in the transverse direction, due to frame and shear wall action of the EOS-HSM, is the primary load transfer mechanism assumed in the analysis. The bending moments and shear forces at critical locations in the EOS-HSM concrete components are calculated by performing an analysis using the ANSYS analytical model of the EOS-HSM as described in Section 3.9.4.6. The resulting moments and forces are included in the EOS-HSM load combination results reported in Table 3.9.4-7 to Table 3.9.4-10.

Conservatively, the design basis extreme wind pressure loads are assumed to be equal to those calculated for the DBT (based on 360 mph wind speed) in the formulation of EOS-HSM load combination results.

In addition, the adequacy of the EOS-HSM to resist tornado missile loads is checked using the modified National Defense Research Committee (NDRC) empirical formulae [3.9.4-13] for local damage evaluation, and response chart solution method [3.9.4-18] for global response. These evaluations are described in Section 3.9.4.10.6.

3.9.4.9.2 Earthquake (Seismic) Load (E) Analysis

The design basis seismic load used for analysis of the EOS-HSM components is as discussed in Section 2.3.4. Based on U.S. NRC (NRC) Regulatory Guide 1.61 [3.9.4-3], a damping value of four percent is used for seismic analysis of steel structural components and a damping value of seven percent is used for seismic analysis of concrete components of EOS-HSM. An evaluation of the frequency content of the loaded EOS-HSM is performed to determine the amplified accelerations associated with the design basis seismic response spectra for EOS-HSM.

The design basis accelerations for the EOS-HSM are amplified based on the results of the frequency analysis of the EOS-HSM. The results of the frequency analysis of the EOS-HSM structure (which includes a simplified model of the DSC) yield a lowest frequency of 18.7 Hz in the transverse direction and 32.7 Hz in the longitudinal direction. The lowest vertical frequency exceeds 45 Hz; therefore the spectral acceleration is not amplified in vertical direction. Thus, based on the Regulatory Guide 1.60 response spectra amplifications, the corresponding seismic accelerations used for the design of the EOS-HSM are 0.936g and 0.628g in the transverse and longitudinal directions, respectively, and 0.333g in the vertical direction. The resulting amplified accelerations are given in Table 3.9.4-3.

An equivalent static analysis of the EOS-HSM is performed using the ANSYS model described in Section 3.9.4.6 by applying the amplified seismic accelerations load. These amplified accelerations are determined based on the frequency analysis of the EOS-HSM. The frequency analysis of EOS-HSM and multi-segment design EOS-HSMS was performed individually and found that EOS-HSMS yields bounding amplified acceleration. Therefore, the bounding amplified acceleration derived from modal analysis of EOS-HSMS is conservatively used for both EOS-HSM and EOS-HSMS.

The responses for each orthogonal direction are combined using the square root of the sum of the squares (SRSS) method. The resulting moments and forces due to combined seismic load are included in the EOS-HSM load combination results.

For sites having higher zero period acceleration than analyzed, more than one module may need to tie together to prevent significant sliding or to prevent the modules from banging into each other causing unacceptable damage. The reinforcement requirement may also need to be reviewed, and additional rebar may be added for such sites.

The stability evaluation of EOS-HSM due to seismic load is discussed in Appendix 3.9.7.

3.9.4.9.3 Flood Load (FL) Analysis

Since the source of flooding is site specific, the exact source, or quantity of flood water, should be established by the licensee. However, for this generic evaluation of the EOS-HSM, bounding flooding conditions are specified that envelope those that are postulated for most plant sites. As described in Section 2.3.3, the design basis flooding load is specified as a 50-foot static head of water and a maximum flow velocity of 15 feet per second. Each licensee should confirm that this represents a bounding design basis for their specific ISFSI site.

Since the EOS-HSM is open to the atmosphere, static differential pressure due to flooding is not a design load.

The maximum drag pressure, D, acting on the EOS-HSM due to a 15 fps flood water velocity is calculated as follows:

$$D = \frac{C_D \rho_w V^2}{2g} \qquad [3.9.4\text{-}20]$$

Where:

V = 15 fps, Flood water velocity

C_D = 2.0, Drag coefficient for flat plate

ρ_w = 62.4 lb/ft^3, Flood water density

g = 32.2 ft/sec^2, Acceleration due to gravity

D = Drag pressure (psf)

The resulting flood induced drag pressure is: D = 436 psf.

The following flood load cases are considered to account for different flow direction:

- Case 1: Flood water flow from front to rear of EOS-HSM
- Case 2: Flood water flow from rear to front of EOS-HSM
- Case 3: Flood water flow from right side to left side of EOS-HSM or vice versa

ANSYS FEM described in Section 3.9.4.6 is used for the structural evaluation. The results for flood load case are obtained by enveloping results from above load cases.

The stability evaluation of EOS-HSM due to flood load is discussed in Appendix 3.9.7.

3.9.4.9.4 Accident Blocked Vent Thermal (T_a) Stress Analysis

This accident conservatively postulates the complete blockage of the EOS-HSM ventilation air inlet and outlet openings.

Since the EOS-HSMs are located outdoors; there is a remote probability that the ventilation air inlet and outlet vent openings could become blocked by debris from events such as flooding, high wind and tornados. Design features, such as the perimeter security fence and the redundant protected location of the air inlet, and outlet vent openings and the screens reduce the probability of occurrence of such an accident. Nevertheless, for this conservative generic analysis, such an accident is postulated to occur and is analyzed.

The postulated accident thermal event occurs due to blockage of the air inlet and outlet vents under off-normal ambient temperatures range from -40 ºF to 117 ºF.

ANSYS FEM described in Section 3.9.4.6 is used for the structural analysis for accident blocked vent condition.

3.9.4.10 Structural Evaluation

The load categories associated with normal operating conditions, off-normal conditions and postulated accident conditions are described previously. The load combination results and design strengths of EOS-HSM components are presented in this section.

3.9.4.10.1 EOS-HSM Concrete Components

To determine the required strength (internal axial forces, shear forces, and bending moments) for each EOS-HSM concrete component, linear elastic finite element analyses are performed for the normal, off-normal, and accident loads using the analytical models described in Section 3.9.4.6 for mechanical and thermal loads.

The concrete design loads are multiplied by load factors and combined to simulate the most adverse load conditions. The load combinations listed in Table 3.9.4-5 are used to evaluate the concrete components. The bounding load combination results for each component are presented in Table 3.9.4-7 to Table 3.9.4-10. The notations for the components of forces and moments and the concrete component planes in which capacities are computed are shown in Figure 3.9.4-5. The thermal stresses of EOS-HSM concrete components used in the load combination results are based on thermal results that bound those reported in Chapter 4. All load combination results are less than computed section capacities.

The required strength, U, for critical sections of concrete is calculated in accordance with the requirements of ANSI 57.9 [3.9.4-10] and ACI 349-06 [3.9.4-12], including the strength reduction factors defined in ACI 349-06, Section 9.3. The design strength of EOS-HSM concrete components exceeds the factored design loads. Thus, the EOS-HSM concrete components are adequate to perform their intended function. EOS-HSM construction details such as construction joints and reinforcement bar splices is detailed on the construction drawings.

3.9.4.10.2 DSC Support Structure

The DSC main support beams, stiffener plates, extension baseplates, DSC stop plates and braces members of the DSC support structure are evaluated using the allowable strength design method of the AISC Manual of Steel Construction [3.9.4-14]. The maximum temperature used in the stress analysis of the support steel bounds the maximum temperature reported in Chapter 4.

The load combination results for each of these components are provided in Table 3.9.4-17 to Table 3.9.4-22. The maximum value of demand to capacity ratio of DSC support structure is less than 1.0. Thus, DSC support structure is adequately strong to resist the reasonably foreseeable loads applied to it.

3.9.4.10.3 EOS-HSM Shield Door

The shield door is free to grow in the radial direction when subjected to thermal loads. Therefore, there are no stresses in the door due to thermal growth. The dead weight, tornado wind, differential pressure and flood loads cause insignificant stresses in the door compared to stresses due to missile impact load. Therefore, the door is evaluated only for the missile impact load.

The minimum thickness of concrete component to prevent perforation, and scabbing are 18.5 inches and 27.7 inches, respectively. Thus, the 30.5-inch thick door is adequate to protect from local damage due to missile impact. The computed maximum ductility ratio for the door is less than 1, which satisfies the ductility requirement if compared against the allowable ductility ratio of 10 as per ACI 349-06 [3.9.4-12]. Therefore, the concrete door meets the ductility requirement and is adequate to protect from global effect of missile impact.

For the door anchorage, the controlling load is tornado generated differential pressure drop load. The maximum tensile force per bolt (four door attachment bolts), is 7.6 kips. The design strength of door attachment embedment (nonductile) as per Section D.3.6.3 of ACI 349-06 [3.9.4-12] is 17.99 kips, which is greater than 7.6 kips, thus satisfying the ACI 349-06 code requirement.

3.9.4.10.4 EOS-HSM Heat Shield

The roof heat shield assembly consists of four panels. Each panel section is a v-shaped in transverse direction with v-notch at the center of the EOS-HSM width. The roof heat shield panels are connected to the roof by fifteen, ¾-10UNC bolts. The natural lateral frequency of a typical panel/connection stud system is determined from ANSYS computer code. The maximum interaction ratio for combined axial and bending stress in the connection bolts is 0.503, which is less than 1.0. The maximum bending moment in roof heat shield panel is 22.29 in-lb/in., which is also less than the panel moment capacity of 59.59 in-lb/in.

The side wall heat shield assembly also consists of four panels. The side wall heat shield panels are attached to the EOS-HSM base unit side wall by seventeen ½-13UNC bolts on both sides. The maximum interaction ratio for combined axial and bending stress in connection bolts is 0.563, which is less than 1.0. The maximum bending moment in side heat shield panel is 46.98 in-lb/in, which is also less than the panel moment capacity of 59.59 in-lb/in.

The maximum temperature used in the stress analysis of the heat shields bounds the maximum temperatures reported in Chapter 4. The size of the slot hole provided in the panel at the connection bolt location is sufficiently large to allow for free thermal expansion. Therefore, neither of roof heat shield panel and side wall heat shield panel is subjected to thermal stress.

3.9.4.10.5 EOS-HSM DSC Axial Restraint

The DSC axial restraint consists of a capped steel tube embedment located within the bottom center of the round access opening of the EOS-HSM front wall, and a 2-inch by 4-inch solid bar steel retainer that drops into the embedment cavity after DSC transfer is complete. The drop-in retainer extends approximately 5 inches above the top of embedment to provide axial restraint of the DSC. The maximum seismically induced shear load in the retainer is 140.5 kips. The allowable shear strength of the axial retainer is 196.0 kips. The maximum seismically induced moment in the retainer is 281.0 in-kips taking a moment arm of 2 inches, conservatively. The allowable flexural strength of axial retainer is 344.9 in-kips. Hence, the DSC axial retainer design is adequate to perform its intended function.

3.9.4.10.6 Evaluation of Concrete Components for Missile Loading

Missile impact effects are assessed in terms of local damage and overall structural response. Local damage that occurs in the immediate vicinity of the impact area is assessed in terms of penetration, perforation, spalling and scabbing. Evaluation of local effects is essential to ensure that protected items (the DSC and fuel) would not be damaged by a missile perforating a protective barrier, or by secondary missiles such as scabbing particles. Evaluation of overall structural response is essential to ensure that protected items are not damaged or functionally impaired by deformation or collapse of the impacted structure.

The tornado-generated missiles are conservatively assumed to strike normal to the surface with the long axis of the missile parallel to the line of flight to maximize the local effects. Plastic deformation to absorb the energy input by the tornado-generated missile load is desirable and acceptable, provided that the overall integrity of the structure is not impaired. Due to complex physical process associated with missile impact effects, the EOS-HSM structure is primarily evaluated conservatively by application of empirical formulae.

3.9.4.10.6.1 Local Damage Evaluation

Local missile impact effects consist of (a) missile penetration into the target, (b) missile perforation through the target, and (c) spalling and scabbing of the target. This also includes punching shear in the region of the target. Per F.7.2.3 of ACI 349-06 [3.9.4-12], if the concrete thickness is at least 20% greater than that required to prevent perforation, the punching shear requirement of the code need not be checked.

The following enveloping missiles are considered for local damage:

- Utility wooden pole
- Armor piercing artillery shell
- 12-inch diameter schedule 40 steel pipe

Large deformable missiles such as automobiles are incapable of producing significant local damage. Concrete thickness satisfying the global structural response requirements including punching shear is considered to preclude unacceptable local damage. Therefore, the local effects from an automobile are evaluated using punching shear criteria of ACI 349-06 [3.9.4-12].

The following empirical formulae are used to determine the local damage effects on reinforced concrete target:

A. Modified NDRC formulas for penetration depth [3.9.4-13]:

$$x = \sqrt{4KNWd\left(\frac{v_o}{1000\ d}\right)^{1.8}}\ , \text{ for } x/d \leq 2.0$$

$$x = \left[KNW\left(\frac{v_o}{1000\ d}\right)^{1.8}\right] + d\ , \text{ for } x/d > 2.0$$

Where,

x = Missile penetration depth, inches

K= concrete penetrability factor = $\frac{180}{\sqrt{f_c'}}$

N = projectile shape factor
= 0.72 flat nosed
= 0.84 blunt nosed
= 1.0 bullet nosed (spherical end)
= 1.14 very sharp nose

W = weight of missile, lb

v_o = striking velocity of missile, fps

d = effective projectile diameter, inches.
for a solid cylinder, d = diameter of projectile and
for a non-solid cylinder, $d = (4A_c/\pi)^{1/2}$

A_c = projectile impact area, in^2

B. Modified NDRC formula for perforation thickness [3.9.4-13]:

$$\frac{e}{d} = 3.19\left(\frac{x}{d}\right) - 0.718\left(\frac{x}{d}\right)^2\ , \text{ for } x/d \leq 1.35$$

$$\frac{e}{d} = 1.32 + 1.24\left(\frac{x}{d}\right)\ , \text{ for } 1.35 \leq x/d \leq 13.5$$

Where,

e = perforation thickness, in.

In order to provide an adequate margin of safety the design thickness $t_d = 1.2e$ [3.9.4-12]

C. Modified NDRC formula for scabbing thickness [3.9.4-13]:

$$\frac{s}{d} = 7.91\left(\frac{x}{d}\right) - 5.06\left(\frac{x}{d}\right)^2 \text{ , for } x/d \le 0.65$$

$$\frac{s}{d} = 2.12 + 1.36\left(\frac{x}{d}\right) \text{ , for } 0.65 \le x/d \le 11.75$$

Where,

s = scabbing thickness, in.

In order to provide an adequate margin of safety the design thickness td = 1.2s [3.9.4-12]

The concrete targets of the EOS-HSM that may be subjected to local damage due to missile impact are:

- 44-inch thick roof
- 42-inch thick (minimum) front wall
- 36-inch thick end shield wall
- 36-inch thick rear shield wall
- 30.5-inch thick shielding door

The minimum thickness of concrete target components listed above is 30.5 inches. So, the required perforation thickness and require scabbing thickness is compared against 30.5 inches to ensure the adequacy of design.

3.9.4.10.6.1.1 Local Impact Effects of Utility Wooden Pole Missile

Per section 6.4.1.2.5 of [3.9.4-13], utility wooden pole missiles do not have sufficient strength to penetrate a concrete target and that the scabbing thickness required for wood missiles is substantially less than that required for a steel missile with the same mass and velocity. Practically, wooden pole missiles do not appear to be capable of causing local damage to the 12-inch or thicker walls (also see Section 2.1.1 of [3.9.4-18]). Since none of the concrete targets are less than 12 inches thick, the postulated wood missiles do not cause any local damage to the EOS-HSM concrete component.

3.9.4.10.6.1.2 Local Impact Effects of Armor Piercing Artillery Shell Missile

The penetration depth for this missile is calculated using the NDRC Formula as given in Section 3.9.4.10.6.1 (a) and the parameters used in the formula are as listed below:

d = 8.0 in.	effective diameter of missile
W = 276 lb	weight of missile

v_o = 185 fps striking velocity of missile

f'_c = 5000 psi concrete compressive strength

K = 180/√5000 = 2.55 concrete penetrability factor

N = 0.84 projectile shape factor (blunt nosed)

Penetration depth, x = 4.6 in. for x/d (= 0.58) ≤ 2.0

Perforation thickness, e = 12.9 in. for x/d (= 0.58) ≤ 1.35

Required perforation thickness = 1.2*12.9 = 15.5 in. < 30.5 in.

Scabbing thickness, s = 23.1 in. for x/d (= 0.58) ≤ 0.65

Required scabbing thickness = 1.2*23.1 = 27.7 in. < 30.5 in.

Therefore, penetration, perforation and scabbing of the concrete components of EOS-HSM do not occur due to this missile impact.

3.9.4.10.6.1.3 Local Impact Effects of 12-Inch Diameter Schedule 40 Steel Pipe Missile

The penetration depth for this missile is calculated using the NDRC Formula as given in Section 3.9.4.10.6.1 (A) and the parameters used in the formula are as listed below:

ϕ = 12.75 in. outer diameter of 12" dia. schedule 40 steel pipe.

A_c = 15.74 in^2 missile impact area (cross sectional area of steel)

$d = (4*15.74/\pi)^{1/2}$ = 4.5 in. effective diameter of missile

W = 750 lb weight of missile

v_o = 154 fps striking velocity of missile

f'_c = 5000 psi concrete compressive strength

K = 180/√5000 = 2.55 concrete penetrability factor

N = 0.72 projectile shape factor (flat nosed)

Penetration depth, x = 7.6 in. for x/d (= 1.69) ≤ 2.0

Perforation thickness, e = 15.4 in. for 1.35 ≤ x/d (= 1.69) ≤ 13.5

Required perforation thickness = 1.2*15.4 = 18.5 in. < 30.5 in. OK

Scabbing thickness, s = 19.9 in. for 0.65 ≤ x/d (= 1.69) ≤ 11.75

Required scabbing thickness = 1 .2*19.9 = 23.9 in. < 30.5 in. OK

Therefore, penetration, perforation and scabbing of the concrete components of EOS-HSM do not occur due to this missile impact.

3.9.4.10.6.2 Global Structural Response

When a missile strikes a structure, large forces develop at the missile-structure interface, which decelerate the missile and accelerate the structure. The response of the structure depends on the dynamic properties of the structure and the time dependent nature of the applied loading (interface force-time function). The force-time function is, in turn, dependent on the type of impact (elastic or plastic) and the nature and extent of local damage.

In an elastic impact, the missile and the structure deform elastically, remain in contact for a short period of time (duration of impact), and subsequently disengage due to the action of elastic interface restoring forces.

In a plastic impact, the missile or the structure (or both) may sustain permanent deformation or damage (local damage). Elastic restoring forces are small, and the missile and the structure tend to remain in contact after impact. Plastic impact is much more common than elastic impact, which is rarely encountered. Test data have indicated that the impact from all postulated tornado-generated missiles can be characterized as a plastic impact.

If the interface forcing function can be defined or conservatively idealized, the structure can be modeled mathematically, and conventional analytical or numerical techniques can be used to predict structural response. If the interface forcing function cannot be defined, the same mathematical model of the structure can be used to determine structural response by application of conservation of momentum and energy balance techniques with due consideration for type of impact (elastic or plastic).

In either case, in lieu of a more rigorous analysis, a conservative estimate of structural response can be obtained by first determining the response of the impacted structural element, and then applying its reaction forces to the supporting structure. The predicted structural response enables assessment of structural design adequacy in terms of strain energy capacity, deformation limits, stability and structural integrity.

The overall structural response of each component as a whole (global response) is determined by single degree of freedom analysis using response charts solution method of [3.9.4-18].

The following enveloping missiles are considered for global structural response:

- Utility wooden pole
- Armor piercing artillery shell
- 12-inch diameter schedule 40 steel pipe
- Automobile missile

The peak interface force and impact duration for each missile are calculated as follows:

A. Utility Wooden Pole Missile

For wooden missile, the interface forcing function is a rectangular pulse having a force magnitude of F and duration t_i, per Section 2.3.1 of [3.9.4-18]

$F = PA$

$t_i = M_m \nu_c/F$

Where,

F = interface force (lb)

P = interface pressure (psi) = 2500 psi for wood missiles [3.9.4-18]

A = cross sectional area of the missile (in^2) = π * 13.52/4 = 143.1 in^2

t_i = impact duration (sec)

W_m = weight of missile (lb) = 1124 lb

M_m = missile mass (lb-sec^2/ft) = W_m/g = 1124 lb /32.2 ft/sec^2 = 34.9 lb-sec^2/ft

ν_c = change in velocity during impact (conservatively = ν_s) (fps) = 180 fps

Therefore,

F = 358 kip and t_i = 0.018 sec

B. Armor Piercing Artillery Shell

For solid steel missile, the concrete is a soft target per section 6.4.2 of [3.9.4-13] with a penetration depth of 4.6 in. The interface forcing function is a rectangular pulse per Section 6.4.2.1.1 of [3.9.4-13].

$F = W_m V_0^2/2gX$

$t_i = 2X/V_0$

Where,

F = interface force (lb)

t_i = impact duration (sec)

W_m = missile weight (lb) = 276 lb

V_0 = initial velocity of the missile (fps) = 185 fps

X = penetration depth = 4.6 in.

Therefore,

F = 383 kip and t_i = 0.00414 sec

C. 12-Inch Diameter Schedule 40 Steel Pipe

For steel pipe missile, the interface forcing function is a triangular pulse per Section 2.3.2 of [3.9.4-18].

$t_i = 400M_m /PA$

$F = (2M_m\nu_s)/t_i$

Where,

F = peak interface force (lb)

P = collapse stress of pipe (psi) = 60000 psi

A = cross sectional metal area of the missile (in^2) = 15.74 in^2

t_i = impact duration (sec)

W_m = weight of missile (lb) = 750 lb

M_m = missile mass (lb-sec^2/ft) = W_m/g = 750 lb /32.2 ft/sec^2 = 23.29 lb-sec^2/ft

ν_s = striking velocity of missile = 154 fps

Therefore,

F = 718 kip and t_i = 0.01 sec

D. Automobile Missile

For automobile missile, the interface forcing function per 2.3.3 of [3.9.4-18] is as follows:

$F_t = 0.625\ \nu_c\, W \sin(20t)$ $0 < t \leq 0.0785$ sec

$F_t = 0$ $t > 0.0785$ sec

Where,

F_t = force as a function of time (lb)

W = weight of automobile (lb) = 4000 lb

ν_c = change in velocity during impact (conservatively = ν_s) (fps) = 195 fps

Therefore,

F = 488 kip and t_i = 0.0785 sec

The end wall, rear wall, base front wall, roof and door of EOS-HSM are evaluated for global response, since these components may interface with missile loading. The end/rear walls and door are idealized as a simply supported plate while the base front wall and roof are idealized as simply supported beam for structural response. The yield resistance and fundamental period of vibration of concrete components is then determined based on the assumed idealized boundary condition using the equations given in Section 4.4 of [3.9.4-18]. The calculated value of yield resistance, R_y, and fundamental period of vibration, T_n, for different concrete components are tabulated below.

Component	R_y (kip)	T_n (sec)
End Wall	446.1	0.0180
Rear Wall	919.9	0.0065
Base Front Wall	1182.5	0.0045
Roof	402.0	0.0301
Door	1211.0	0.002124

In the response chart solution method, the structural response is determined by entering the chart with calculated values of C_T and C_R to determine the ductility ratio, μ, which is compared against the allowable ductility ratio as given in Appendix F of ACI 349-06 [3.9.4-12]. The dimensionless ratios, C_T and C_R, are defined as follows:

$$C_R = \frac{R_y}{F} \qquad C_T = \frac{t_i}{T_n}$$

The maximum value of ductility ratio of all five components is found to be less than 10. The allowable ductility ratio per ACI 349-06 [3.9.4-12] is 10. Hence, the global response of EOS-HSM is within deformation limit meeting the ductility requirement.

Each component is also evaluated for punching shear capacity with interfacing utility wooden pole missile and automobile missile. All the components have punching shear capacity greater than the peak missile interface force.

3.9.4.11 Conclusions

The load categories associated with normal operating conditions, off-normal conditions and postulated accident conditions are described and analyzed in previous sections. The load combination results for EOS-HSM components important-to-safety are also presented. Comparison of the results with the corresponding design capacity shows that the design strength of the EOS-HSM is greater than the strength required for the most critical load combination.

3.9.4.12 References

3.9.4-1 Code of Federal Regulation Title 10, Part 72 (10CFR Part 72), "Licensing Requirements for the Independent Storage of Spent Nuclear Fuel, High-Level Radioactive Waste, and Reactor-Related Greater than Class C Waste."

3.9.4-2 U.S. Nuclear Regulatory Commission, Regulatory Guide 1.60, "Design Response Spectra for Seismic Design of Nuclear Power Plants," Revision 1, 1973.

3.9.4-3 U.S. Nuclear Regulatory Commission, Regulatory Guide 1.61, "Damping Values for Seismic Design of Nuclear Power Plants," Revision 1, March 2007.

3.9.4-4 U.S. Nuclear Regulatory Commission, Regulatory Guide 1.76, "Design Basis Tornado for Nuclear Power Plants," Revision 0, April 1974.

3.9.4-5 U.S. Nuclear Regulatory Commission, Regulatory Guide 1.92, "Combining Modal Responses and Spatial Components in Seismic Response Analysis," Revision 3, October 2012.

3.9.4-6 U.S. Nuclear Regulatory Commission, Regulatory Guide 1.122, "Development of Floor Design Response Spectra for Seismic Design of Floor-Supported Equipment or Components," Revision 1, 1978.

3.9.4-7 NUREG-0800, Standard Review Plan, Section 3.5.1.4, "Missiles Generated by Natural Phenomena," Revision 2, July 1981.

3.9.4-8 NUREG-0800, Standard Review Plan, Section 3.3.1, "Wind Loading," Section 3.3.2 "Tornado Loads," and Section 3.5.1.4 "Missiles Generated by Tornado and Extreme Winds," Revision 3, March 2007.

3.9.4-9 NUREG-1536, "Standard Review Plan for Spent Fuel Dry Storage Systems at a General License Facility," Revision 1, U.S. Nuclear Regulatory Commission, July 2010.

3.9.4-10 ANSI/ANS 57.9-1984, "Design Criteria for an Independent Spent Fuel Storage Installation (Dry Storage Type)," American National Standards Institute, American Nuclear Society.

3.9.4-11 ACI-318-08, "Building Code Requirement for Structural Concrete," American Concrete Institute.

3.9.4-12 ACI 349-06, "Code Requirements for Nuclear Safety Related Concrete Structures," American Concrete Institute.

3.9.4-13 American Society of Civil Engineers, "Structural Analysis and Design of Nuclear Plant Facilities," ASCE Publication No. 58.

3.9.4-14 American Institute of Steel Construction, AISC Manual of Steel Construction, 13th Edition.

3.9.4-15 American Society of Civil Engineers, "Minimum Design Loads for Buildings and Other Structures," ASCE 7-10 (formerly ANSI A58.1).

3.9.4-16 AREVA Inc., "Updated Final Safety Analysis Report for the Standardized NUHOMS® Horizontal Modular Storage System for Irradiated Nuclear Fuel," Revision 14, USNRC Docket Number 72-1004, September 2014.

3.9.4-17 Bechtel Power Corporation, "Design of Structures for Missile Impact," Topical Report BCTOP-9A, Revision 2, San Francisco, California.

3.9.4-18 Bechtel Corporation, "Design Guide Number C-2.45 for Design of Structures for Tornado Missile Impact," Rev. 0, April 1982.

3.9.4-19 "ANSYS Computer Code and User's Manual", Release 14.0.3.

3.9.4-20 Binder, Raymond C., "Fluid Mechanics," 3rd Edition, Prentice-Hall, Inc, 1973.

Table 3.9.4-1
Design Pressures for Tornado Wind Flowing from Front Wall to Rear Wall and Vice Versa

Component	Velocity Pressure, q_v (psf)	External Pressure Coefficient, C_p	Internal Pressure Coefficient, (GC_{pi})	Max. Design Pressure, $q_v*(G*C_p-GC_{pi})$ (psf)
Windward(Front/Rear Wall)	254	0.80	±0.18	218
Leeward(Rear/Front Wall)		-0.30(1)		-110
Side(Right Side Wall)		-0.70		-197
Side(Left Side Wall)		-0.70		-197
Roof		-1.30		-326

Notes:

1. The C_p value is taken for L/B = 268”/116” ≈ 2.0.
2. The gust effect factor, G=0.85 considering the EOS-HSM as rigid.

Table 3.9.4-2
Design Pressures for Tornado Wind Flowing from Right Side to Left Side Wall and Vice Versa

Component	Velocity Pressure, q_v (psf)	External Pressure Coefficient, C_p	Internal Pressure Coefficient, (GC_{pi})	Max. Design Pressure, $q_v*(G*C_p-GC_{pi})$ (psf)
Side(Front Wall)	254	-0.70	±0.18	-197
Side(Rear Wall)		-0.70		-197
Windward(Right/Left Side Wall)		0.80		218
Leeward(Left/Right Side Wall)		-0.50(1)		-154
Roof		-1.30		-326

Notes:

1. The C_p value is taken for L/B = 116”/268” ≈ 0.4
2. The gust effect factor, G=0.85 considering the EOS-HSM as rigid.

Table 3.9.4-3
Spectral Acceleration Applicable to Different Components of EOS-HSM for Seismic Analysis

Direction	Frequency (Hz)	Spectral Acceleration Corresponding to Design ZPA (Design ZPA = 0.5g horizontal & 0.333 g vertical)		
		at 3% Damping (for DSC)	at 4% Damping (for DSC support structure)	at 7% Damping (for concrete components)
X (Transverse)	18.7	1.229g	1.156g	0.936g
Y (Vertical)	60.3	0.333g	0.333g	0.333g
Z (Longitudinal)	32.7	0.694g	0.677g	0.628g

Table 3.9.4-4
Load Cases for EOS-HSM Concrete Components Evaluation

Design Load Type	Load Notation	Design Parameters	Applicable Codes / References
Normal			
Dead	DL	Includes self-weight with 160 pcf density for concrete and 0.28 pci for steel support structure.	ANSI/ANS 57.9-1984 [3.9.4-10]
Live	LL	Design live load of 200 psf on roof which includes snow and ice load and DSC weight of 135 kip applied on DSC support rails.	ANSI/ANS 57.9-1984 [3.9.4-10] & ASCE 7-10 [3.9.4-15]
Normal Handling	R_O	The concrete module is evaluated for 140 kip DSC insertion load as a normal handling load. The DSC weight is also applied at both rail support locations (4 points).	
Normal Thermal	T_O	DSC with spent fuel rejecting up to 50.0 kW of decay heat. Extreme ambient air temp. -20°F and 100°F. Reference temperature = 70°F.	
Off-Normal/Accidental			
Off-Normal Handling	R_a	For the steel support structure the magnitude of this load is 135 kip both for DSC insertion and retrieval, applied to one rail. The DSC weight is also applied at one rail support location (two points).	
Accidental Thermal	T_a	Enveloped of Off-Normal and Accidental Thermal (vent blocked) condition. Accidental thermal condition is same as off-normal condition with ambient temperature range of -40°F to 117°F. Reference temperature = 70°F	
Earthquake	E	Zero period acceleration of 0.5g in horizontal and 0.333g in vertical direction with enhancement in frequency above 9 Hz and 7% damping.	NRC Reg. Guide 1.60 [3.9.4-2] & Reg. Guide 1.61 [3.9.4-3]
Flood	FL	Maximum flood height of 50 ft and max. velocity of water 15 ft/sec	10 CFR Part 72 [3.9.4-1]
Wind/Tornado Wind	W/W_t	Maximum wind speed of 360 mph, and a pressure drop of 3 psi	ASCE 7-10 [3.9.4-15] & NRC Reg Guide 1.76 [3.9.4-4]
Tornado Generated Missile	W_m	4 types of tornado-generated missiles	NUREG-0800 Section 3.5.1.4 [3.9.4-7]

Table 3.9.4-5
Load Combination for EOS-HSM Concrete Components Evaluation

Combination Number	Load Combination	Event
C1	1.4 DL + 1.7 (LL + R_o)	Normal
C2	1.05 DL + 1.275 (LL + T_o + W)	Off-Normal – Wind
C3	1.05 DL + 1.275 (LL + T_o + R_a)	Off-Normal – Handling
C4	DL + LL + T_o + E	Accident – Earthquake
C5	DL + LL + T_o + W_t	Accident – Tornado
C6	DL + LL + T_o + FL	Accident – Flood
C7	DL + LL + Ta	Accident – Thermal

Note: See Table 3.9.4-4 for notation.

Table 3.9.4-6
Strength Reduction Factors for Concrete

Type of Stress	Strength Reduction Factor, ϕ
Tension - Controlled	0.90
Compression - Controlled	0.65
Shear	0.75
Torsion	0.75
Bearing	0.65

Note: The strength reduction factors are taken from ACI 349-06, Section 9.3 [3.9.4-12].

Table 3.9.4-7
Demand of EOS-HSM Concrete Components for Shear Forces and Moments

Component	Load Combination	M_1 (in-kip/ft)	M_2 (in-kip/ft)	V_{o1} (kip/ft)	V_{o2} (kip/ft)	V_i (kip/ft)
1. Rear Wall Bottom (32”)	C1 through C6	338.7	708.7	6.3	9.8	51.6
	C7	232.8	270.8	1.9	2.7	25.3
2. Rear Wall Top (12”)	C1 through C6	36.9	106.6	5.1	6.4	13.7
	C7	24.5	69.3	4.2	2.9	7.6
3. Front Wall Bottom (54”)	C1 through C6	1024.0	1877.2	14.2	13.0	57.6
	C7	1049.1	1735.2	3.1	3.1	25.2
4. Front Wall Top (42”)	C1 through C6	949.7	1768.7	28.5	25.6	90.4
	C7	1353.1	2485.3	26.1	24.4	48.3
5. Side Wall Bottom (24”)	C1 through C6	269.3	182.9	15.4	14.8	23.5
	C7	143.4	396.3	14.3	18.6	11.1
6. Side Wall Bottom (14”)	C1 through C6	91.4	38.0	11.4	6.1	14.4
	C7	64.0	117.2	12.1	12.7	11.1
7. Side Wall Top (12”)	C1 through C6	285.3	195.0	12.3	11.9	38.5
	C7	341.2	151.8	10.6	10.6	46.5
8. Roof (44”)	C1 through C6	622.2	1831.5	46.1	49.5	21.5
	C7	283.6	1004.2	11.6	24.3	22.5

Table 3.9.4-8
Demand of EOS-HSM Concrete Components for Axial Forces and Moments

Component	Load Combination	T_1 (kip/ft)	T_2 (kip/ft)	C_1 (kip/ft)	C_2 (kip/ft)	M_{1P} (in-kip/ft)	M_{2P} (in-kip/ft)
1. Rear Wall Bottom (32”)	C1 through C6	33.8	32.1	46.4	104.4	299.6	428.3
	C7	13.4	5.5	40.5	44.6	66.4	124.1
2. Rear Wall Top (12”)	C1 through C6	9.5	23.6	7.5	29.6	36.9	43.4
	C7	7.1	40.0	15.1	15.8	20.1	45.8
3. Front Wall Bottom (54”)	C1 through C6	72.2	65.6	51.3	122.3	1019.5	773.8
	C7	19.8	0.0	32.0	59.8	485.3	0.0
4. Front Wall Top (42”)	C1 through C6	97.7	77.5	86.6	256.2	737.5	1137.7
	C7	22.1	32.8	38.7	98.9	1352.7	1796.9
5. Side Wall Bottom (24”)	C1 through C6	28.0	37.6	48.2	70.2	267.5	158.6
	C7	22.5	58.7	28.0	38.8	97.1	324.9
6. Side Wall Bottom (14”)	C1 through C6	19.4	16.5	47.6	15.9	75.9	37.9
	C7	31.5	62.9	21.9	6.1	64.0	117.2
7. Side Wall Top (12”)	C1 through C6	27.5	49.7	157.1	103.7	44.4	49.0
	C7	56.9	11.7	138.0	108.7	64.5	132.3
8. Roof (44”)	C1 through C6	24.4	67.5	35.4	107.1	621.8	1817.3
	C7	11.5	59.9	4.8	90.8	239.4	751.2

Table 3.9.4-9
Demand of EOS-HSMS Concrete Components for Shear Forces and Moments

Component	Load Combination	M_1 (in-kip/ft)	M_2 (in-kip/ft)	V_{o1} (kip/ft)	V_{o2} (kip/ft)	V_i (kip/ft)
1. Rear Wall Bottom (32”)	C1 through C6	335.6	694.6	6.9	11.3	55.5
	C7	215.2	297.1	2.2	2.5	24.5
2. Rear Wall Top (12”)	C1 through C6	69.4	110.3	4.9	7.7	52.9
	C7	25.1	66.2	3.2	3.0	8.5
3. Front Wall Bottom (54”)	C1 through C6	970.2	1882.1	13.4	13.0	60.8
	C7	1028.4	1436.7	3.6	3.1	26.2
4. Front Wall Top (42”)	C1 through C6	1077.5	1501.8	28.7	28.3	130.5
	C7	1500.8	2424.0	24.8	21.4	46.8
5. Side Wall Bottom (24”)	C1 through C6	193.1	161.2	13.3	12.6	20.9
	C7	140.6	409.0	14.6	17.4	13.1
6. Side Wall Bottom (14”)	C1 through C6	67.4	38.9	10.9	6.6	15.4
	C7	58.5	115.7	12.0	12.0	9.8
7. Side Wall Top (12”)	C1 through C6	265.9	224.6	12.1	12.1	59.3
	C7	307.9	138.6	10.6	10.6	37.7
8. Roof (44”)	C1 through C6	623.2	1839.1	39.3	49.8	22.3
	C7	291.1	979.2	10.2	21.8	20.8

Table 3.9.4-10
Demand of EOS-HSMS Concrete Components for Axial Forces and Moments

Component	Load Combination	T_1 (kip/ft)	T_2 (kip/ft)	C_1 (kip/ft)	C_2 (kip/ft)	M_{1P} (in-kip/ft)	M_{2P} (in-kip/ft)
1. Rear Wall Bottom (32”)	C1 through C6	25.0	42.4	49.3	108.5	248.3	344.0
	C7	14.6	10.9	39.7	47.3	58.8	295.8
2. Rear Wall Top (12”)	C1 through C6	51.4	43.7	306.1	132.2	44.1	29.1
	C7	7.5	34.8	21.9	22.4	21.2	42.4
3. Front Wall Bottom (54”)	C1 through C6	54.1	88.6	75.0	117.7	800.5	412.6
	C7	20.5	0.0	35.3	62.5	486.1	0.0
4. Front Wall Top (42”)	C1 through C6	111.6	103.8	426.5	336.5	352.2	907.9
	C7	45.6	80.0	65.8	163.9	1500.8	992.9
5. Side Wall Bottom (24”)	C1 through C6	34.7	28.2	49.3	60.0	181.8	159.6
	C7	21.0	55.2	26.4	33.8	98.8	342.5
6. Side Wall Bottom (14”)	C1 through C6	20.6	15.0	45.9	16.8	64.3	38.9
	C7	29.8	57.3	21.0	10.2	57.2	115.7
7. Side Wall Top (12”)	C1 through C6	50.8	62.0	257.1	233.8	40.9	63.2
	C7	51.8	58.5	121.8	240.2	63.3	62.7
8. Roof (44”)	C1 through C6	24.9	76.4	38.8	114.5	623.0	1824.9
	C7	10.4	46.9	4.9	94.0	246.1	746.4

Table 3.9.4-11
Ultimate Shear/Moment Capacities of Concrete Components

Component	Thermal Condition	V_{ui} kips/ft	V_{uo1} kips/ft	V_{uo2} kips/ft	M_{u1} kip-in/ft	M_{u2} kip-in/ft
1. Rear Wall Bottom (32")	Normal	90.4	38.3	38.3	886.8	886.8
	Accident	85.6	36.3	36.3	837.1	837.1
2. Rear Wall Top (12")	Normal	65.0	12.8	12.8	290.4	290.4
	Accident	61.4	12.2	12.2	273.8	273.8
3. Front Wall Bottom (54")	Normal	196.0	64.3	64.3	3,791.7	3,791.7
	Accident	185.4	61.0	61.0	3,578.1	3,578.1
4. Front Wall Top (42")	Normal	180.7	49.0	49.0	2,875.6	2,875.6
	Accident	170.9	46.5	46.5	2,712.9	2,712.9
5. Side Wall Bottom (24")	Normal	102.1	27.8	27.8	919.3	919.3
	Accident	96.6	26.4	26.4	867.3	867.3
6. Side Wall Bottom (14")	Normal	89.4	15.1	15.1	489.8	489.8
	Accident	84.5	14.3	14.3	461.7	461.7
7. Side Wall Top (12")	Normal	86.8	12.6	12.6	404.0	404.0
	Accident	82.1	11.9	11.9	380.6	380.6
8. Roof (44")	Normal	151.4	51.5	51.5	2,283.1	2,283.1
	Accident	143.3	48.9	48.9	2,154.6	2,154.6

Notes:

V_{ui} = Minimum of ultimate in plane shear capacities in planes 1 and 2.
V_{uo1} = Minimum ultimate out of plane shear capacity in plane 1.
V_{uo2} = Minimum ultimate out of plane shear capacity in plane 2.
M_{u1} = Minimum ultimate moment capacity in plane 1.
M_{u2} = Minimum ultimate moment capacity in plane 2.
Planes 1 and 2 are defined in Figure 3.9.4-5.

Table 3.9.4-12
Ultimate Axial/Moment Capacities of Concrete Components

Component	Thermal Condition	P_{tu} kips/ft	P_{cu} kips/ft	P_{ub1} kips/ft	P_{ub2} kips/ft	M_{ub1} kip-in/ft	M_{ub2} kip-in/ft
1. Rear Wall Bottom (32”)	Normal	59.6	880.4	490.2	490.2	4,802.8	4,802.8
	Accident	56.3	793.9	465.0	465.0	4,367.5	4,367.5
2. Rear Wall Top (12”)	Normal	59.6	350.0	163.0	163.0	747.1	747.1
	Accident	56.3	316.5	154.6	154.6	687.3	687.3
3. Front Wall Bottom (54”)	Normal	152.7	1,513.4	822.0	822.0	14,501.4	14,501.4
	Accident	144.2	1,365.9	779.7	779.7	13,222.4	13,222.4
4. Front Wall Top (42”)	Normal	152.7	1,195.1	625.7	625.7	9,097.3	9,097.3
	Accident	144.2	1,079.5	593.5	593.5	8,318.6	8,318.6
5. Side Wall Bottom (24”)	Normal	85.9	682.2	355.5	355.5	2,951.3	2,951.3
	Accident	81.1	616.2	337.2	337.2	2,699.1	2,699.1
6. Side Wall Bottom (14”)	Normal	85.9	417.0	191.9	191.9	1,081.2	1,081.2
	Accident	81.1	377.5	182.1	182.1	995.7	995.7
7. Side Wall Top (12”)	Normal	85.9	364.0	159.1	159.1	806.6	806.6
	Accident	81.1	329.8	151.0	151.0	744.4	744.4
8. Roof (44”)	Normal	114.5	1,227.8	659.5	659.5	9,425.2	9,425.2
	Accident	108.1	1,108.0	625.5	625.5	8,597.8	8,597.8

Notes:

P_{tu} = Minimum of ultimate tensile capacities in planes 1 and 2.
P_{cu} = Minimum of ultimate compressive capacities in plane 1 and 2.
P_{ub1} = Minimum of ultimate balanced section compressive capacity in plane 1.
P_{ub2} = Minimum of ultimate balanced section compressive capacity in plane 2.
M_{ub1} = Minimum of ultimate balanced section moment capacity in plane 1.
M_{ub2} = Minimum of ultimate balanced section moment capacity in plane 2.
Planes 1 and 2 are defined in Figure 3.9.4-5.

Table 3.9.4-13
Comparison of Highest Combined Shear Forces/Moments with the Capacities of EOS-HSM
3 Pages

Component	Load Combination	Quantity	V_1 Kips/ft	V_{o1} kips/ft	V_{o2} kips/ft	M_1 kip-in/ft	M_2 kip-in/ft
1. Rear Wall Bottom (32")	C1 through C6	Computed	51.62	6.26	9.79	338.75	708.70
		Capacity	90.43	38.26	38.26	886.79	886.79
		Ratio	0.57	0.16	0.26	0.38	0.80
	C7	Computed	25.29	1.86	2.71	232.79	270.83
		Capacity	85.58	36.30	36.30	837.08	837.08
		Ratio	0.30	0.05	0.07	0.28	0.32
2. Rear Wall Top (12")	C1 through C6	Computed	13.70	5.12	6.40	36.93	106.65
		Capacity	64.97	12.81	12.81	290.38	290.38
		Ratio	0.21	0.40	0.50	0.13	0.37
	C7	Computed	7.64	4.22	2.95	24.52	69.33
		Capacity	61.43	12.15	12.15	273.80	273.80
		Ratio	0.12	0.35	0.24	0.09	0.25
3. Front Wall Bottom (54")	C1 through C6	Computed	57.56	14.24	13.02	1023.97	1877.23
		Capacity	195.97	64.28	64.28	3791.72	3791.72
		Ratio	0.29	0.22	0.20	0.27	0.50
	C7	Computed	25.23	3.12	3.11	1049.12	1735.23
		Capacity	185.37	60.98	60.98	3578.11	3578.11
		Ratio	0.14	0.05	0.05	0.29	0.48

Table 3.9.4-13
Comparison of Highest Combined Shear Forces/Moments with the Capacities of EOS-HSM
3 Pages

Component	Load Combination	Quantity	V_I Kips/ft	V_{o1} kips/ft	V_{o2} kips/ft	M_1 kip-in/ft	M_2 kip-in/ft
4. Front Wall Top (42")	C1 through C6	Computed	90.42	28.50	25.62	949.69	1768.70
		Capacity	180.69	49.00	49.00	2875.63	2875.63
		Ratio	0.50	0.58	0.52	0.33	0.62
	C7	Computed	48.32	26.12	24.35	1353.14	2485.27
		Capacity	170.88	46.49	46.49	2712.91	2712.91
		Ratio	0.28	0.56	0.52	0.50	0.92
5. Side Wall Bottom (24")	C1 through C6	Computed	23.50	15.39	14.78	269.28	182.86
		Capacity	102.12	27.84	27.84	919.26	919.26
		Ratio	0.23	0.55	0.53	0.29	0.20
	C7	Computed	11.06	14.31	18.56	143.44	396.28
		Capacity	96.57	26.41	26.41	867.25	867.25
		Ratio	0.11	0.54	0.70	0.17	0.46
6. Side Wall Bottom (14")	C1 through C6	Computed	14.39	11.42	6.10	91.36	38.03
		Capacity	89.39	15.11	15.11	489.85	489.85
		Ratio	0.16	0.76	0.40	0.19	0.08
	C7	Computed	11.13	12.14	12.65	63.98	117.21
		Capacity	84.50	14.34	14.34	461.69	461.69
		Ratio	0.13	0.85	0.88	0.14	0.25

Table 3.9.4-13
Comparison of Highest Combined Shear Forces/Moments with the Capacities of EOS-HSM
3 Pages

Component	Load Combination	Quantity	V_1 Kips/ft	V_{o1} kips/ft	V_{o2} kips/ft	M_1 kip-in/ft	M_2 kip-in/ft
7. Side Wall Top (12")	C1 through C6	Computed	38.48	12.32	11.88	285.32	195.00
		Capacity	86.84	12.57	12.57	403.96	403.96
		Ratio	0.44	0.98	0.95	0.71	0.48
	C7	Computed	46.54	10.56	10.64	341.15	151.85
		Capacity	82.08	11.92	11.92	380.58	380.58
		Ratio	0.57	0.89	0.89	0.90	0.40
8. Roof (44")	C1 through C6	Computed	21.46	46.12	49.54	622.18	1831.53
		Capacity	151.43	51.55	51.55	2283.14	2283.14
		Ratio	0.14	0.89	0.96	0.27	0.80
	C7	Computed	22.51	11.56	24.29	283.58	1004.18
		Capacity	143.25	48.90	48.90	2154.63	2154.63
		Ratio	0.16	0.24	0.50	0.13	0.47

Notes:

Load Combinations C1 through C6 include normal thermal condition and C7 includes accidental thermal condition.

Table 3.9.4-14
Comparison of Highest Combined Axial Forces/Moments with the Capacities of EOS-HSM
3 Pages

Component	Load Combination	Quantity	P (Comp) kips/ft	P_1 (Tens) kips/ft	P_2 (Tens.) kips/ft	M_{1p} (1) kip-in/ft	M_{2p} (1) kip-in/ft
1. Rear Wall Bottom (32")	C1 through C6	Computed	104.39	33.78	32.11	299.64	428.28
		Capacity	880.39	59.64	59.64	427.42	738.10
		Ratio	0.12	0.57	0.54	0.70	0.58
	C7	Computed	44.56	13.37	5.46	66.43	124.05
		Capacity	793.88	56.33	56.33	826.20	806.31
		Ratio	0.06	0.24	0.10	0.08	0.15
2. Rear Wall Top (12")	C1 through C6	Computed	29.63	9.50	23.56	36.93	43.42
		Capacity	349.99	59.64	59.64	279.91	238.59
		Ratio	0.08	0.16	0.40	0.13	0.18
	C7	Computed	15.84	7.09	40.00	20.08	45.85
		Capacity	316.52	56.33	56.33	249.52	79.84
		Ratio	0.05	0.13	0.71	0.08	0.57
3. Front Wall Bottom (54")	C1 through C6	Computed	122.27	72.22	65.59	1019.49	773.80
		Capacity	1513.35	152.68	152.68	1998.10	3368.23
		Ratio	0.08	0.47	0.43	0.51	0.23
	C7	Computed	59.82	19.82	0.00	485.33	0.00
		Capacity	1365.94	144.20	144.20	3244.10	3578.11
		Ratio	0.04	0.14	0.00	0.15	0.00

Table 3.9.4-14
Comparison of Highest Combined Axial Forces/Moments with the Capacities of EOS-HSM
3 Pages

Component	Load Combination	Quantity	P (Comp) kips/ft	P_1 (Tens) kips/ft	P_2 (Tens.) kips/ft	M_{1p} [1] kip-in/ft	M_{2p} [1] kip-in/ft
4. Front Wall Top (42")	C1 through C6	Computed	256.17	97.70	77.54	737.46	1137.66
		Capacity	1195.11	152.68	152.68	2524.84	1880.68
		Ratio	0.21	0.64	0.51	0.29	0.60
	C7	Computed	98.93	22.08	32.83	1352.68	1796.91
		Capacity	1079.52	144.20	144.20	2297.59	2299.51
		Ratio	0.09	0.15	0.23	0.59	0.78
5. Side Wall Bottom (24")	C1 through C6	Computed	70.20	27.97	37.58	267.46	158.64
		Capacity	682.20	85.88	85.88	664.87	738.53
		Ratio	0.10	0.33	0.44	0.40	0.21
	C7	Computed	38.81	22.46	58.73	97.14	324.92
		Capacity	616.18	81.11	81.11	627.12	331.04
		Ratio	0.06	0.28	0.72	0.15	0.98
6. Side Wall Bottom (14")	C1 through C6	Computed	47.63	19.43	16.50	75.91	37.93
		Capacity	417.00	85.88	85.88	450.17	484.24
		Ratio	0.11	0.23	0.19	0.17	0.08
	C7	Computed	21.85	31.53	62.90	63.98	117.21
		Capacity	377.50	81.11	81.11	337.69	236.42
		Ratio	0.06	0.39	0.78	0.19	0.50

Table 3.9.4-14
Comparison of Highest Combined Axial Forces/Moments with the Capacities of EOS-HSM
3 Pages

Component	Load Combination	Quantity	P (Comp) kips/ft	P_1 (Tens) kips/ft	P_2 (Tens.) kips/ft	M_{1p} (1) kip-in/ft	M_{2p} (1) kip-in/ft
7. Side Wall Top (12")	C1 through C6	Computed	157.07	27.52	49.71	44.42	49.00
		Capacity	363.96	85.88	85.88	386.56	170.14
		Ratio	0.43	0.32	0.58	0.11	0.29
	C7	Computed	138.02	56.91	11.68	64.54	132.35
		Capacity	329.77	81.11	81.11	114.93	358.64
		Ratio	0.42	0.70	0.14	0.56	0.37
8. Roof (44")	C1 through C6	Computed	107.11	24.43	67.55	621.82	1817.34
		Capacity	1227.83	114.51	114.51	2237.29	2106.43
		Ratio	0.09	0.21	0.59	0.28	0.86
	C7	Computed	90.83	11.47	59.85	239.44	751.16
		Capacity	1107.99	108.15	108.15	2085.65	1488.26
		Ratio	0.08	0.11	0.55	0.11	0.50

Notes:

1. M_{1p} and M_{2p} are moments at the same location and for the same load combination as P_1 and P_2. M_{1p} and M_{2p} occur at the same location simultaneously with P_1 and P_2, i.e. $M_1 = [(P_{tu} - P_1)/P_{tu}]*M_{u1}$.
2. Load Combinations C1 to C6 include normal thermal, C7 include accident thermal.

Table 3.9.4-15
Load Cases for DSC Support Structure Evaluation

Load Type Nomenclature	Load Type Description
D	Dead load – self weight of rails
L	Live load – weight of the DSC
Ro	Normal handling load
To	Normal thermal load
Ra	Off-normal handling load
Ta	Envelope of off-normal and accident thermal loads
E	Earthquake load

Table 3.9.4-16
Load Combination for DSC Support Structure Evaluation

Load Combination ID	Load Combination	Event
N1	1.0 S > D + L + Ro	Normal
N2	1.0 S > D + L + Ro	Normal – Insertion/Extraction
N3	1.3 S > D + L + Ra + To	Off-normal – Handling
A5S	1.6 S > D + L + E + To	Accident – Earthquake
A5V	1.4 Sv > D + L + E + To	Accident – Earthquake
A8S	1.7 S > D + L + Ta	Accident – Thermal
A8V	1.4 Sv > D + L + Ta	Accident – Thermal

Table 3.9.4-17
Summary of Demand to Capacity Ratio (D/C Ratio) for the Whole Cross Section

Load Combination	Demand/Capacity Ratio	Maximum D/C Ratio and Controlling Action
N3 Strong	0.118	0.729 in Weak Axis Bending in load case A5 Seismic
N1 Weak	0.193	
A5S Weak	0.729	
A8S Weak	0.002	

Table 3.9.4-18
Summary of Demand to Capacity Ratio (D/C Ratio) for the Flange Elements

	Flange Demand/Capacity Type Ratio			Maximum D/C Ratio and Controlling Action
Load Combination	Axial Compression	Strong Bending	Weak Bending	
N1	0.314	0.02	0.228	0.388 Axial Compression in load case N3
N3	0.388	0.226	0.225	
A5S	0.265	0.022	0.229	
A8S	0.114	0.012	0.136	
N2	0.3	0.023	0.271	

Table 3.9.4-19
Summary of Demand to Capacity Ratio (D/C Ratio) for the Web Elements

Load Combination	Web Demand/Capacity Type Ratio			Maximum D/C Ratio and Controlling Action
	Axial Compression	Strong Bending	Weak Bending	
N1	0.747	0.08	0.012	0.761 in Axial Compression in load case A5 Seismic
N3	0.7	0.007	0.007	
A5S	0.761	0.076	0.014	
A8S	0.407	0.038	0.008	
N2	0.693	0.091	0.012	

Table 3.9.4-20
Summary of Demand to Capacity Ratio (D/C Ratio) for the Stiffener Elements

Load Combination	Stiffener Demand/Capacity Type Ratio			Maximum D/C Ratio and Controlling Action
	Axial Compression	Strong Bending	Weak Bending	
N1	0.162	0.023	0.707	0.805 in Weak Axis Bending in load case A5 Seismic
N3	0.059	0.372	0.372	
A5S	0.153	0.026	0.805	
A8S	0.096	0.014	0.434	
N2	0.156	0.02	0.529	

Table 3.9.4-21
Summary of Demand to Capacity Ratio (D/C Ratio) for the Accessories

Item	Demand/Capacity Ratio
Stop plate	0.784
DSC seismic impact	0.027
Extension baseplate	0.864
Lateral braces	0.636

Table 3.9.4-22
Summary of Demand to Capacity Ratio (D/C Ratio) for the Welds

Weld between	Demand/Capacity Ratio
Stop plate and rail	0.363
Extension baseplate and rail	0.141
Stiffener and lateral brace	0.291
Stiffener plate and rail	0.668

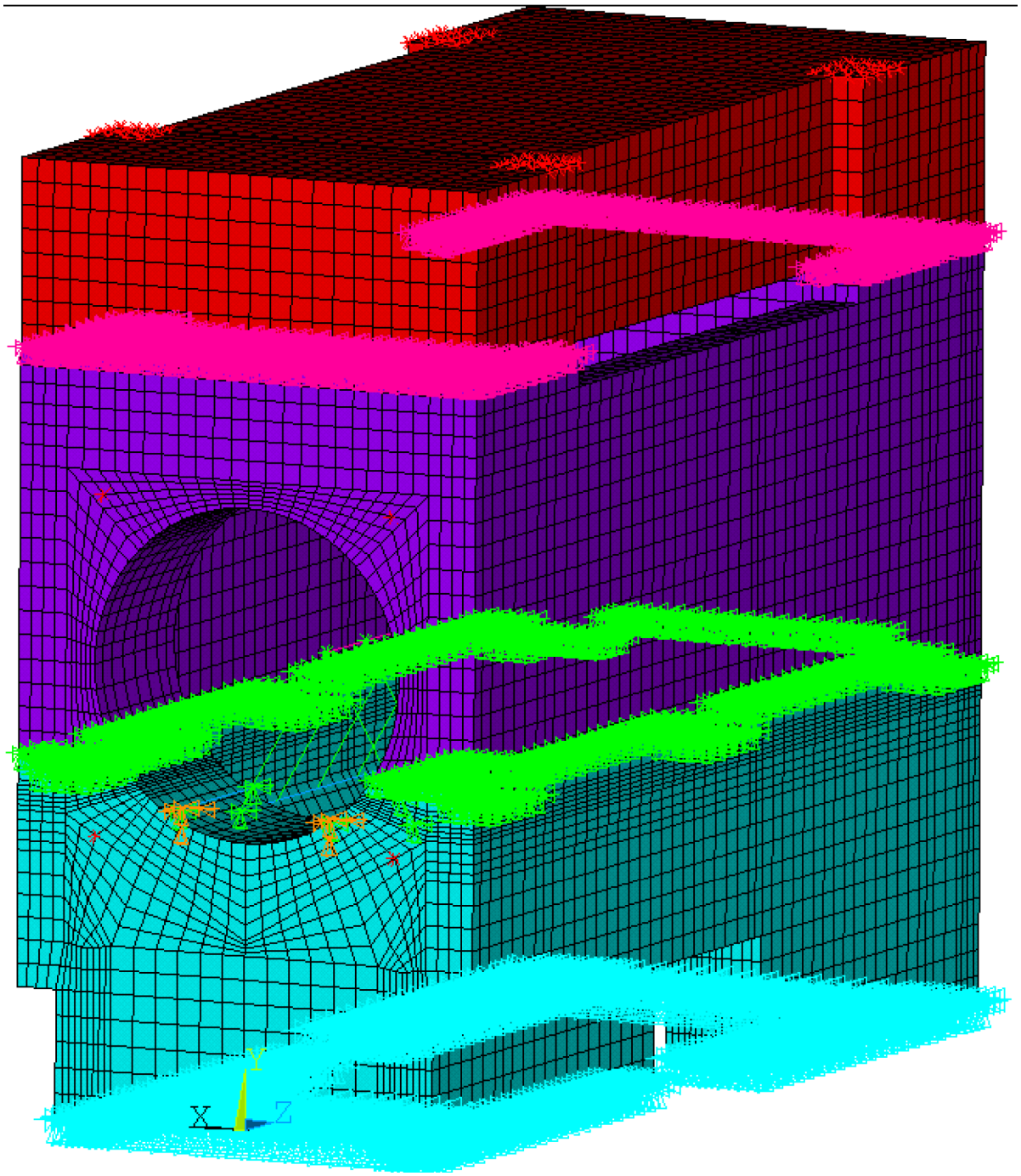

Figure 3.9.4-1
Analytical Model of EOS-HSM for Mechanical Load Analysis

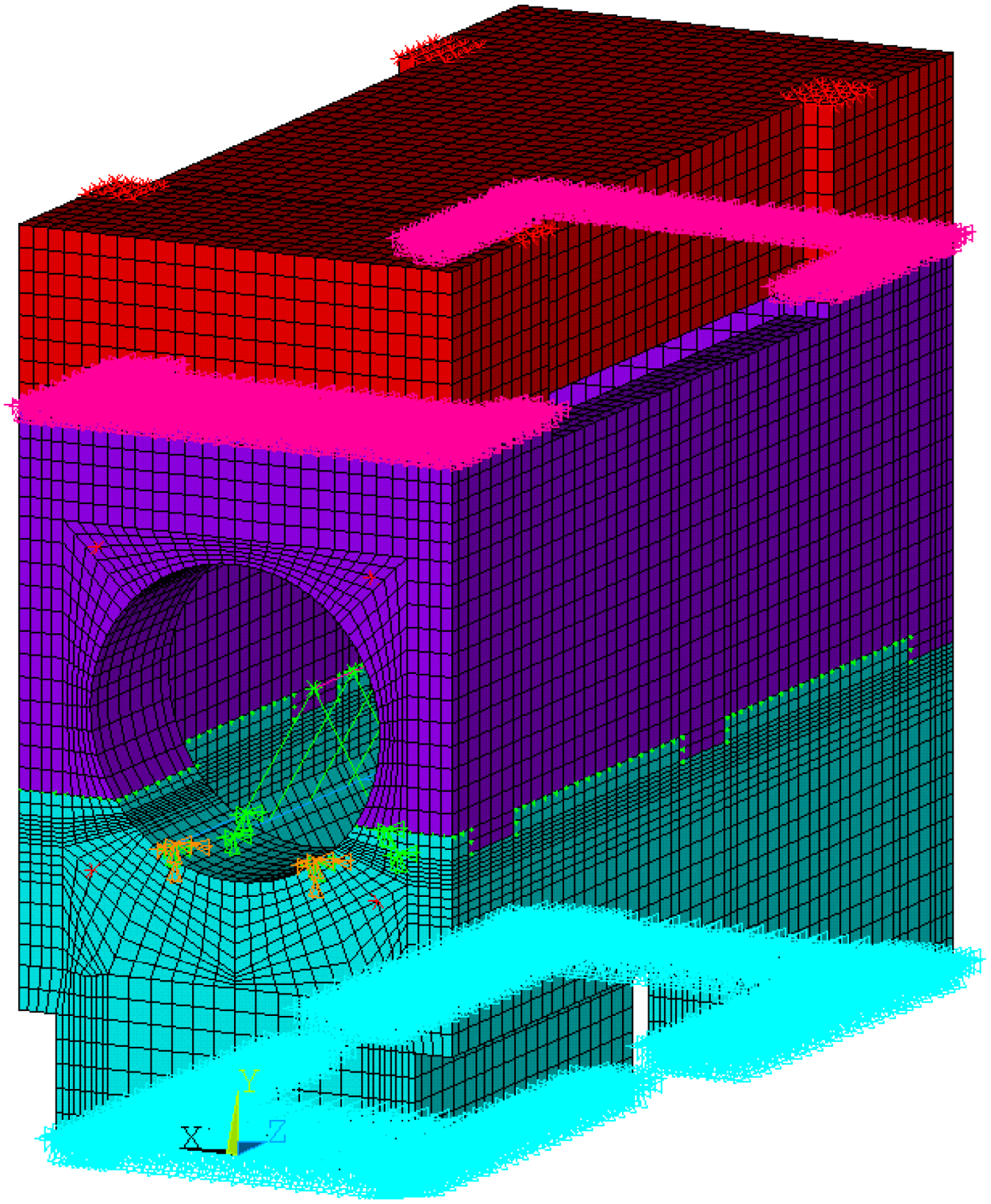

Figure 3.9.4-2
Analytical Model of EOS-HSMS for Mechanical Load Analysis
(Node to Node Contact at Segment Joint interface)

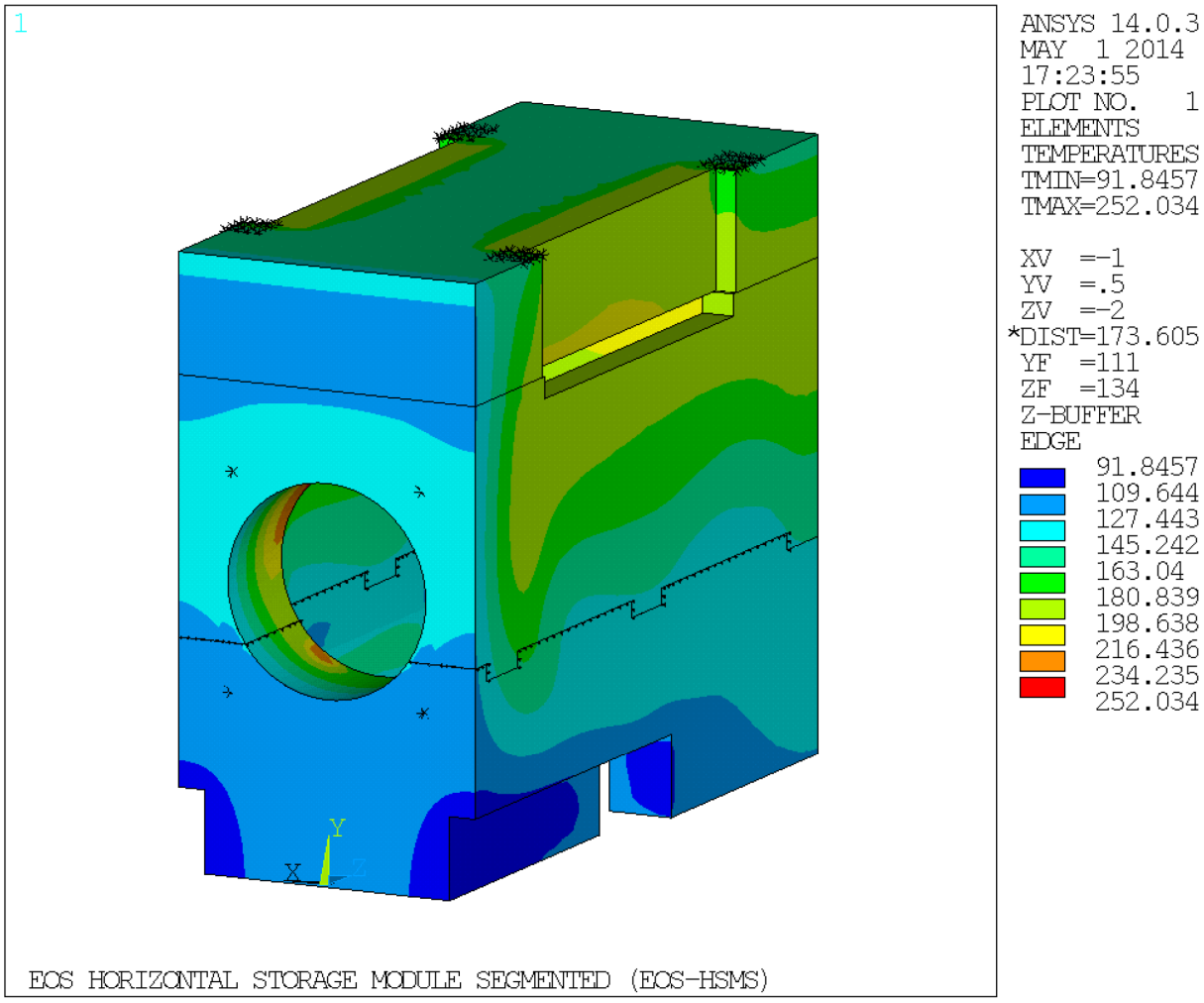

Figure 3.9.4-3
Temperature distribution of EOS-HSMS for Normal Thermal Hot Condition

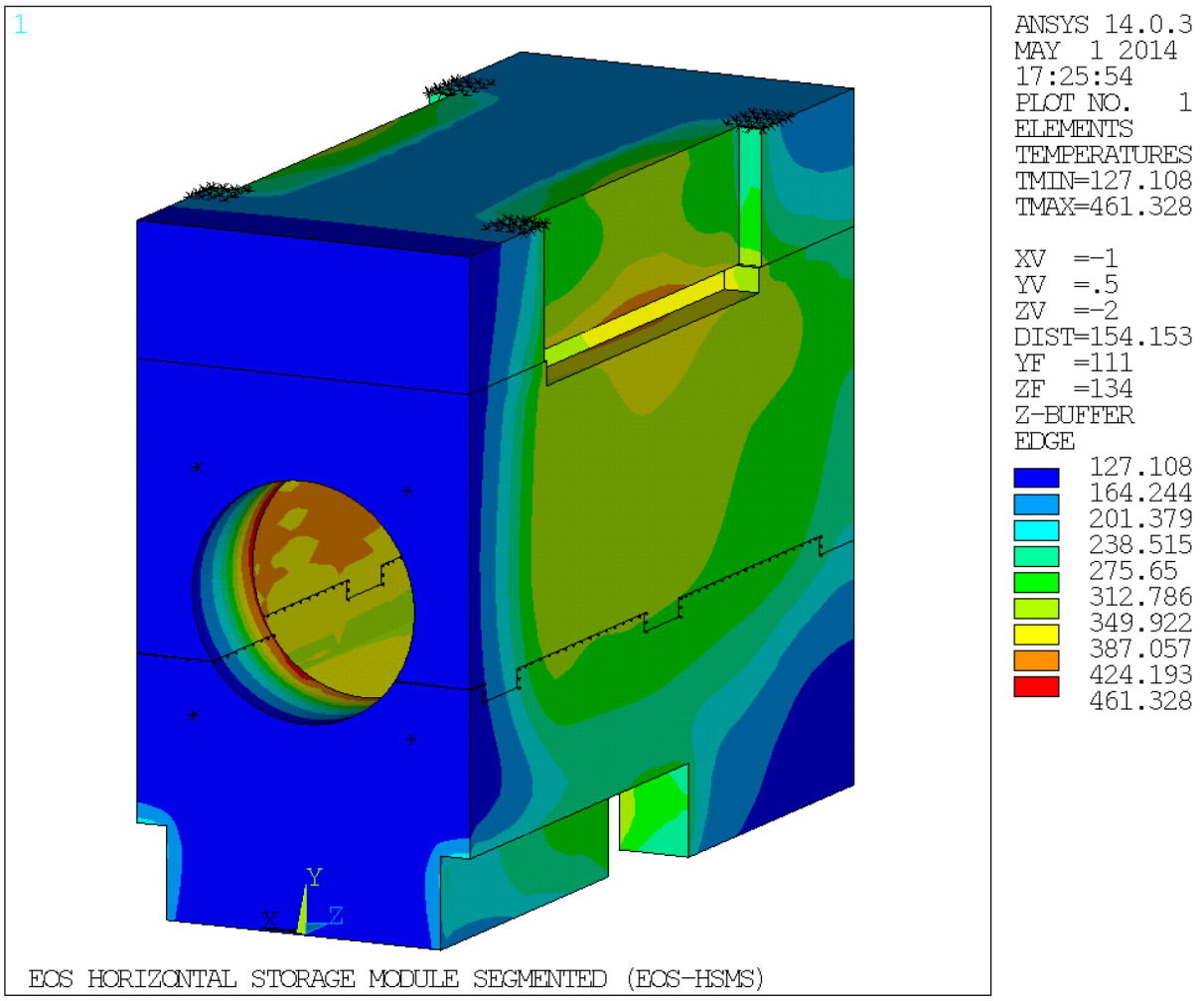

Figure 3.9.4-4
Temperature distribution of EOS-HSMS for Blocked Vent Accident Thermal Condition

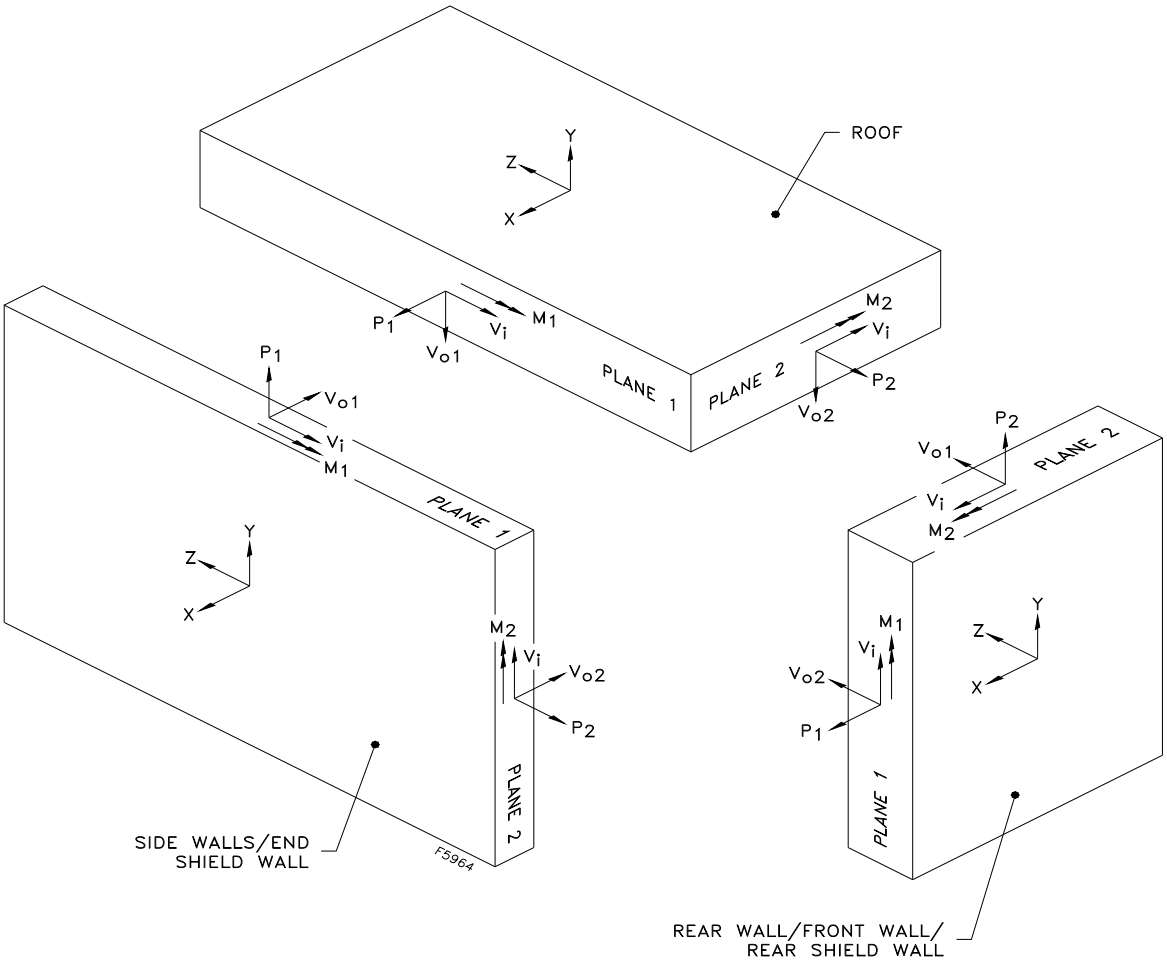

Figure 3.9.4-5
Symbolic Notation of Forces and Moments of EOS-HSM Concrete Components

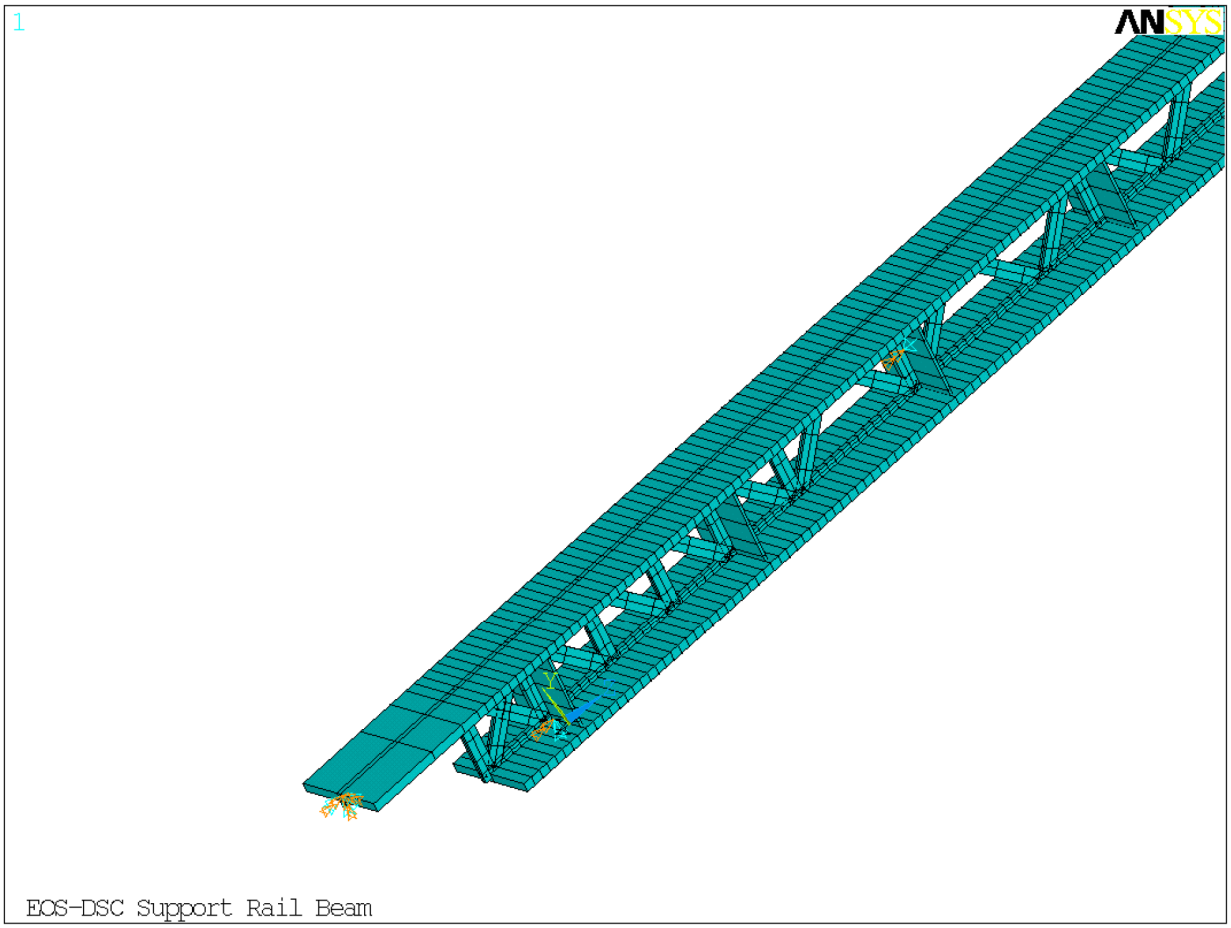

Figure 3.9.4-6
Analytical Model of the W12x136 DSC Main Support Beam with Stiffeners and Open Web

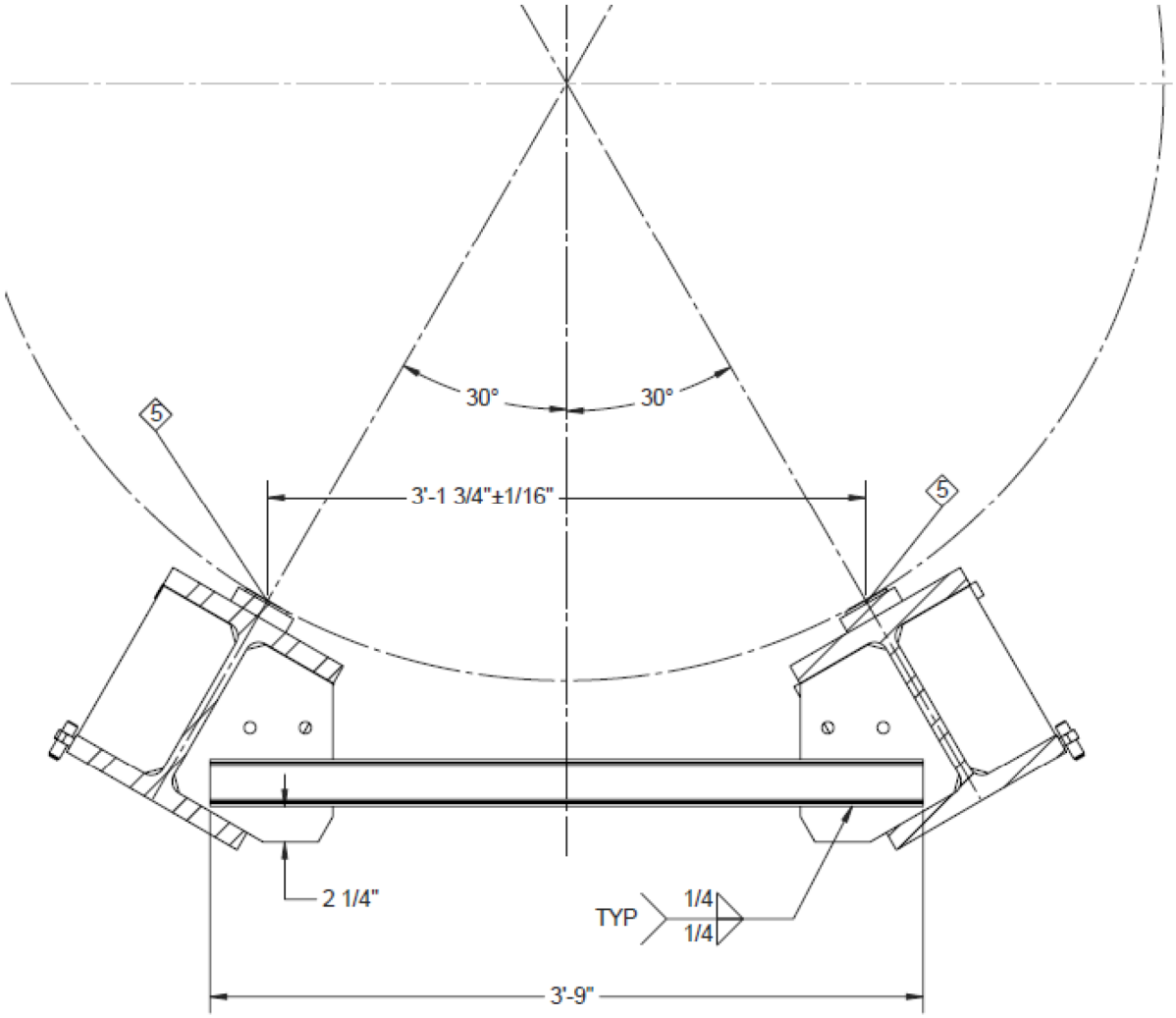

Figure 3.9.4-7
Components of DSC Support Structure

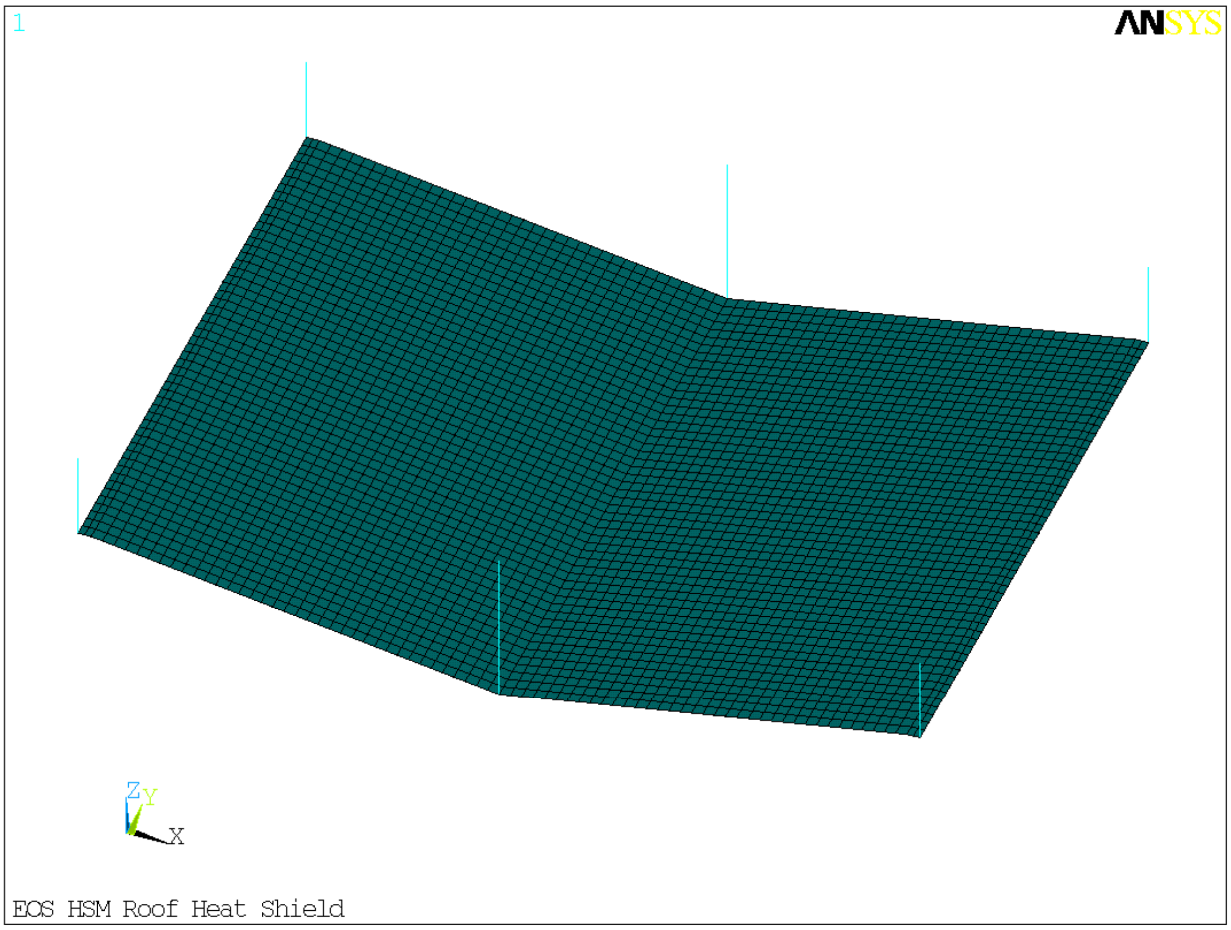

Figure 3.9.4-8
Analytical Model of Coupled Roof Heat Shield and Connection Studs

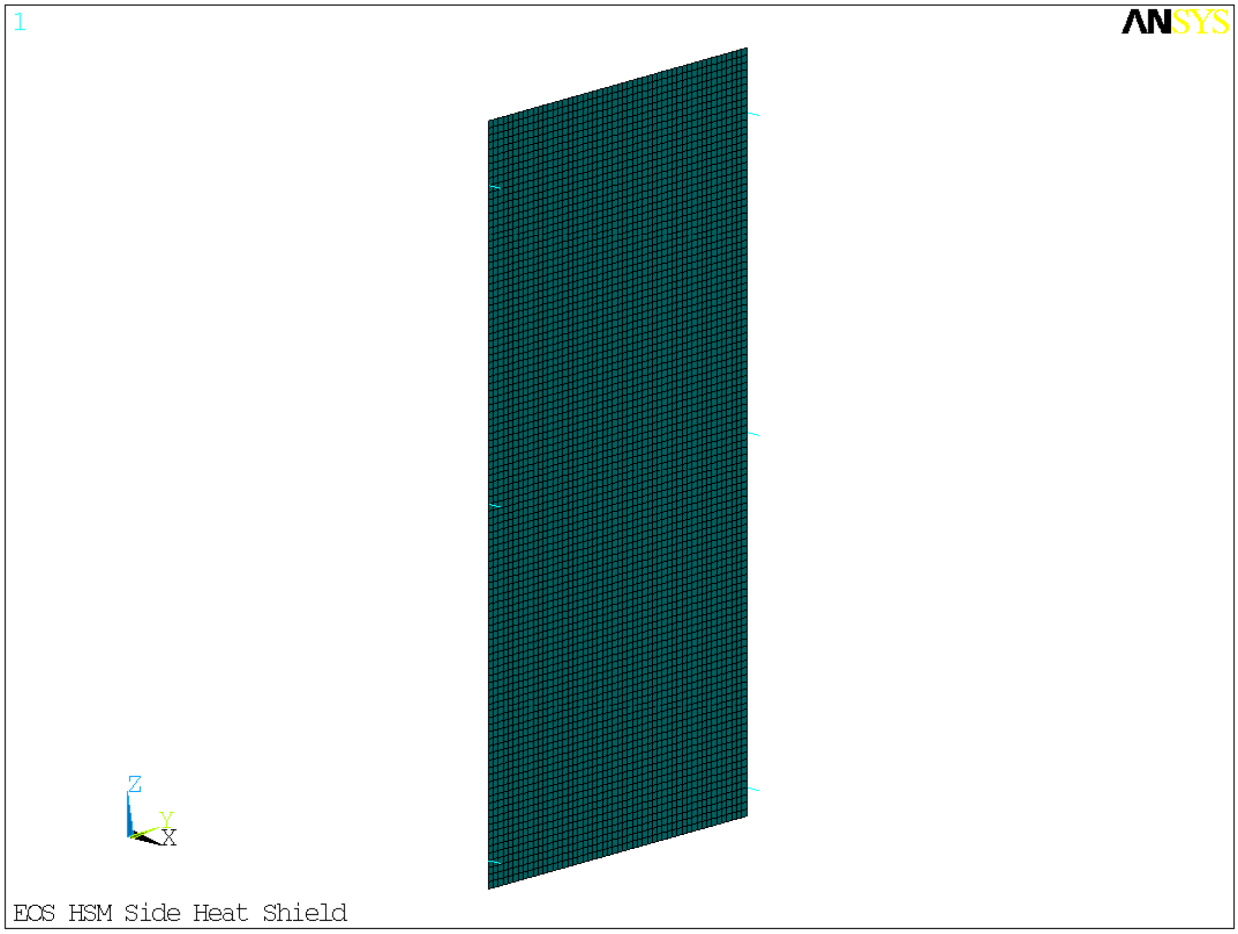

Figure 3.9.4-9
Analytical Model of Coupled Side Heat Shield and Connection Studs